TRƯỜNG ĐẠI HỌC THỦ ĐÔ HÀ NỘI
HANOI METROPOLITAN UNIVERSITY

TẠP CHÍ
KHOA HỌC

SCIENCE JOURNAL OF HANOI METROPOLITAN UNIVERSITY

ISSN 2354-1504

SỐ 31 – KHOA HỌC TỰ NHIÊN VÀ CÔNG NGHỆ

THÁNG 5 – 2019

TẠP CHÍ KHOA HỌC TRƯỜNG ĐẠI HỌC THỦ ĐÔ HÀ NỘI

SCIENTIFIC JOURNAL OF HANOI METROPOLITAN UNIVERSITY

(Tạp chí xuất bản định kì 1 tháng/số)

Giấy phép hoạt động báo chí số 571/GP-BTTTT cấp ngày 26/10/2015
In 200 cuốn tại Trường ĐH Thủ đô Hà Nội. In xong và nộp lưu chiểu tháng 5/2019

MỤC LỤC

Trang

EQUIVALENCE RELATIONS AND THE APPLICATION OF EQUIVALENCE RELATIONS IN TEACHING FRACTIONS IN PRIMARY

Nguyen Van Hao[1], Nguyen Thi Thu Hang[2], Dao Thi Ngoc Bich[3]

[1]*Department of Mathematics, Hanoi Pedagogical University 2*

[2]*Department of Primary Education, Hanoi Pedagogical University 2*

[3]*Department of basic science, Viet Tri University of industry*

Abstract: *In this paper, we would like to present the application of equivalence relations in teaching fractions in Primary.*

Keywords: *Equivalence relations, the application of equivalence relations.*

Email: nguyenvanhaodhsphn2@gmail.com

Received 21 April 2019
Accepted for publication 25 May 2019

1. INTRODUCTION

In Primary, the content of Math knowledge is the first knowledge of Mathematics, although simple but is the basic knowledge, foundation for each student's future learning process. One of the basic views when developing programs and textbooks for Primary Mathematics it is the presentation of mathematical knowledge in the light of modern advanced mathematics. So, the application of advanced mathematics in teaching mathematics in Primary has extremely significant. In this paper, we illustrate an in-depth understanding of equivalence relations that is important in orienting and teaching some fractional problems in Primary.

2. CONTENT

2.1. Preliminaries

To present some applications on equivalence relations in teaching fractions in Primary, we would like to repeat some of the most basic knowledge about this concept. For more details on this problem, we can refer to the references [1] and [2].

2.1.1. Two - way relationship

Define 1. A certain S subset of Descartes multiplication $X \times Y$ is called the two - way relationship above on $X \times Y$.

One element $(x;y) \in S$ we say x has a two - way relationship S with y and from now, we write xSy instead of writing is $(x;y) \in S$. When $Y = X$ to simply say S is a two-way relationship on X instead of speaking S is a two - way relationship on $X \times X$.

Example. For two set $X = \{1,2,3\}$ and $Y = \{a,b\}$. Then, Descartes multiplication of X and Y is

$$X \times Y = \{(1;a),(1;b),(2;a),(2;b),(3;a),(3;b)\}$$

Thus, we immediately see that in Descartes multiplication $X \times Y$, the following subsets are the two-way relationship on $X \times Y$

$$S_1 = \{(1;a),(1;b),(2;a)\}$$

$$S_2 = \{(2;b),(3;a),(3;b)\}$$

$$S_3 = \{(1;a),(2;a),(3;a)\}$$

In the conventional way, we write the two-way relationship between the elements in the above relationship, respectively is

$$1S_1a, 1S_1b, 2S_1a$$

$$2S_2b, 3S_2a, 3S_2b$$

$$1S_3a, 2\,\mathrm{S}_3\,a, 3S_3a$$

2.1.2. Equivalence relations

Define 2. A two - way relationship S on the set X is called an equivalence relation if the following three conditions are satisfied:

(i) Reflex: For every $x \in X$ then xSx.

(ii) Symmetry: For every $x, y \in X$ if xSy then ySx.

(iii) Bridge: For every $x, y, z \in X$ if xSy and ySz then xSz.

When two - way relationship S is equivalence relations, we often change S by symbol "$\sim$" and if $a \sim b$ then read is "a equivalent to b".

Define 3. Suppose that "$\sim$" is a equivalence relations on set X and $a \in X$. Set of all elements $x \in X$, they are equivalent with a denoted by $C(a)$ or $\overline{a}$. It mean that

$$\overline{a} = C(a) = \left\{x \in X : x \sim a\right\}$$

This is called a class equivalent to a according to the equivalence relation "$\sim$" on the set X.

2.1.3. The nature of fractions

Let $\mathbb{N}$ be a natural number set and $\mathbb{N}^* = \mathbb{N} \setminus \{0\}$. On the Descartes product $\mathbb{N} \times \mathbb{N}^*$, we define relationship "$\sim$" as follows for any $\frac{a}{b}, \frac{c}{d} \in \mathbb{N} \times \mathbb{N}^*$ we say that

$\frac{a}{b} \sim \frac{c}{d}$ if and only if $a \times d = b \times c$.

It is easy to check that "$\sim$" is equivalence relations. Each pair of numbers in order $(a;b)$ with $a \in \mathbb{N}$ and $b \in \mathbb{N}^*$ we call a non - negative fraction. The set all non - negative fractions, we denote $\mathbb{Q}^+$. Như vậy $\mathbb{Q}^+ = {}^{\mathbb{N}\times\mathbb{N}^*}\!/_{\sim}$.

The concept of non - negative fractions in this curriculum is consistent with the concept of fractions formed in Primary schools. This way of forming fractions is the foundation for building rational numbers $\mathbb{Q}$.

2.2. The applications of equivalence relations in teaching fractions in Primary

In the primary mathematics program, fractions are formed based on equivalence relations. Therefore, we can understand the fraction problems easily and teaching for students when understanding the theory of equivalence relations. We illustrate that through a number of problems below.

2.2.1. Some typical problems

Problem 1 $\left([3], \text{Exercise} 153, \text{page} 19\right)$. Find x to have equal fractions

$a)\ \frac{2}{3} = \frac{12}{x}$ $\qquad$ $c)\ \frac{14}{56} = \frac{1}{x}$

$b)\ \frac{24}{36} = \frac{x}{12}$ $\qquad$ $d)\ \frac{x}{125} = \frac{2}{5}$

Method 1. The teacher suggests that students use nature of the two equal fractions to solve this problem. Guide students to reduce to the same denominator or compact fractions was known to get new fractions has a numerator or denominator similar to the fraction containing x.

$a)$ We have

$$\frac{2}{3}=\frac{2\times 6}{3\times 6}=\frac{12}{18}.$$

It is easy to see that the two fractions $\frac{12}{18}$ and $\frac{12}{x}$ have numerator equal to 12 so these two fractions are equal, the denominator must be equal. Then, we have

$$\frac{2}{3}=\frac{12}{x}$$

$$\frac{12}{18}=\frac{12}{x}$$

$$x=18$$

Thus $x=18$.

$b)$ We have

$$\frac{24}{36}=\frac{24:3}{36:3}=\frac{8}{12}.$$

It is easy to see that the two fractions $\frac{8}{12}$ and $\frac{x}{12}$ have denominator equal to 12 so these two fractions are equal, the numerator must be equal. It folows that

$$\frac{24}{36}=\frac{x}{12}$$

$$\frac{8}{12}=\frac{x}{12}$$

$$x=8$$

Thus $x=8$.

Parts $c)$ and $d)$ same as parts $a)$ and $b)$.

Method 2. Teachers guide students to solve the above problem based on the theory of equivalence relations. This method helps students solve faster, no need to transform known fractions to get a new fraction with a numerator or denominator by numerator or denominator of fraction containing x. Based on this nature, we can guide students to solve as follows

$a)\ \dfrac{2}{3}=\dfrac{12}{x}$

It means that

$$2\times x=3\times 12$$

or

$$2\times x=36.$$

Students apply the formula to find unknown factors to find x

$$x=36:2$$

$$x=18$$

Thus $x=18$.

Part $b),\mathrm{c})$ and $d)$ same as part $a)$.

Problem 2 $\left([3],\mathrm{Exercie}\,157,\mathrm{page}\,19\right)$. Give fraction $\dfrac{11}{16}$. Need to add both the numerator and denominator of that fraction with the same number is how many to get a new fraction which value is $\dfrac{4}{5}$?.

The teacher suggested that when adding both the numerator and the denominator of the fraction $\dfrac{11}{16}$ with the same number, subtraction the denominator and numerator of the new fraction remain unchanged and equal

$$16-11=5.$$

On the other hand, we have the ratio between the denominator and the numerator of the new fraction is $\dfrac{5}{4}$. Then, the problem takes the form of finding two numbers when knowing the subtraction and the ratio of the two numbers. We have a diagram

New denominator

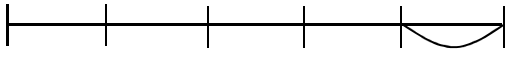

New numerator

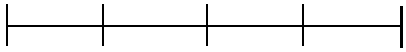

New numerator is

$$5 : (5-4) \times 4 = 20$$

The number to be added to the numerator and the denominator of the old fraction is

$$20 - 11 = 9.$$

Try again

$$\frac{11+9}{16+9} = \frac{20}{25} = \frac{4}{5}.$$

So, the natural number need to look for is 9.

2.2.2. Some similar problems

Problem 3 $\Big([3], \text{Exercise}\, 152, \text{ page } 19\Big)$. Find x is a natural number, know

$a)$ Fraction $\dfrac{x}{33}$ has a value of 4.

$b)$ Fraction $\dfrac{5}{x}$ has a value of $\dfrac{1}{2}$.

Problem 4 $\Big([3], \text{Exercise}\, 197, \text{ page } 19\Big)$. Need to reduce both the numerator and denominator of the fraction $\dfrac{3}{5}$ how many units to get the new fraction equal to $\dfrac{1}{2}$?.

Problem 5 $\Big([3], \text{Exercise}\, 160, \text{ page } 20\Big)$. Need to add the numerator and denominator of the fraction $\dfrac{13}{19}$ how many units to get the new fraction equal to $\dfrac{5}{7}$?.

Problem 6 $\Big([4], \text{Exercise}\, 3, \text{ page } 112\Big)$. Write the appropriate number in the box

$a)$ $\dfrac{50}{75} = \dfrac{10}{\square} = \dfrac{\square}{3}$ $\qquad$ $b)$ $\dfrac{3}{5} = \dfrac{\square}{10} = \dfrac{9}{\square} = \dfrac{\square}{20}$

Problem 7 $\left([4], \text{Exercise } 3, \text{ page } 114\right)$. Write the appropriate number in the box

$$\frac{54}{72} = \frac{27}{\square} = \frac{\square}{12} = \frac{3}{\square}$$

Problem 8 $\left([5], \text{Exercise } 4, \text{ page } 4\right)$. Write the appropriate number in the box

$a)\ 1 = \dfrac{6}{\square}$ $\qquad$ $b)\ 0 = \dfrac{\square}{5}$

3. CONCLUSION

In this article, we present some application of equivalence relations in teaching fractions in Primary to find solutions to present the answer accordance with level of primary students. Application of equivalence relations will help teacher guide students solve problems and help improve teaching effctiveness.

REFERENCES

1. Nguyễn Đình Trí, Tạ Văn Đĩnh, Nguyễn Hồ Quỳnh (2009), *Toán cao cấp tập 1,* - Nxb Giáo dục.
2. Trần Diên Hiển, Nguyễn Tiến Tài, Nguyễn Văn Ngọc (2001), *Lý thuyết số*, - Nxb Đại học Sư phạm.
3. Nguyễn Áng, Dương Quốc Ấn, Hoàng Thị Phước Hảo (2017), *Toán bồi dưỡng học sinh lớp 4*, - Nxb Giáo dục Việt Nam.
4. Đỗ Đình Hoan, Nguyễn Áng, Vũ Quốc Chung, Đỗ Tiến Đạt, Đỗ Trung Hiệu, Trần Diên Hiển, Đào Thái Lai, Phạm Thanh Tâm, Kiều Đức Thành, Lê Tiến Thành, Vũ Dương Thụy (2017), *Toán 4,* - Nxb Giáo dục Việt Nam.
5. Đỗ Đình Hoan, Nguyễn Áng, Đặng Tự Ân, Vũ Quốc Chung, Đỗ Tiến Đạt, Đỗ Trung Hiệu, Đào Thái Lai, Trần Văn Lý, Phạm Thanh Tâm, Kiều Đức Thành, Lê Tiến Thành, Vũ Dương Thụy (2017), *Toán 5*, - Nxb Giáo dục Việt Nam.

QUAN HỆ TƯƠNG ĐƯƠNG VÀ ỨNG DỤNG CỦA QUAN HỆ TƯƠNG ĐƯƠNG TRONG DẠY HỌC PHÂN SỐ Ở TIỂU HỌC

Tóm tắt: *Trong bài báo này, chúng tôi trình bày ứng dụng của quan hệ tương đương trong dạy học phân số ở Tiểu học.*

Từ khóa: *quan hệ tương đương, ứng dụng của quan hệ tương đương.*

A ALGORITHM FOR SOLVING A SEPTADIAGONAL LINEAR SYSTEMS

Nguyen Thi Thu Hoa
Hanoi Metropolitan University

Abstract: *In this paper, we present efficient computational and symbolic algorithm for solving a septadiagonal linear system. Using computer algebra systems such as Maple, Mathematica, Matlab, Python is straightforward. Some example are given. All calculations are implemented by some codes produced in Python.*

Keywords: *Septadiagonal matrices; Linear systems; Computer algebra systems (CAS).*

Email: hoantt@hnmu.edu.vn
Received 13 March 2019
Accepted for publication 25 May 2019

1. INTRODUCTION

The septadiagonal linear system (SLS) take the following form:

$$AX = Y \tag{1}$$

where

$$\widetilde{A} = \begin{pmatrix} D_0 & E_0 & F_0 & G_0 & 0 & ... & 0 \\ C_1 & D_1 & E_1 & F_1 & G_1 & ... & 0 \\ B_2 & C_2 & D_2 & E_2 & ... & ... & 0 \\ A_3 & B_3 & C_3 & D_4 & ... & ... & G_{N-3} \\ 0 & A_4 & B_4 & ... & ... & ... & F_{N-2} \\ ... & ... & ... & ... & C_{N-1} & D_{N-1} & E_{N-1} \\ 0 & ... & 0 & A_N & B_N & C_N & D_N \end{pmatrix} \tag{2}$$

N is a positive integer number, $N \geq 4, X = (x_0, \dots, x_N)^T, Y = (y_0, \dots, y_N)^T, x_i, y_i \in \mathbf{R}$.

This kind of linear systems arise in areas of science and engineering [2, 3, 4, 5]. So in recent years, researchers solve these systems. The author in [] presented the efficient computational algorithms for solving nearly septadiagonal linear systems. The algorithms depend on the LU factorization of the nearly pentadiagonal matrix. In [], the authors discussed a symbolic algorithm for solving septadiagonal linear systems via transformations, …

In this paper,we introduce efficient algorithm base on the LU factorization of the septadiagonal matrix. This work is organized as follow: in Section 2, numerical algorithm for solving SLS are presented. In Section 3, the numerical results are discussed. In the last Section, Section 5, conclusion of the work is presented.

2. NUMERICAL ALGORITHM FOR SOLVING SLS

In this section, we are going to build a new numerical algorithm for computing the solution of septadiagonal linear system.

Assume that

$$\alpha = (\alpha_0, \dots, \alpha_{N-1}), \beta = (\beta_0, \dots, \beta_N), \gamma = (\gamma_1, \dots, \gamma_N), \mu = (\mu_0, \dots, \mu_{N-2}), \gamma' = (\gamma'_2, \dots, \gamma'_N),$$

$$\psi = (\psi_0, \dots, \psi_N), \gamma = (\gamma_1, \dots, \gamma_N), \alpha_i, \beta_i, \gamma_i, \mu_i, \gamma'_i, \psi_i \in \mathbf{R}.$$

If use the LU decomposition of the matrix $\widetilde{A}$, then we have:

$$\widetilde{A} = \begin{pmatrix} 1 & 0 & \dots & & & 0 \\ \gamma_1 & 1 & 0 & \dots & & 0 \\ \gamma'_2 & \gamma_2 & \dots & \dots & & \\ A_3 & \gamma'_3 & \dots & \dots & 0 & \dots \\ 0 & A_4 & \dots & & \dots & 0 \\ \dots & & \dots & & & 1 \\ 0 & \dots & 0 & A_N & \gamma'_N & \gamma_N \end{pmatrix} \begin{pmatrix} \beta_0 & \alpha_0 & \mu_0 & G_0 & 0 & \dots & 0 \\ 0 & \beta_1 & \alpha_1 & \mu_1 & G_1 & 0 & 0 \\ \dots & \dots & \dots & \dots & \dots & \dots & \\ & & & & & & G_{N-3} \\ & & & & & \alpha_{N-2} & \mu_{N-2} \\ & & & & & \beta_{N-1} & \alpha_{N-1} \\ 0 & \dots & & & & 0 & \beta_N \end{pmatrix}. \quad (3)$$

Assume that

$$\begin{pmatrix} \beta_0 & \alpha_0 & \mu_0 & G_0 & 0 & \dots & 0 \\ 0 & \beta_1 & \alpha_1 & \mu_1 & G_1 & 0 & 0 \\ \dots & \dots & \dots & \dots & \dots & \dots & \\ & & & & & & G_{N-3} \\ & & & & & \alpha_{N-2} & \mu_{N-2} \\ & & & & & \beta_{N-1} & \alpha_{N-1} \\ 0 & \dots & & & & 0 & \beta_N \end{pmatrix} \begin{pmatrix} x_0 \\ x_1 \\ \dots \\ \\ \\ \\ x_N \end{pmatrix} = \begin{pmatrix} \psi_0 \\ \psi_1 \\ \dots \\ \\ \\ \\ \psi_N \end{pmatrix}. \quad (4)$$

From (3) and (4) we have

$$\beta_0 = D_0, \alpha_0 = E_0, \mu_0 = F_0,$$

$$\gamma_1 = \frac{C_1}{\beta_0}, \mu_1 = F_1 - \gamma_1 G_0, \beta_1 = D_1 - \alpha_0 \gamma_1, \alpha_1 = E_1 - \gamma_1 \mu_0,$$

$$\gamma_2' = \frac{B_2}{\beta_0}, \gamma_2 = \frac{C_2 - \gamma_2'\alpha_0}{\beta_1}, \alpha_2 = E_2 - \gamma_2\mu_1 - \gamma_2' G_0,$$

$$\beta_2 = D_2 - \alpha_1\gamma_2 - \mu_0\gamma_2'$$

$$\mu_2 = F_2 - \gamma_2 G_1,$$

$$\gamma_i' = \frac{B_i - A_i \dfrac{\alpha_{i-3}}{\beta_{i-3}}}{\beta_{i-2}}$$

$$\gamma_i = \frac{C_i - \gamma_i'\alpha_{i-2} - A_i \dfrac{\mu_{i-3}}{\beta_{i-3}}}{\beta_{i-1}},$$

$$\alpha_i = E_i - \gamma_i\mu_{i-1} - \gamma_i' G_{i-2}, \beta_i = D_i - A_i \frac{G_{i-3}}{\beta_{i-3}} - \alpha_{i-1}\gamma_i - \mu_{i-2}\gamma_i',$$

$$\beta_i = D_i - A_i \frac{G_{i-3}}{\beta_{i-3}} - \alpha_{i-1}\gamma_i - \mu_{i-2}\gamma_i', \mu_i = F_i - \gamma_i G_{i-1},$$

$$\beta_i = D_i - A_i \frac{G_{i-3}}{\beta_{i-3}} - \alpha_{i-1}\gamma_i - \mu_{i-2}\gamma_i', \mu_i = F_i - \gamma_i G_{i-1},\ i = 3, \ldots, N-2.$$

$$\gamma_{N-1}' = \frac{B_{N-1} - A_{N-1} \dfrac{\alpha_{N-4}}{\beta_{N-4}}}{\beta_{N-2}}, \alpha_{N-1} = E_{N-1} - \gamma_{N-1}\mu_{N-2} - \gamma_{N-1}' G_{N-3},$$

$$\gamma_{N-1} = \frac{C_{N-1} - \gamma_{N-1}'\alpha_{N-3} - \dfrac{A_{N-1}\mu_{N-4}}{\beta_{N-4}}}{\beta_{N-2}},$$

$$\alpha_{N-1} = E_{N-1} - \gamma_{N-1}\mu_{N-2} - \gamma_{N-1}' G_{N-3}, \beta_{N-1} = D_{N-1} - A_{N-1} \frac{G_{N-4}}{\beta_{N-4}} - \alpha_{N-2}\gamma_{N-1} - \mu_{N-3}\gamma_{N-1}',$$

$$\gamma_N' = \frac{B_N - A_N \dfrac{\alpha_{N-3}}{\beta_{N-3}}}{\beta_{N-2}}, \gamma_N = \frac{C_N - \gamma_N'\alpha_{N-2} - A_N \dfrac{\mu_{N-3}}{\beta_{N-3}}}{\beta_{N-1}},$$

$$\beta_N = D_N - A_N \frac{G_{N-3}}{\beta_{N-3}} - \alpha_{N-1}\gamma_N - \mu_{N-2}\gamma_N'.$$

It is to see that, the LU decomposition (3) exists only if $\beta_i \neq 0, i = 1, \ldots, n-1$.

Algorithm. To solve the general septadiagonal linear system (1), we may procced as follows:

Step 1. Set

$$\beta_0 = D_0, \alpha_0 = E_0, \mu_0 = F_0.$$

Step 2. Compute

$$\gamma_1 = \frac{C_1}{\beta_0}, \mu_1 = F_1 - \gamma_1 G_0, \beta_1 = D_1 - \alpha_0\gamma_1, \alpha_1 = E_1 - \gamma_1\mu_0,$$

$$\gamma_2' = \frac{B_2}{\beta_0}, \gamma_2 = \frac{C_2 - \gamma_2'\alpha_0}{\beta_1}, \alpha_2 = E_2 - \gamma_2\mu_1 - \gamma_2' G_0,$$

$$\beta_2 = D_2 - \alpha_1\gamma_2 - \mu_0\gamma_2'$$

$$\mu_2 = F_2 - \gamma_2 G_1.$$

Step 3. For i = 3…, N – 2 compute

$$\gamma_i' = \frac{B_i - A_i \frac{\alpha_{i-3}}{\beta_{i-3}}}{\beta_{i-2}}$$

$$\gamma_i = \frac{C_i - \gamma_i'\alpha_{i-2} - A_i \frac{\mu_{i-3}}{\beta_{i-3}}}{\beta_{i-1}},$$

$$\alpha_i = E_i - \gamma_i\mu_{i-1} - \gamma_i' G_{i-2}, \beta_i = D_i - A_i \frac{G_{i-3}}{\beta_{i-3}} - \alpha_{i-1}\gamma_i - \mu_{i-2}\gamma_i',$$

$$\beta_i = D_i - A_i \frac{G_{i-3}}{\beta_{i-3}} - \alpha_{i-1}\gamma_i - \mu_{i-2}\gamma_i', \mu_i = F_i - \gamma_i G_{i-1},$$

$$\beta_i = D_i - A_i \frac{G_{i-3}}{\beta_{i-3}} - \alpha_{i-1}\gamma_i - \mu_{i-2}\gamma_i', \mu_i = F_i - \gamma_i G_{i-1},$$

Step 4. Compute

$$\gamma_{N-1}' = \frac{B_{N-1} - A_{N-1} \frac{\alpha_{N-4}}{\beta_{N-4}}}{\beta_{N-2}}, \alpha_{N-1} = E_{N-1} - \gamma_{N-1}\mu_{N-2} - \gamma_{N-1}' G_{N-3},$$

$$\gamma_{N-1} = \frac{C_{N-1} - \gamma_{N-1}'\alpha_{N-3} - \frac{A_{N-1}\mu_{N-4}}{\beta_{N-4}}}{\beta_{N-2}},$$

$$\alpha_{N-1} = E_{N-1} - \gamma_{N-1}\mu_{N-2} - \gamma'_{N-1}G_{N-3}, \beta_{N-1} = D_{N-1} - A_{N-1}\frac{G_{N-4}}{\beta_{N-4}} - \alpha_{N-2}\gamma_{N-1} - \mu_{N-3}\gamma'_{N-1},$$

$$\gamma'_N = \frac{B_N - A_N\frac{\alpha_{N-3}}{\beta_{N-3}}}{\beta_{N-2}}, \gamma_N = \frac{C_N - \gamma'_N\alpha_{N-2} - A_N\frac{\mu_{N-3}}{\beta_{N-3}}}{\beta_{N-1}},$$

$$\beta_N = D_N - A_N\frac{G_{N-3}}{\beta_{N-3}} - \alpha_{N-1}\gamma_N - \mu_{N-2}\gamma'_N.$$

Step 5. Compute the solution

$$x_N = \frac{\psi_N}{\beta_N}, x_{N-1} = \frac{\psi_{N-1} - x_N\alpha_{N-1}}{\beta_{N-1}}, x_{N-2} = \frac{\psi_{N-2} - x_{N-1}\alpha_{N-2} - x_N\mu_{N-2}}{\beta_{N-2}},$$

for i = N – 3, N – 2,…, 0 compute

$$x_i = \frac{\psi_i - x_{i+1}\alpha_i - x_{i+2}\mu_i - x_{i+3}G_i}{\beta_i},$$

where: $\psi_0 = y_0, \psi_1 = y_1 - \gamma_1\psi_0, \psi_2 = y_2 - \gamma_2\psi_1 - \gamma'_2\psi_0$ and for i = 3, …, N we have

$$\psi_i = y_i - \frac{A_i\psi_{i-3}}{\beta_{i-3}} - \gamma_i\psi_{i-1} - \gamma'_i\psi_{i-2}.$$

3. PYTHON CODE AND ILLUSTRATIVE EXAMPLES

In this section, we give Python code to solve septadiagonal linear systems. After that this code is used for some examples.

3.1. Python code to solve septadiagonal linear systems

We have Python code to solve septadiagonal linear systems:

```
Code python giai he pttt 7 dg cheo
Beta[0] = D[0]
if Beta[0]== 0:
Beta[0]= s
D[0]= s
Alpha[0] = E[0]
Mu[0] = F[0]
Gamma[1] = C[1]/Beta[0]
Mu[1] = F[1] - Gamma[1] * G[0]
```

```
Beta[1] = D[1] - Alpha[0]*Gamma[1]
if Beta[1]== 0:
    Beta[1]= s
Alpha[1] = E[1] - Gamma[1]*Mu[0]
Gamma_P[2] = B[2]/Beta[0]
Gamma[2] = (C[2] - Gamma_P[2]*Alpha[0])/Beta[1]
Alpha[2] = E[2] - Gamma[2]*Mu[1] - Gamma_P[2]*G[0]
Beta[2] = D[2] - Alpha[1]*Gamma[2] - Mu[0]*Gamma_P[2]
if Beta[2]== 0:
    Beta[2]= s
Mu[2] = F[2] - Gamma[2]*G[1]
for i in range(3,N-1):
    Gamma_P[i] = (B[i] - A[i]*Alpha[i-3]/Beta[i-3])/Beta[i-2]
    Gamma[i] = (C[i] - Gamma_P[i]*Alpha[i-2] - A[i]*Mu[i-3]/Beta[i-3])/Beta[i-1]
    Alpha[i] = E[i] - Gamma[i]*Mu[i-1] - Gamma_P[i]*G[i-2]
    Beta[i] = D[i] - A[i] * G[i-3]/Beta[i-3] - Alpha[i-1]*Gamma[i] - Mu[i-2]*Gamma_P[i]
    if Beta[i]== 0:
    Beta[i]= s
Mu[i] = F[i] - Gamma[i]*G[i-1]
Gamma_P[N-1] = (B[N-1] - A[N-1]*Alpha[N-4]/Beta[N-4])/Beta[N-3]
Gamma[N-1] = (C[N-1] - Gamma_P[N-1]*Alpha[N-3] - A[N-1]*Mu[N-4]/Beta[N-4])/Beta[N-2]
Alpha[N-1] = E[N-1] - Gamma[N-1]*Mu[N-2] - Gamma_P[N-1]*G[N-3]
Beta[N-1] = D[N-1] - A[N-1]*G[N-4]/Beta[N-4] - Alpha[N-2]*Gamma[N-1] - Mu[N-
    3]*Gamma_P[N-1]
    if Beta[N-1]== 0:
    Beta[N-1]= s
Gamma_P[N] = (B[N] - A[N]*Alpha[N-3]/Beta[N-3])/Beta[N-2]
Gamma[N] = (C[N] - Gamma_P[N]*Alpha[N-2] - A[N]*Mu[N-3]/Beta[N-3])/Beta[N-1]
Beta[N] = D[N] - A[N]*G[N-3]/Beta[N-3] - Alpha[N-1]*Gamma[N] - Mu[N-2]*Gamma_P[N]
    if Beta[N]== 0:
    Beta[N]= s
    Psi[0] = f[0]
    Psi[1] = f[1] - Gamma[1]*Psi[0]
    Psi[2] = f[2] - Gamma[2]*Psi[1] - Gamma_P[2]*Psi[0]
```

```
for i in range (3,N+1):
    Psi[i] = f[i] - A[i]*Psi[i-3]/Beta[i-3] - Gamma[i]*Psi[i-1] - Gamma_P[i]*Psi[i-2]
    delta = [0 for i in range(N+1)]
    delta[N] = Psi[N]/Beta[N]
    delta[N-1] = (Psi[N-1] - delta[N]*Alpha[N-1])/Beta[N-1]
    delta[N-2] = (Psi[N-2] - delta[N-1]*Alpha[N-2] - Mu[N-2]*delta[N])/Beta[N-2]
for i in range(N-3,-1,-1):
delta[i] = (Psi[i] - delta[i+1] * Alpha[i] - delta[i+2] * Mu[i] - G[i]*delta[i+3])/Beta[i].
```

3.2. Illustrative examples

Example 1. Find the solution of the following septadiagonal linear system following:

$$\begin{cases} x_0 + 2x_1 + 3x_2 + 4x_3 = 30 \\ -3x_0 + 4x_1 + x_2 + 2x_3 + x_4 = 21 \\ 2x_0 - x_1 + 5x_2 + 7x_3 + 8x_4 + 2x_5 = 95 \\ x_0 + 3x_1 + 4x_2 + 5x_3 + 6x_4 + x_5 + x_6 = 82 \\ x_1 + 5x_2 + 2x_3 + 3x_4 + 4x_5 + 5x_6 = 99 \\ 2x_2 + 3x_3 + 4x_4 + 5x_5 + x_6 = 75 \\ x_3 + x_4 + 2x_5 + x_6 = 28. \end{cases}$$

Solution.

We have N = 6, D = (1, 4, 5, 5,3, 5, 1), E = (2, 1, 7, 6, 4, 1), F = (3, 2, 8, 1, 5), G = (4, 1, 2, 1), A = (1, 1, 2, 1), B = (2, 3, 5, 3, 1), C = (-3, -1, 4, 2, 4, 2), y = (30, 21, 95, 82, 99, 75, 28). The numerical result is x = (1, 2, 3, 4, 5, 6, 7).

Example 2. Find the solution of the following septadiagonal linear system following:

$$\begin{pmatrix} 81 & -12 & 33 & 24 & 0 & 0 \\ -13 & 4 & 1 & 3 & 32 & 0 \\ 12 & -10 & 15 & 7 & 8 & 2 \\ 112 & 2 & 14 & 25 & 6 & 4 \\ 0 & 1 & 5 & 2 & 3 & 4 \\ 0 & 0 & 2 & 3 & 4 & 5 \end{pmatrix} \begin{pmatrix} x_0 \\ x_1 \\ x_2 \\ x_3 \\ x_4 \\ x_5 \end{pmatrix} = \begin{pmatrix} -222 \\ 212 \\ -71 \\ -96 \\ 42 \\ 24 \end{pmatrix}.$$

Solution.

From the above system, we see that, N = 5, D = (81, 4, 15, 25, 3, 5), E = (-12, 1, 7, 6, 4), F = (33, 3, 8, 4), G = (24, 32, 2), A = (112, 1, 2), B = (12, 3, 5, 3), C = (-13, -10, 14, 2, 4). We find approximation solution of this equation x = (-1, 12, 3, -4, 5, 2).

4. CONCLUSION

In this work, we used the LU factorization of the septadiagonal matrix to biuld a new algorithm. Using numerical examples we have obtained that the Algorithm works well.

Hence, it may be come auseful tool for solving linear systems of septadiagonal type.

REFERENCES

1. S. S. Askar and A. A. Karawia (2015), "On solving pentadiagonal linear systems via transformations", *Mathematical Problems in Engineering*, Vol. **2015**, pp.1-9.
2. S.Battal Gazi Karakoça, Halil Zeybek (2016), "Solitary - wave solutions of the GRLW equation using septic B - spline collocation method", *Applied Mathematics and Computation*, Vol. **289**, pp.159-171.
3. H. Che, X. Pan, L. Zhang and Y. Wang (2012), "Numerical analysis of a linear - implicit average scheme for generalized Benjamin - Bona - Mahony - Burgers equation", J. *Applied Mathematics*, Vol. **2012**, pp.1-14.
4. D. J. Evans and K. R. Raslan (2005), "Solitary waves for the generalized equal width (GEW) equation", *International J. of Computer Mathematics*, Vol. **82(4)**, pp.445-455.
5. C. M. García - Lospez, J.I.Ramos (2012), "Effects of convection on a modified GRLW equation", *Applied Mathematics and Computation*, Vol. **219**, pp.4118-4132.
6. Halil Zeybek, S.Battal Gazi Karakoça (2016), "A numerical investigation using lumped Galerkin approch with cubic B – spline", Springer Plus, 5:199.
7. A. A. Karawia and S. A. El-Shehawy (2009), "Nearly pentadiagonal linear systems", Math. NA, Vol. **26**, pp.1-7.

THUẬT TOÁN GIẢI HỆ PHƯƠNG TRÌNH TUYẾN TÍNH BẢY ĐƯỜNG CHÉO

Tóm tắt*: Trong bài báo này, chúng ta trình bày thuật toán hiệu quả để giải các hệ phương trình tuyến tính bảy đường chéo. Thuật toán trình bày thích hợp với các ngôn ngữ lập trình như Maple, Matlab, Mathematica, Python. Các kết quả số được trình bày bằng ngôn ngữ lập trình Python minh họa hiệu quả của thuật toán.*

Từ khóa*: Ma trận bảy đường chéo, hệ phương trình tuyến tính, tính toán các hệ đại số.*

WEIGHTED MULTILINEAR HARDY-CESÀRO OPERATORS ON SPACES OF HERZ TYPES

Nguyen Thi Hong
Hanoi Metropolitan University

Abstract: *The aim of this paper is investigated the boundedness of the weighted multilinear Hardy-Cesàro operators on weighted functional spaces of Herz types.*

Keywords: *Weighted bilinear Hardy-Cesàro operator; Herz spaces; Morrey-Herz spaces.*

Email: nthong@hnmu.vn
Received 23 March 2019
Accepted for publication 25 May 2019

1. INTRODUCTION

Let me give a brief history of results on these operators. In 1984, Carton-Lebrun and Fosset [1] considered a Hausdorff operator of special kind, which is called the weighted Hardy operator U_ψ, such as the following

$$U_\psi f(x) = \int_0^1 f(tx)\psi(t)dt\,, x \in R^n. \tag{1.1}$$

The authors showed the boundedness of U_ψ on Lebesgue spaces and $BMO(R^n)$ space. In 2001, J. Xiao [16] obtained that U_ψ is bounded on $L^p(R^n)$ if and only if

$$\int_0^1 t^{-\frac{n}{p}}\ \psi(t)dt < \infty. \tag{1.2}$$

Meanwhile, the corresponding operator norm was worked out. The result seems to be of interest as it is related closely to the classical Hardy integral inequality. Also, J. Xiao obtained the $BMO(R^n)$ bounds of U_ψ which sharpened and extended the main result of Carton-Lebrun and Fosset in [1].

In 2012, Chuong and Hung [6] introduced the weighted Hardy-Cesàro operator, a more general form of U_ψ in the real case as

Definition 1.1. Let $\psi: [0,1] \to [0,\infty)$, $s: [0,1] \to R$ be measurable functions. The weighted Hardy-Cesàro operator $U_{\psi,s}$, associated to the parameter curve $s(x,t) := s(t)x$, is defined by

$$U_{\psi,s}f(x) = \int_0^1 f(s(t)x)\psi(t)\,dt, \tag{1.3}$$

for all measurable complex valued functions f on R^n.

With certain conditions on functions s and ω , the authors [6] proved $U_{\psi,s}$ is bounded on weighted Lebesgue spaces and weighted BMO spaces. The corresponding operator norms are worked out too. The authors also give a necessary condition on the weight function ψ, for the boundedness of the commutators of operator $U_{\psi,s}$ on $L^r_\omega(R^n)$ with symbols in $BMO_\omega(R^n)$.

In 2015, Hung and Ky introduced the weighted multilinear Hardy-Cesàro operator which was defined as following

Definition 1.2. Let $m, n \in N$, $\psi: [0,1]^n \to [0,\infty)$, $s_1, \dots, s_m : [0,1]^n \to R$ be measurable functions. Given $f_1, \dots, f_m: R^d \to C$ be measurable functions.

The weighted multilinear Hardy-Cesàro operator $U^{m,n}_{\psi,\vec{s}}$, is defined by

$$U^{m,n}_{\psi,\vec{s}}(f_1, \dots, f_m)(x) = \int_{[0,1]^n}\left(\prod_{k=1}^m f_k(s_k(t)x)\right)\psi(t)dt \tag{1.4}$$

where $\vec{s} = (s_1, \dots, s_m)$.

In [22], the authors obtain the sharp bounds of $U^{m,n}_{\psi,\vec{s}}$ on the product of Lebesgue spaces and central Morrey spaces. They also proved sufficient and necessary conditions of the weighted functions so that the commutators of $U^{m,n}_{\psi,\vec{s}}$ (with symbols in central BMO space) are bounded on the product of central Morrey spaces.

In 2014, Gong, Fu, Ma investigate the weighted multilinear Hardy operators (see [20]) on the product Herz spaces and the product Morrey-Herz spaces, respectively. They obtained the bounds of this operators on the product these spaces.

From all above analysis, it makes me investigate the boundedness and norm of operator in (1.4) from product of spaces of Herz and Morrey-Herz.

The paper is organized as followed. In Section 2 we give the notation and definitions that we shall use in the sequel. In Section 3 we state the main results on the boundedness of $U^{m,n}_{\psi,\vec{s}}$ on the product of Herz spaces. In Section 4, we present the main results on the boundedness of $U^{m,n}_{\psi,\vec{s}}$ on the product of Morrey-Herz spaces.

2. BASIC NOTIONS AND LEMMAS

Since Herz space is a natural generalization of weighted Lebesgue spaces with power weights, researcher are also interested in studying the boundedness of $U^{m,n}_{\psi,\vec{s}}$ on the Herz spaces. To make the description more clear below, we review the definition of the Herz

spaces now. In the following $\chi_k = \chi_{C_k}$; $C_k = B_k \setminus B_{k-1}$ and $B_k = \{x \in R^d: |x| \leq 2^k$, for $k \in Z$, $\widetilde{C_k} = C_k$, $\widetilde{C_0} = B_0$, and $\widetilde{\chi_k} = \chi_{C_k}$ for $k \in N$ and χ_E is the characteristic function of a set E.

Definition 2.1. Let $\alpha \in R, 0 < p \leq \infty, 0 < q < \infty$.

The homogeneous Herz spaces $\dot{K}_q^{\alpha,p}(R^d)$, is defined by

$$\dot{K}_q^{\alpha,p}(R^d) = \{f \in L_{loc}^q(R^d \setminus \{0\}): \|f\|_{\dot{K}_q^{\alpha,p}(R^d)} < \infty\}, \tag{2.1}$$

where

$$\|f\|_{\dot{K}_q^{\alpha,p}(R^d)} = \left\{\sum_{k=-\infty}^{\infty} 2^{k\alpha p} \|f\chi_k\|_{L^q(R^d)}^p\right\}^{\frac{1}{p}} \tag{2.2}$$

(2) The inhomogeneous Herz spaces $K_q^{\alpha,p}(R^d)$, is defined by

$$K_q^{\alpha,p}(R^d) = \{f \in L_{loc}^q(R^d): \|f\|_{K_q^{\alpha,p}(R^d)} < \infty\}, \tag{2.3}$$

where

$$\|f\|_{K_q^{\alpha,p}(R^d)} = \left\{\sum_{k=0}^{\infty} 2^{k\alpha p} \|f\chi_k\|_{L^q(R^d)}^p\right\}^{\frac{1}{p}} \tag{2.4}$$

with usual modifications made when $p = \infty$ or $q = \infty$.

Next, I recall definition of Morrey-Herz spaces (see [20])

Definition 2.2. Let $\alpha \in R, 0 < p < \infty, 0 < q < \infty$ and $\lambda \geq 0$.

The homogeneous Morrey-Herz space $M\dot{K}_{p,q}^{\alpha,\lambda}(R^d)$, is defined by

$$M\dot{K}_{p,q}^{\alpha,\lambda}(R^d) = \{f \in L_{loc}^q(R^d \setminus \{0\}): \|f\|_{M\dot{K}_{p,q}^{\alpha,\lambda}(R^d)} < \infty\}, \tag{2.5}$$

where:

$$\|f\|_{M\dot{K}_{p,q}^{\alpha,\lambda}(R^d)} = \sup_{k_0 \in Z} 2^{-k_0\lambda} \left\{\sum_{k=-\infty}^{k_0} 2^{k\alpha p} \|f\chi_k\|_{L^q(R^d)}^p\right\}^{\frac{1}{p}} \tag{2.6}$$

The inhomogeneous Morrey-Herz spaces $MK_{p,q}^{\alpha,\lambda}(R^d)$, is defined by

$$MK_{p,q}^{\alpha,\lambda}(R^d) = \{f \in L_{loc}^q(R^d): \|f\|_{MK_{p,q}^{\alpha,\lambda}(R^d)} < \infty\}, \tag{2.7}$$

where

$$\|f\|_{MK_{p,q}^{\alpha,\lambda}(R^d)} = \sup_{k_0 \in N} 2^{-k_0\lambda} \left\{\sum_{k=0}^{k_0} 2^{k\alpha p} \|f\tilde{\chi}_k\|_{L^q(R^d)}^p\right\}^{\frac{1}{p}} \tag{2.8}$$

with usual modifications made when $p = \infty$ or $q = \infty$.

From the above definitions, it is not difficult to note that $\dot{K}_p^{0,p}(R^d) = K_p^{0,p}(R^d) = L^p(R^d); \dot{K}_p^{\frac{\alpha}{p},p}(R^d) = K_p^{\frac{\alpha}{p},p}(R^d) = L^p(|x|^\alpha dx)(R^d)$ *for all* $0 < p \leq \infty$ *and* $\alpha \in R$.

Moreover the homogeneous Herz spaces $\dot{K}_q^{\alpha,p}(R^d)$, the homogeneous Morrey-Herz spaces $M\dot{K}_{p,q}^{\alpha,\lambda}(R^d)$ and the Morrey spaces $M^{q,\lambda}(R^d)$ satify $M\dot{K}_{p,q}^{\alpha,0}(R^d) = \dot{K}_p^{\alpha,p}(R^d)$; $M^{q,\lambda}(R^d) \subset M\dot{K}_{q,q}^{0,\lambda}(R^d)$.

Throughout this paper $\omega(x)$ will be denote a nonnegative measurable function on R^d. Remember that a measurable function f belongs to $L_\omega(R^d)$ if

$$||f||_{L_\omega(R^d)} = \left(\int_{R^d}|f(x)|^p\,\omega(x)dx\right)^{\frac{1}{p}} < \infty. \tag{2.9}$$

Definition 2.3. Let γ be a real number. Let W_γ be the set of all functions ω on R^d, which are measurable, $\omega(x) > 0$ for almost everywhere $x \in R^d$. $0 < \int_{S_d}\omega(y)\sigma(y)dy < \infty$ and are absolutely homogeneous of degree γ, that is $\omega(tx) = |t|^\gamma\omega(x)$, for all $t \in R \setminus \{0\}, x \in R^d$.

3. BOUNDEDNESS OF $U_{\psi,\vec{s}}^{m,n}$ ON THE PRODUCT OF HERZ-TYPE SPACES

This section will be devoted to state and prove results on the boundedness of $U_{\psi,\vec{s}}^{2,n}, U_{\psi,\vec{s}}^{m,n}$ on the product of Herz-type spaces. Throughout the whole paper, $S_d = \{x \in R^d : |x| = 1\}$ and we also denote $S_d = \frac{2\pi^{\frac{d}{2}}}{\Gamma(\frac{d}{2})}$. By ω we will denote a weight from W_γ, where $\gamma > -d$. We also denote by ψ a nonnegative and measurable function on $[0,1]^n$.

Theorem 3.1. Let $\alpha, \alpha_1, \alpha_2 \in R, 1 < p, p_i, q, q_i < \infty$, for $i = 1,2$ and

$$\alpha_1 + \alpha_2 = \alpha$$
$$\frac{1}{q_1} + \frac{1}{q_2} = \frac{1}{q}$$
$$\frac{1}{p_1} + \frac{1}{p_2} = \frac{1}{p}$$

then $U_{\psi,\vec{s}}^{2,n}$ is bounded from $\dot{K}_{q_1}^{\alpha_1,p_1}(R^d) \times \dot{K}_{q_2}^{\alpha_2,p_2}(R^d) \to \dot{K}_q^{\alpha,p}(R^d)$ if

$$\int_{[0,1]^n}\left(\prod_{i=1}^2|s(t)|^{-\alpha-\frac{d}{q_i}}\right)\psi(t)dt, \tag{3.1}$$

Conversely, if $\alpha_1 = \alpha_2 = \frac{1}{2}\alpha$, $q_i = 2q, p_i = 2p, i = 1,2$ and $U_{\psi,\vec{s}}^{2,n}$ is bounded from $\dot{K}_{q_1}^{\alpha_1,p_1}(R^d) \times \dot{K}_{q_2}^{\alpha_2,p_2}(R^d) \to \dot{K}_q^{\alpha,p}(R^d)$, then (3.1) holds.

Moreover, in that case, one has

$$||U_{\psi,\vec{s}}^{2,n}||_{\dot{K}_{q_1}^{\alpha_1,p_1}(R^d)\times\dot{K}_{q_2}^{\alpha_2,p_2}(R^d)\to\dot{K}_q^{\alpha,p}(R^d)} \simeq \int_{[0,1]^n}\left(\prod_{i=1}^2|s(t)|^{-\alpha-\frac{d}{q_i}}\right)\psi(t)dt. \tag{3.2}$$

In general case, we have the following theorem

Theorem 3.2. Let $\alpha, \alpha_1, \alpha_2, \dots, \alpha_m \in \mathrm{R}, 1 < \mathrm{p}, \mathrm{p_i}, \mathrm{q}, \mathrm{q_i} < \infty$, for $i = 1, \dots, m$ and

$$\alpha_1 + \alpha_2 + \cdots + \alpha_m = \alpha$$
$$\frac{1}{q_1} + \frac{1}{q_2} + \cdots + \frac{1}{q_m} = \frac{1}{q}$$
$$\frac{1}{p_1} + \frac{1}{p_2} + \cdots + \frac{1}{p_m} = \frac{1}{p}$$

then $U_{\psi,\vec{s}}^{m,n}$ is bounded from $\dot{K}_{q_1}^{\alpha_1,p_1}(R^d) \times \dot{K}_{q_2}^{\alpha_2,p_2}(R^d) \times \dots \times \dot{K}_{q_m}^{\alpha_m,p_m}(R^d) \to \dot{K}_q^{\alpha,p}(R^d)$ if

$$\int_{[0,1]^n} \left(\prod_{i=1}^m |s(t)|^{-\alpha - \frac{d}{q_i}} \right) \psi(t) dt, \tag{3.3}$$

Conversely, if $\alpha_1 = \alpha_2 = \cdots = \alpha_m = \frac{1}{m}\alpha$, $q_i = mq, p_i = mp, i = 1, 2, \dots, m$ and $U_{\psi,\vec{s}}^{m,n}$ is bounded from $\dot{K}_{q_1}^{\alpha_1,p_1}(R^d) \times \dot{K}_{q_2}^{\alpha_2,p_2}(R^d) \times \dots \times \dot{K}_{q_m}^{\alpha_m,p_m}(R^d) \to \dot{K}_q^{\alpha,p}(R^d)$, then (3.3) holds.

Moreover, in that case, one has

$$||U_{\psi,\vec{s}}^{m,n}||_{\dot{K}_{q_1}^{\alpha_1,p_1}(R^d) \times \dot{K}_{q_2}^{\alpha_2,p_2}(R^d) \times \dots \times \dot{K}_{q_m}^{\alpha_m,p_m}(R^d) \to \dot{K}_q^{\alpha,p}(R^d)} \simeq$$
$$\int_{[0,1]^n} \left(\prod_{i=1}^m |s(t)|^{-\alpha - \frac{d}{q_i}} \right) \psi(t) dt. \tag{3.4}$$

Proof of Theorem 3.1. Since $\frac{1}{q_1} + \frac{1}{q_2} = \frac{1}{q}$, by Hölder, Minkowski inequalities and change variable we have:

$$||U_{\psi,\vec{s}}^{2,n}(f_1, f_2)\chi_k||_{L^q(R^d)}$$

$$= \left(\int_{C_k} \left| \int_{[0,1]^n} \left(\prod_{i=1}^2 f_i(s_k(t)x) \right) \psi(t) dt \right|^q dx \right)^{\frac{1}{q}}$$

$$\leq \int_{[0,1]^n} \left(\int_{C_k} \left| \prod_{i=1}^2 f_i(s_k(t)x) \right| dx \right)^{\frac{1}{q}} \psi(t) dt$$

$$\leq \int_{[0,1]^n} \prod_{i=1}^2 \left(\int_{C_k} |f_i(s_i(t)x)|^{q_i} dx \right)^{\frac{1}{q_i}} \psi(t) dt$$

$$= \int_{[0,1]^n} \prod_{i=1}^2 \left(\int_{s_i(t)C_k} |f_i(x)|^{q_i} |s_i(t)|^{-d} dx \right)^{\frac{1}{q_i}} \psi(t) dt$$

$$= \int_{[0,1]^n} \left(\prod_{i=1}^{2} |s_i(t)|^{-\frac{d}{q_i}} \right) \left(\int_{s_1(t)C_k} |f_1(x)|^{q_1} dx \right)^{\frac{1}{q_1}} \left(\int_{s_2(t)C_k} |f_2(x)|^{q_2} dx \right)^{\frac{1}{q_2}} \psi(t) dt.$$

For the arbitrary $s_1(t), s_2(t) \in R$, so we find $m, l \in Z$ such that $2^{m-1} < s_1(t) \leq 2^m$ and $2^{l-1} < s_2(t) \leq 2^l$. Thus

$$\leq \int_{[0,1]^n} \left(\prod_{i=1}^{2} |s(t)|^{-\frac{d}{q_i}} \right) \left(\int_{2^{k+m-2}<|x|\leq 2^{k+m}} |f_1(x)|^{q_1} dx \right)^{\frac{1}{q_1}}$$

$$\times \left(\int_{2^{k+l-2}<|x|\leq 2^{k+l}} |f_2(x)|^{q_2} dx \right)^{\frac{1}{q_2}} \psi(t) dt$$

$$\leq \int_{[0,1]^n} (\|f_1 \chi_{k+m-1}\|_{L^{q_1}} + \|f_1 \chi_{k+m}\|_{L^{q_1}})(\|f_2 \chi_{k+l-1}\|_{L^{q_2}} + \|f_2 \chi_{k+l}\|_{L^{q_2}}) \times$$

$$\left(\prod_{i=1}^{2} |s_i(t)|^{-\frac{d}{q_i}} \right) \psi(t) dt. \tag{3.3}$$

For $\frac{1}{p_1} + \frac{1}{p_2} = \frac{1}{p}$ and $\alpha_1 + \alpha_2 = \alpha$, by Hölder inequality and Minkowski inequality given

$$||U_{\psi,\vec{s}}^{2,n}||_{\dot{K}_q^{\alpha,p}(R^d)}$$

$$= \left(\sum_{k=-\infty}^{\infty} 2^{k\alpha p} ||U_{\psi,\vec{s}}^{2,n} \chi_k||_{L^q}^p \right)^{\frac{1}{p}}$$

$$\leq \left(\sum_{k=-\infty}^{\infty} 2^{k\alpha p} \left(\int_{[0,1]^n} (\|f_1 \chi_{k+m-1}\|_{L^{q_1}} + \|f_1 \chi_{k+m}\|_{L^{q_1}}) \right. \right.$$

$$\left. \left. \times (\|f_2 \chi_{k+l-1}\|_{L^{q_2}} + \|f_2 \chi_{k+l}\|_{L^{q_2}}) \left(\prod_{i=1}^{2} |s_i(t)|^{-\frac{d}{q_i}} \right) \psi(t) dt \right)^p \right)^{\frac{1}{p}}$$

$$\leq \int_{[0,1]^n} \left(\sum_{k=-\infty}^{\infty} 2^{k\alpha p} (\|f_1 \chi_{k+m-1}\|_{L^{q_1}} + \|f_1 \chi_{k+m}\|_{L^{q_1}})^p \right.$$

$$\left. \times (\|f_2 \chi_{k+l-1}\|_{L^{q_2}} + \|f_2 \chi_{k+l}\|_{L^{q_2}})^p \right)^{\frac{1}{p}} \left(\prod_{i=1}^{2} |s_i(t)|^{-\frac{d}{q_i}} \right) \psi(t) dt$$

$$\leq \int_{[0,1]^n} \left(\sum_{k=-\infty}^{\infty} 2^{k\alpha_1 p_1} (\|f_1 \chi_{k+m-1}\|_{L^{q_1}} + \|f_1 \chi_{k+m}\|_{L^{q_1}})^{p_1} \right)^{\frac{1}{p_1}}$$

$$\times \left(\sum_{k=-\infty}^{\infty} 2^{k\alpha_2 p_2} (\|f_2 \chi_{k+l-1}\|_{L^{q_2}} + \|f_2 \chi_{k+l}\|_{L^{q_2}})^{p_2} \right)^{\frac{1}{p_2}}$$

$$\times \left(\prod_{i=1}^{2} |s_i(t)|^{-\frac{d}{q_i}} \right) \psi(t) dt$$

$$\leq \int_{[0,1]^n} \left\{ \left(\sum_{k=-\infty}^{\infty} 2^{k\alpha_1 p_1} (\|f_1 \chi_{k+m-1}\|_{L^{q_1}})^{p_1} \right)^{\frac{1}{p_1}} \right.$$

$$\left. + \left(\sum_{k=-\infty}^{\infty} 2^{k\alpha_1 p_1} (\|f_1 \chi_{k+m}\|_{L^{q_1}})^{p_1} \right)^{\frac{1}{p_1}} \right\}$$

$$\times \left\{ \left(\sum_{k=-\infty}^{\infty} 2^{k\alpha_2 p_2} (\|f_2 \chi_{k+l-1}\|_{L^{q_2}})^{p_2} \right)^{\frac{1}{p_2}} \right.$$

$$\left. + \left(\sum_{k=-\infty}^{\infty} 2^{k\alpha_2 p_2} (\|f_2 \chi_{k+l}\|_{L^{q_2}})^{p_2} \right)^{\frac{1}{p_2}} \right\} \times \times \left(\prod_{i=1}^{2} |s_i(t)|^{-\frac{d}{q_i}} \right) \psi(t) dt$$

$$\leq \|f_1\|_{\dot{K}_{q_1}^{\alpha_1,p_1}(R^d)} \|f_2\|_{\dot{K}_{q_2}^{\alpha_2,p_2}(R^d)} \int_{[0,1]^n} (2^{-(m-1)\alpha_1} + 2^{-m\alpha_1})(2^{-(l-1)\alpha_2} + 2^{-l\alpha_2})$$

$$\times \left(\prod_{i=1}^{2} |s_i(t)|^{-\frac{d}{q_i}} \right) \psi(t) dt$$

$$\leq \|f_1\|_{\dot{K}_{q_1}^{\alpha_1,p_1}(R^d)} \|f_2\|_{\dot{K}_{q_2}^{\alpha_2,p_2}(R^d)} \int_{[0,1]^n} \left(\prod_{i=1}^{2} |s_i(t)|^{-\frac{d}{q_i}} \right) \psi(t) dt.$$

So

$$||U_{\psi,\vec{s}}^{2,n}||_{\dot{K}_q^{\alpha,p}(R^d)} \leq \|f_1\|_{\dot{K}_{q_1}^{\alpha_1,p_1}(R^d)} \|f_2\|_{\dot{K}_{q_2}^{\alpha_2,p_2}(R^d)} \int_{[0,1]^n} \left(\prod_{i=1}^{2} |s_i(t)|^{-\frac{d}{q_i}} \right) \psi(t) dt. \quad (3.4)$$

From the above inequalities, we have that the first conclusion in Theorem 3.1 holds.

On the other hand, we suppose that $U_{\psi,\vec{s}}^{2,n}$ is bounded from

$$\dot{K}_{q_1}^{\alpha_1,p_1}(R^d) \times \dot{K}_{q_2}^{\alpha_2,p_2}(R^d) \to \dot{K}_{q}^{\alpha,p}(R^d)$$

and $U_{\psi,\vec{s}}^{2,n}$ has the operator norm $||U_{\psi,\vec{s}}^{2,n}||_{\dot{K}_{q_1}^{\alpha_1,p_1}(R^d)\times \dot{K}_{q_2}^{\alpha_2,p_2}(R^d)\to \dot{K}_{q}^{\alpha,p}(R^d)}$. For any $0 < \epsilon < 1$, let

$$f_1(x) = \begin{cases} 0\,, if\ x \le 1 \\ x^{-\alpha_1-\frac{d}{q_1}-\epsilon}, if\ x > 1, \end{cases} \tag{3.5}$$

$$f_2(x) = \begin{cases} 0\,, if\ x \le 1 \\ x^{-\alpha_1-\frac{d}{q_1}-\epsilon}, if\ x > 1, \end{cases} \tag{3.6}$$

Obviously, $\|f_1\chi_k\|_{L^{q_1}} = \|f_2\chi_k\|_{L^{q_2}} = 0$, when $k = 0, -1, -2, \ldots$. So, for any positive integer k, it is easy to get that

$$\|f_1\chi_k\|_{L^{q_1}}^{q_1} = \int_{2^{k-1}<|x|<2^k} |x|^{\left(-\alpha_1-\frac{d}{q_1}-\epsilon\right)q_1} dx$$

$$= 2^{k(-\alpha_1-\epsilon)q_1} \frac{S_d(2^{q_1(\alpha_1+\epsilon)}-1)}{q_1(\alpha_1+\epsilon)}$$

where $S_d = \frac{2\,\pi^{\frac{d}{2}}}{\Gamma(\frac{d}{2})}$. Thus

$$\|f_1\chi_k\|_{L^{q_1}} = 2^{-k(\alpha_1+\epsilon)} \left(\frac{S_d(2^{q_1(\alpha_1+\epsilon)}-1)}{q_1(\alpha_1+\epsilon)}\right)^{\frac{1}{q_1}} \tag{3.7}$$

A simple computation gives

$$\|f_1\|_{\dot{K}_{q_1}^{\alpha_1,p_1}(R^d)} = 2^{-\epsilon} \left(\frac{S_d(2^{q_1(\alpha_1+\epsilon)}-1)}{q_1(\alpha_1+\epsilon)}\right)^{\frac{1}{q_1}} \left(\frac{1}{1-2^{-\epsilon p_1}}\right)^{\frac{1}{p_1}} \tag{3.8}$$

Similarly, we obtain

$$\|f_2\|_{\dot{K}_{q_2}^{\alpha_2,p_2}(R^d)} = 2^{-\epsilon} \left(\frac{S_d(2^{q_2(\alpha_2+\epsilon)}-1)}{q_2(\alpha_2+\epsilon)}\right)^{\frac{1}{q_2}} \left(\frac{1}{1-2^{-\epsilon p_2}}\right)^{\frac{1}{p_2}} \tag{3.9}$$

For each $i = 1, 2$. For each $x \in R^d$ which $|x| \ge 1$, let

$$S_x = \cap_{i=1}^{2}\{t \in [0,1]^n : |s_i(t)x| > 1\}.$$

From the assumption $|s_i(t_1, \ldots, t_n)| > \min\{t_1^{\beta}, \ldots, t_m^{\beta}\}$ a.e $t = (t_1, \ldots, t_n) \in [0,1]^n$, there exists a null subset E of $[0,1]^n$ so that S_x contains $\left[\frac{1}{|x|^{\frac{1}{\beta}}}, 1\right]^n \setminus E$.

$$U_{\psi,\vec{s}}^{2,n}(f_1, f_2)(x) = \int_{[0,1]^n} f_1(s_1(t)x) f_2(s_2(t)x)\psi(t)dt$$

$$= |x|^{-\alpha-\frac{d}{q}-2\epsilon} \int_{S_x} \prod_{i=1}^{2} |s_i(t)|^{-\alpha_i-\frac{d}{q_i}-\epsilon} \psi(t)dt.$$

Hence

$$\left\| U_{\psi,\vec{s}}^{2,n}(f_1,f_2) \right\|_{\dot{K}_q^{\alpha,p}(R^d)}^{p} =$$

$$= \sum_{k=1}^{\infty} 2^{k\alpha p} \left\| U_{\psi,\vec{s}}^{2,n}(f_1,f_2)\chi_k(x) \right\|_{L^q(R^d)}^{p}$$

$$= \sum_{k=1}^{\infty} 2^{k\alpha p} \left(\int_{|x|>1} \left| |x|^{-\alpha-\frac{d}{2}-2\epsilon} \chi_k(x) \int_{S_x} \prod_{i=1}^{2} |s_i(t)|^{-\alpha_i-\frac{d}{q_i}-\epsilon} \psi(t)dt \right|^q dx \right)^{\frac{p}{q}}$$

$$\geq \sum_{k=1}^{\infty} 2^{k\alpha p} \left(\int_{|x|\geq\epsilon^{-\beta}} |x|^{-q\alpha-d-2q\epsilon} \chi_k(x)dx \right)^{\frac{p}{q}} \left| \int_{[\epsilon,1]^n} \left(\prod_{i=1}^{2} |s_i(t)|^{-\alpha_i-\frac{d}{q_i}-\epsilon} \right) \psi(t)dt \right|^p.$$

Since $1 < \epsilon^{-\beta} \in R$, it is easy to find a positive integer l such that $2^{l-1} \leq \epsilon^{-\beta} < 2^l$. Thus, we have

$$\geq \sum_{k=l+1}^{\infty} 2^{k\alpha p} S_d^{\frac{p}{q}} \left(\int_{2^{k-1}}^{2^k} r^{-(\alpha+2\epsilon)q-1} dr \right)^{\frac{p}{q}} \left| \int_{[\epsilon,1]^n} \left(\prod_{i=1}^{2} |s_i(t)|^{-\alpha_i-\frac{d}{q_i}-\epsilon} \right) \psi(t)dt \right|^p$$

$$= \sum_{k=l+1}^{\infty} 2^{k\alpha p} S_d^{\frac{p}{q}} 2^{-kp(\alpha+2\epsilon)} \left(\frac{2^{(\alpha+2\epsilon)q} - 1}{q(\alpha+2\epsilon)} \right)^{\frac{p}{q}} \left| \int_{[\epsilon,1]^n} \left(\prod_{i=1}^{2} |s_i(t)|^{-\alpha_i-\frac{d}{q_i}-\epsilon} \right) \psi(t)dt \right|^p$$

$$= S_d^{\frac{p}{q}} \left(\frac{2^{(\alpha+2\epsilon)q} - 1}{q(\alpha+2\epsilon)} \right)^{\frac{p}{q}} \sum_{k=l+1}^{\infty} 2^{-2\epsilon kp} \left| \int_{[\epsilon,1]^n} \left(\prod_{i=1}^{2} |s_i(t)|^{-\alpha_i-\frac{d}{q_i}-\epsilon} \right) \psi(t)dt \right|^p$$

$$= S_d^{\frac{p}{q}} \left(\frac{2^{(\alpha+2\epsilon)q} - 1}{q(\alpha+2\epsilon)} \right)^{\frac{p}{q}} \frac{2^{-2\epsilon(l+1)p}}{1-2^{-2\epsilon p}} \left| \int_{[\epsilon,1]^n} \left(\prod_{i=1}^{2} |s_i(t)|^{-\alpha_i-\frac{d}{q_i}-\epsilon} \right) \psi(t)dt \right|^p$$

Since $q_1 = q_2 = 2q, \alpha_1 = \alpha_2 = \frac{1}{2}\alpha$ and $\frac{1}{p} = \frac{1}{p_1} + \frac{1}{p_2}$, $p_1 = p_2 = 2p$, we have

$$||U_{\psi,\vec{s}}^{2,n}(f_1,f_2)||_{\dot{K}_q^{\alpha,p}(R^d)}$$

$$\geq 2^{-2\epsilon(l+1)} S_d^{\frac{1}{q}} \left(\frac{2^{(\alpha+2\epsilon)q} - 1}{q(\alpha+2\epsilon)} \right)^{\frac{1}{q}} \left(\frac{1}{1-2^{-2\epsilon p}} \right)^{\frac{1}{p}} \left| \int_{[\epsilon,1]^n} \left(\prod_{i=1}^{2} |s_i(t)|^{-\alpha_i-\frac{d}{q_i}-\epsilon} \right) \psi(t)dt \right|$$

$$\geq \epsilon^{2\epsilon\beta}\|f_1\|_{\dot{K}_{q_1}^{\alpha_1,p_1}(R^d)}\|f_2\|_{\dot{K}_{q_2}^{\alpha_2,p_2}(R^d)}\left|\int_{[\epsilon,1]^n}\left(\prod_{i=1}^{2}|s_i(t)|^{-\alpha_i-\frac{d}{q_i}-\epsilon}\right)\psi(t)dt\right|$$

This implies that

$$||U_{\psi,\vec{s}}^{2,n}||_{\dot{K}_{q_1}^{\alpha_1,p_1}(R^d)\times\dot{K}_{q_2}^{\alpha_2,p_2}(R^d)\to\dot{K}_{q}^{\alpha,p}(R^d)} \geq \epsilon^{2\epsilon\beta}\left|\int_{[\epsilon,1]^n}\left(\prod_{i=1}^{2}|s_i(t)|^{-\alpha_i-\frac{d}{q_i}-\epsilon}\right)\psi(t)dt\right| \quad (3.10)$$

Notice that $\left|s_{i(t)}\right|^{-\epsilon} \leq \min\{t_1,\dots,t_n\}^{-\epsilon\beta} \geq \epsilon^{-\epsilon\beta} \to 1 \; when \; \epsilon \to 0^+$

Thus, letting $\epsilon \to 0^+$ and by Fatou's lemma we obtain

$$||U_{\psi,\vec{s}}^{2,n}||_{\dot{K}_{q_1}^{\alpha_1,p_1}(R^d)\times\dot{K}_{q_2}^{\alpha_2,p_2}(R^d)\to\dot{K}_{q}^{\alpha,p}(R^d)} \geq \left|\int_{[0,1]^n}\left(\prod_{i=1}^{2}|s_i(t)|^{-\alpha_i-\frac{d}{q_i}}\right)\psi(t)dt\right|$$

$$||U_{\psi,\vec{s}}^{2,n}||_{\dot{K}_{q_1}^{\alpha_1,p_1}(R^d)\times\dot{K}_{q_2}^{\alpha_2,p_2}(R^d)\to\dot{K}_{q}^{\alpha,p}(R^d)} \geq \int_{[0,1]^n}\left(\prod_{i=1}^{2}|s_i(t)|^{-\alpha_i-\frac{d}{q_i}}\right)\psi(t)dt \quad (3.11)$$

Thus, (3.1) holds.

The proof of the theorem 3.2 is general of the proof of theorem 3.1, so I omit it.

4. BOUNDEDNESS OF $U_{\psi,\vec{s}}^{2,n}$ ON THE PRODUCT OF MORREY-HERZ SPACES

This section will be devoted to state and prove results on the boundedness of $U_{\psi,\vec{s}}^{2,n}, U_{\psi,\vec{s}}^{m,n}$ on the product of Morrey-Herz spaces.

Theorem 4.1. Let $\alpha_1,\alpha_2 \in R, \lambda,\lambda_i > 0, 1 < p,p_i,q,q_i < \infty, i = 1,2$ and $\alpha_1+\alpha_2 = \alpha$, $\frac{1}{q_1}+\frac{1}{q_2}=\frac{1}{q};\frac{1}{p_1}+\frac{1}{p_2}=\frac{1}{p};\ \lambda_1+\lambda_2=\lambda$. Then, $U_{\psi,\vec{s}}^{2,n}$ is bounded from $M\dot{K}_{p_1,q_1}^{\alpha_1,\lambda_1}(R^d)\times M\dot{K}_{p_2,q_2}^{\alpha_2,\lambda_2}(R^d)$ to $M\dot{K}_{p,q}^{\alpha,\lambda}(R^d)$ if

$$\int_{[0,1]^n}\left(\prod_{i=1}^{2}|s_i(t)|^{-\alpha_i-\frac{d}{q_i}+\lambda_i}\right)\psi(t)dt < \infty \quad (4.1)$$

Conversely, if $\alpha_1=\alpha_2=\frac{1}{2}\alpha, \lambda_1=\lambda_2=\frac{1}{2}\lambda, q_i = 2q, p_i = 2p, i = 1,2$ and $U_{\psi,\vec{s}}^{2,n}$ is bounded from $M\dot{K}_{p_1,q_1}^{\alpha_1,\lambda_1}(R^d)\times M\dot{K}_{p_2,q_2}^{\alpha_2,\lambda_2}(R^d)$ to $M\dot{K}_{p,q}^{\alpha,\lambda}(R^d)$ then (4.1) holds.

Moreover, in this case, one has

$$||U_{\psi,\vec{s}}^{2,n}||_{M\dot{K}_{p_1,q_1}^{\alpha_1,\lambda_1}(R^d)\times M\dot{K}_{p_2,q_2}^{\alpha_2,\lambda_2}(R^d)\to M\dot{K}_{p,q}^{\alpha,\lambda}(R^d)} \simeq \int_{[0,1]^n}\left(\prod_{i=1}^{2}|s_i(t)|^{-\alpha_i-\frac{d}{q_i}+\lambda_i}\right)\psi(t)dt \quad (4.2)$$

In general case, we have the following theorem:

Theorem 4.2. Let $\alpha_1, \alpha_2, \dots, \alpha_m \in R, \lambda, \lambda_i > 0, 1 < p, p_i, q, q_i < \infty, i = 1,2, \dots, m$ and $\alpha_1 + \alpha_2 + \cdots + \alpha_m = \alpha$, $\frac{1}{q_1} + \frac{1}{q_2} + \cdots + \frac{1}{q_m} = \frac{1}{q}; \frac{1}{p_1} + \frac{1}{p_2} + \cdots + \frac{1}{p_m} = \frac{1}{p}$; $\lambda_1 + \lambda_2 + \cdots + \lambda_m = \lambda$. Then, $U_{\psi,\vec{s}}^{m,n}$ is bounded from $M\dot{K}_{p_1,q_1}^{\alpha_1,\lambda_1}(R^d) \times M\dot{K}_{p_2,q_2}^{\alpha_2,\lambda_2}(R^d) \times \dots \times M\dot{K}_{p_m,q_m}^{\alpha_m,\lambda_m}(R^d)$ to $M\dot{K}_{p,q}^{\alpha,\lambda}(R^d)$ if

$$\int_{[0,1]^n} \left(\prod_{i=1}^m |s_i(t)|^{-\alpha_i - \frac{d}{q_i} + \lambda_i} \right) \psi(t) dt < \infty \tag{4.3}$$

Conversely, if $\alpha_1 = \alpha_2 = \cdots = \alpha_m = \frac{1}{m}\alpha, \lambda_1 = \lambda_2 = \cdots = \lambda_m = \frac{1}{m}\lambda, q_i = mq, p_i = mp, i = 1,2, \dots, m$ and $U_{\psi,\vec{s}}^{m,n}$ is bounded from $M\dot{K}_{p_1,q_1}^{\alpha_1,\lambda_1}(R^d) \times M\dot{K}_{p_2,q_2}^{\alpha_2,\lambda_2}(R^d) \times \dots \times M\dot{K}_{p_m,q_m}^{\alpha_m,\lambda_m}(R^d)$ to $M\dot{K}_{p,q}^{\alpha,\lambda}(R^d)$ then (4.3) holds.

Moreover, in this case, one has

$$\|U_{\psi,\vec{s}}^{m,n}\|_{M\dot{K}_{p_1,q_1}^{\alpha_1,\lambda_1}(R^d) \times M\dot{K}_{p_2,q_2}^{\alpha_2,\lambda_2}(R^d) \times \dots \times M\dot{K}_{p_m,q_m}^{\alpha_m,\lambda_m}(R^d) \to M\dot{K}_{p,q}^{\alpha,\lambda}(R^d)} \simeq \int_{[0,1]^n} \left(\prod_{i=1}^m |s_i(t)|^{-\alpha_i - \frac{d}{q_i} + \lambda_i} \right) \psi(t) dt \tag{4.4}$$

Proof of Theorem 4.1. From the proof of Theorem 3.1, we know that

$$\|U_{\psi,\vec{s}}^{2,n}(f_1, f_2)\chi_k\|_{L^q(R^d)} \le \int_{[0,1]^n} (\|f_1\chi_{k+m-1}\|_{L^{q_1}} + \|f_1\chi_{k+m}\|_{L^{q_1}}) \times$$

$$\times (\|f_2\chi_{k+l-1}\|_{L^{q_2}} + \|f_2\chi_{k+l}\|_{L^{q_2}}) \left(\prod_{i=1}^2 |s_i(t)|^{-\frac{d}{q_i}} \right) \psi(t) dt. \tag{4.3}$$

For $\frac{1}{p_1} + \frac{1}{p_2} = \frac{1}{p}, \alpha_1 + \alpha_2 = \alpha, \lambda = \lambda_1 + \lambda_2$, by Hölder inequality and Minkowski inequality give $\left\| U_{\psi,\vec{s}}^{2,n}(f_1, f_2) \right\|_{M\dot{K}_{p,q}^{\alpha,\lambda}(R^d)}$

$$= \sup_{k_o \in Z} 2^{-k_o\lambda} \left(\sum_{k=-\infty}^{k_o} 2^{k\alpha p} \left\| U_{\psi,\vec{s}}^{2,n}(f_1, f_2)\chi_k \right\|_{L^q}^p \right)^{\frac{1}{p}}$$

$$\le \sup_{k_o \in Z} 2^{-k_o\lambda} \left(\sum_{k=-\infty}^{k_o} 2^{k\alpha p} \left(\int_{[0,1]^n} (\|f_1\chi_{k+m-1}\|_{L^{q_1}} + \|f_1\chi_{k+m}\|_{L^{q_1}}) \right.\right.$$

$$\left.\left. \times (\|f_2\chi_{k+l-1}\|_{L^{q_2}} + \|f_2\chi_{k+l}\|_{L^{q_2}}) \times \left(\prod_{i=1}^2 |s_i(t)|^{-\frac{d}{q_i}} \right) \psi(t) dt \right)^p \right)^{\frac{1}{p}}$$

$$\leq \sup_{k_o\in Z} 2^{-k_o\lambda} \int_{[0,1]^n} \left(\sum_{k=-\infty}^{k_o} 2^{k\alpha p} (\|f_1\chi_{k+m-1}\|_{L^{q_1}} + \|f_1\chi_{k+m}\|_{L^{q_1}})^p \right.$$

$$\left. \times (\|f_2\chi_{k+l-1}\|_{L^{q_2}} + \|f_2\chi_{k+l}\|_{L^{q_2}})^p \right)^{\frac{1}{p}} \left(\prod_{i=1}^{2} |s_i(t)|^{-\frac{d}{q_i}} \right) \psi(t)dt$$

$$\leq \sup_{k_o\in Z} 2^{-k_o\lambda} \int_{[0,1]^n} \left(\sum_{k=-\infty}^{k_o} 2^{k\alpha_1 p_1} (\|f_1\chi_{k+m-1}\|_{L^{q_1}} + \|f_1\chi_{k+m}\|_{L^{q_1}})^{p_1} \right)^{\frac{1}{p_1}}$$

$$\times \left(\sum_{k=-\infty}^{k_o} 2^{k\alpha_2 p_2} (\|f_2\chi_{k+l-1}\|_{L^{q_2}} \right.$$

$$\left. + \|f_2\chi_{k+l}\|_{L^{q_2}})^{p_2} \right)^{\frac{1}{p_2}} \left(\prod_{i=1}^{2} |s_i(t)|^{-\frac{d}{q_i}} \right) \psi(t)dt$$

$$\leq \sup_{k_o\in Z} 2^{-k_o\lambda_1} \int_{[0,1]^n} \left\{ \left(\sum_{k=-\infty}^{k_o} 2^{k\alpha_1 p_1} \|f_1\chi_{k+m-1}\|_{L^{q_1}}^{p_1} \right)^{\frac{1}{p_1}} \right.$$

$$\left. + \left(\sum_{k=-\infty}^{k_o} 2^{k\alpha_1 p_1} \|f_1\chi_{k+m}\|_{L^{q_1}}^{p_1} \right)^{\frac{1}{p_1}} \right\} \times$$

$$\times \sup_{k_o\in Z} 2^{-k_o\lambda_2} \int_{[0,1]^n} \left\{ \left(\sum_{k=-\infty}^{k_o} 2^{k\alpha_2 p_2} \|f_1\chi_{k+m-1}\|_{L^{q_2}}^{p_2} \right)^{\frac{1}{p_2}} \right.$$

$$\left. + \left(\sum_{k=-\infty}^{k_o} 2^{k\alpha_2 p_2} \|f_1\chi_{k+m}\|_{L^{q_2}}^{p_2} \right)^{\frac{1}{p_2}} \right\} \times \left(\prod_{i=1}^{2} |s_i(t)|^{-\frac{d}{q_i}} \right) \psi(t)dt$$

$$\leq \|f_1\|_{M\dot{K}_{p_1,q_1}^{\alpha_1,\lambda_1}(R^d)} \|f_2\|_{M\dot{K}_{p_2,q_2}^{\alpha_2,\lambda_2}(R^d)} \int_{[0,1]^n} \left(2^{-(m-1)\alpha_1} + 2^{-m\alpha_1}\right)\left(2^{-(l-1)\alpha_2} + 2^{-l\alpha_2}\right) \times$$

$$\left(\prod_{i=1}^{2} |s_i(t)|^{-\frac{d}{q_i}+\lambda_i} \right) \psi(t)dt$$

$$\leq \|f_1\|_{M\dot{K}_{p_1,q_1}^{\alpha_1,\lambda_1}(R^d)} \|f_2\|_{M\dot{K}_{p_2,q_2}^{\alpha_2,\lambda_2}(R^d)} \int_{[0,1]^n} \left(\prod_{i=1}^{2} |s_i(t)|^{-\alpha_i-\frac{d}{q_i}+\lambda_i} \right) \psi(t)dt$$

So

$$\left\|U_{\psi,\vec{s}}^{2,n}\right\|_{M\dot{K}_{p,q}^{\alpha,\lambda}(R^d)} \leq$$

$$\|f_1\|_{M\dot{K}_{p_1,q_1}^{\alpha_1,\lambda_1}(R^d)}\|f_2\|_{M\dot{K}_{p_2,q_2}^{\alpha_2,\lambda_2}(R^d)} \int_{[0,1]^n}\left(\prod_{i=1}^{2}|s_i(t)|^{-\alpha_i-\frac{d}{q_i}+\lambda_i}\right)\psi(t)dt \tag{4.4}$$

It means that $U_{\psi,\vec{s}}^{2,n}$ is bounded from $M\dot{K}_{p_1,q_1}^{\alpha_1,\lambda_1}(R^d) \times M\dot{K}_{p_2,q_2}^{\alpha_2,\lambda_2}(R^d)$ to $M\dot{K}_{p,q}^{\alpha,\lambda}(R^d)$

On the other hand, we suppose that $U_{\psi,\vec{s}}^{2,n}$ is bounded from $M\dot{K}_{p_1,q_1}^{\alpha_1,\lambda_1}(R^d) \times M\dot{K}_{p_2,q_2}^{\alpha_2,\lambda_2}(R^d)$ to $M\dot{K}_{p,q}^{\alpha,\lambda}(R^d) and\ U_{\psi,\vec{s}}^{2,n}$ has the operator norm

$$\left\|U_{\psi,\vec{s}}^{2,n}\right\|_{M\dot{K}_{p_1,q_1}^{\alpha_1,\lambda_1}(R^d)\times M\dot{K}_{p_2,q_2}^{\alpha_2,\lambda_2}(R^d)\to M\dot{K}_{p,q}^{\alpha,\lambda}(R^d)}.$$

Let $$f_1(x) = |x|^{-\alpha_1-\frac{d}{q_1}+\lambda_1},\ x \in R^d \tag{4.5}$$

$$f_2(x) = |x|^{-\alpha_2-\frac{d}{q_2}+\lambda_2},\ x \in R^d \tag{4.6}$$

$$\|f_1\chi_k\|_{L^{q_1}} = \left(\int_{2^{k-1}<|x|\leq 2^k}|x|^{\left(-\alpha_1-\frac{d}{q_1}+\lambda_1\right)}dx\right)^{\frac{1}{q_1}} \tag{4.7}$$

$$= 2^{-k(\alpha_1-\lambda_1)}\left(\frac{S_d\left(2^{(\alpha_1-\lambda_1)q_1}-1\right)}{q_1(\alpha_1-\lambda_1)}\right)^{\frac{1}{q_1}}$$

where $S_d = \frac{2\pi^{\frac{d}{2}}}{\Gamma(\frac{d}{2})}$.

A simple computation gives

$$\|f_1\|_{M\dot{K}_{p_1,q_1}^{\alpha_1,\lambda_1}(R^d)} = 2^{\lambda_1}\left(\frac{S_d(2^{(\alpha_1-\lambda_1)q_1}-1)}{q_1(\alpha_1-\lambda_1)}\right)^{\frac{1}{q_1}}\left(\frac{1}{2^{\alpha_1 p_1}-1}\right)^{\frac{1}{p_1}} \tag{4.8}$$

Similarly, we obtain

$$\|f_2\|_{M\dot{K}_{p_2,q_2}^{\alpha_2,\lambda_2}(R^d)} = 2^{\lambda_2}\left(\frac{S_d(2^{(\alpha_2-\lambda_2)q_2}-1)}{q_2(\alpha_2-\lambda_2)}\right)^{\frac{1}{q_2}}\left(\frac{1}{2^{\alpha_2 p_2}-1}\right)^{\frac{1}{p_2}} \tag{4.9}$$

For $\alpha=\alpha_1+\alpha_2$, $\lambda = \lambda_1 + \lambda_2$ and $\frac{1}{q} = \frac{1}{q_1} + \frac{1}{q_2}$, we have

$$U_{\psi,\vec{s}}^{2,n}(f_1,f_2)(x) = \int_{[0,1]^n} f_1(s_1(t)x)f_2(s_2(t)x)\psi(t)dt$$

$$= |x|^{-\alpha-\frac{d}{q}+\lambda}\int_{[0,1]^n}\left(\prod_{i=1}^{2}|s_i(t)|^{-\alpha_i-\frac{d}{q_i}+\lambda_i}\right)\psi(t)dt.$$

Hence

$$\left(\left\|U^{2,n}_{\psi,\vec{s}}(f_1,f_2)\chi_k\right\|^p_{L^q}\right)$$

$$=\left(\int\limits_{R^d}\left|U^{2,n}_{\psi,\vec{s}}(f_1,f_2)(x)\right|^q\chi_k(x)dx\right)^{\frac{p}{q}}$$

$$=\left(\int\limits_{R^d}\left||x|^{-\propto-\frac{d}{q}+\lambda}\chi_k(x)\int\limits_{[0,1]^n}\left(\prod_{i=1}^{2}|s_i(t)|^{-\propto_i-\frac{d}{q_i}+\lambda_i}\right)\psi(t)dt\right|^q dx\right)^{\frac{p}{q}}$$

$$=\left(\int\limits_{2^{k-1}<|x|\le 2^k}|x|^{-q\propto-d+\lambda q}\,dx\right)^{\frac{p}{q}}\left|\int\limits_{[0,1]^n}\left(\prod_{i=1}^{2}|s_i(t)|^{-\propto_i-\frac{d}{q_i}+\lambda_i}\right)\psi(t)dt\right|^p$$

$$=2^{-k(\propto-\lambda)q}\left(\frac{S_d(2^{(\propto-\lambda)q}-1}{(\propto-\lambda)q}\right)\left|\int_{[0,1]^n}\left(\prod_{i=1}^{2}|s_i(t)|^{-\propto_i-\frac{d}{q_i}+\lambda_i}\right)\psi(t)dt\right|^p.$$

Since $\propto_1=\propto_2=\frac{1}{2}\propto, p_1=p_2=2p, q_1=q_2=2q$ and $\lambda_1+\lambda_2=\frac{1}{2}\lambda$, we have

$$\left\|U^{2,n}_{\psi,\vec{s}}(f_1,f_2)\right\|_{M\dot{K}^{\alpha,\lambda}_{p,q}(R^d)}=\sup_{k_o\in Z}2^{-k_o\lambda}\left(\sum_{k=-\infty}^{k_o}2^{k\propto p}\left\|U^{2,n}_{\psi,\vec{s}}(f_1,f_2)\chi_k\right\|^p_{L^q}\right)^{\frac{1}{p}}$$

$$=2^{\lambda}\left(\frac{S_d(2^{(\propto-\lambda)q}-1)}{q(\propto-\lambda)}\right)^{\frac{1}{q}}\left(\frac{1}{2^{\lambda p}-1}\right)^{\frac{1}{p}}\left|\int_{[0,1]^n}\left(\prod_{i=1}^{2}|s_i(t)|^{-\propto_i-\frac{d}{q_i}+\lambda_i}\right)\psi(t)dt\right| .$$

The above gives

$$\left\|U^{2,n}_{\psi,\vec{s}}\right\|_{M\dot{K}^{\alpha_1,\lambda_1}_{p_1,q_1}(R^d)\times M\dot{K}^{\alpha_2,\lambda_2}_{p_2,q_2}(R^d)\to M\dot{K}^{\alpha,\lambda}_{p,q}(R^d)}\ge\left|\int\limits_{[0,1]^n}\left(\prod_{i=1}^{2}|s_i(t)|^{-\propto_i-\frac{d}{q_i}+\lambda_i}\right)\psi(t)dt\right|$$

Since $U^{2,n}_{\psi,\vec{s}}$ is bounded from $M\dot{K}^{\alpha_1,\lambda_1}_{p_1,q_1}(R^d)\times M\dot{K}^{\alpha_2,\lambda_2}_{p_2,q_2}(R^d)$ to $M\dot{K}^{\alpha,\lambda}_{p,q}(R^d)$, we know that (4.1) holds and

$$\left\|U^{2,n}_{\psi,\vec{s}}\right\|_{M\dot{K}^{\alpha_1,\lambda_1}_{p_1,q_1}(R^d)\times M\dot{K}^{\alpha_2,\lambda_2}_{p_2,q_2}(R^d)\to M\dot{K}^{\alpha,\lambda}_{p,q}(R^d)}\simeq\left|\int\limits_{[0,1]^n}\left(\prod_{i=1}^{2}|s_i(t)|^{-\propto_i-\frac{d}{q_i}+\lambda_i}\right)\psi(t)dt\right|$$

The proof of the theorem 4.2 is general of the proof of theorem 4.1, so I omit it.

REFERENCES

1. C. Carton-Lebrun and M. Fosset (1984), "Moyennes et quotients de Taylor dans BMO", - Bull. Soc. Roy. Sci. Liége **53** (2), 85-87.
2. Y. Z. Chen and K. S. Lau (1989), "Some new classes of Hardy spaces", - J. Funct. Anal. **84**, 255-278.
3. F. Chiarenza and M. Frasca (1987), "Morrey spaces and Hardy-Littlewood maximal function", - Rend. Math. Appl. **7**, 273-279.
4. N. M. Chuong and H. D. Hung (2010), "Maximal functions and weighted norm inequalities on Local Fields", - Appl. Comput. Harmon. Anal. **29**, 272-286.
5. N. M. Chuong and H. D. Hung (2010), "A Muckenhoupt's weight problem and vector valued maximal inequalities over local fields", - P-Adic Numb. Ultrametric Anal. Appl., **2**, 305-321.
6. N. M. Chuong and H. D. Hung (2014), "Weighted L^p and weighted BMO − bounds for a new generalized weighted Hardy-Cesàro operator", - Integral Transforms Spec. Funct. **25** (9), 697-710.
7. R. R. Coifman, R. Rochberg, and G. Weiss (1976), "Factorization theorems for Hardy spaces in several variables", - Ann. of Math., **103** (2), 611-635.
8. Z. W. Fu, Z. G. Liu, and S. Z. Lu (2009), "Commutators of weighted Hardy operators on R^n", - Proc. Amer. Math. Soc. **137** (10), 3319-3328.
9. J. García-Cuerva (1989), "Hardy spaces and Beurling algebras", - J. London Math. Soc. **39** (2), 499-513.
10. H. D. Hung (2014), "P-adic weighted Hardy - Cesàro operator and an application to discrete Hardy Inequalities", - J. Math. Anal. Appl. **409**, 868-879.
11. Y. C. Kim (2009), "Carleson measures and the BMO space on the p-adic vector space", - Math. Nachr., **282**, 1278-1304.
12. Y. Komori and S. Shirai (2019), "Weighted Morrey spaces and a singular integral operator", - Math. Nachr. **282** (2), 219-231.
13. F. John and L. Nirenberg (1961), "On functions of bounded mean oscillation", - Comm. Pure and Appl. Math. **14**, 415-426.
14. C. B.Morrey (1938), "On the solutions of quasi-linear elliptic partial differential equations", - Trans. Amer.Math. Soc. **43**, 126-166.
15. K.S. Rim and J. Lee (2006), "Estimates of weighted Hardy-Littlewood averages on the p-adic vector space", - J. Math. Anal. Appl. **324**, 1470-1477.
16. J. Xiao (2001), "L^p and BMO bounds of weighted Hardy-Littlewood Averages", - J. Math. Anal. Appl. **262**, 660-666.
17. Q. Y. Wu (2012), "Boundedness for commutators of fractional p-adic Hardy operators", - J. Ineq. Appl., **2012**:293.
18. Q. Y. Wu and Z. W. Fu (2015), "Weighted p-adic Hardy operators and their commutators on p-adic central Morrey spaces", - To appear in Bull. Malays.Math.Sci.Soc.
19. Q. Y. Wu, L. Mi and Z. W. Fu (2013), "Boundedness of p-adic Hardy operattors and their commutators on p-adic central Morrey and BMO spaces", - J. Funct. Spaces Appl., 359193, 10 pages.

20. S. Gong, Z. W. Fu, B. Ma (2014), "Weighted multilinear Hardy operators on Herz type spaces", - The Sci. World. J., 420480, 10 pages.

21. J. Kuang (2010), "Weighted Morrey-Herz spaces and Applications", - Appl. Math. E-Notes, **10**, 159-166.

22. H. D. Hung, L. D. Ky (2015), "New weighted multilinear operators and commutators of Hardy-Cesàro type", - **35B(6)**, 1-15.

TOÁN TỬ ĐA TUYẾN TÍNH HARDY-CESÀRO TRÊN CÁC KHÔNG GIAN KIỂU HERZ

Tóm tắt: *Mục đích của bài báo này là nghiên cứu tính bị chặn của toán tử đa tuyến tính Hardy-Cesàro trên tích các không gian hàm kiểu Herz.*

Từ khóa: *Toán tử đa tuyến tính Hardy - Cesàro có trọng; Không g□n H□rz; Không g□n Morrey-Herz.*

APPLYING LINEAR RELATIONSHIPS IN VECTOR SPACES TO SOLVE THE PROBLEM CLASS ABOUT INCIDENCE IN PROJECTIVE SPACE

Hoang Ngoc Tuyen
Hanoi Metropolitan University

Abstract: *This article mentions some fundamental concepts and crucial results of linear algebra as well as linear combination, linear span, linear dependence, etc. in vector space and how to use them as an effective tool to determine "the incidence" to affirm the relationships between m-planes in projective space… in projective geometry.*

Keywords: *space, m-plane, linear combination, linear span…*

Email: hntuyen@hnmu.vn
Received 28 March 2019
Accepted for publication 25 May 2019

1. INTRODUCTION

The initial object of Linear Algebra is solving and arguing linear equations. However, in order to have a thorough understanding of the condition for solution, as well as the family of solution, one gives the concept of vector space and this concept becomes the cross-cutting theme of linear algebra. Vector space, then popularized in all areas of Mathematics and has important applications in the fields of science such as Physics, Mechanics ...

One is particularly interested in a model of concept, which is the n-dimensional arithmetic vector space. In this model, each vector is identical to an ordered number set of n components:

$$\alpha \in K^n \leftrightarrow \alpha = (x_1, ...x_n).$$

Linear combination, linear dependence, Vector space generated by vector system ... can be used as a tool to solve a class of problems to confirm the relationship between points, lines, m - plane in $P^n = (X, \pi, V^{n+1})$

2. SOME PREPARED KNOWLEDGE

We always assume K is a field

2.1. Vector space and linear relationships

2.1.1. Vector space

Set M is called a vector space on K if it is equipped with two operations:

(1) Addition vector:

$$+: \begin{array}{l} V \times V \to V \\ (\alpha, \beta) \mapsto \alpha + \beta \end{array}$$

(2) Scalar multiplication:

$$\bullet : K \times V \to V$$
$$(a, \alpha) \mapsto a\alpha$$

These operations satisfy 8-axioms system so that:

- V is the Abel group for summation

- Scalar multiplication has a properties of distribution for scalar summation, distribution for vector summation and has the property of an "impact"

- In addition, the scarlar mulitpication of vectors is standardized.

A vector space on K is also called a K-space vector.

Example:

Call $K^n = \{(x_1,...,x_n) / x_i \in K\}$ a vector space with the two following relations:

$$(x_1,...,x_{n+1}) \sim (y_1,...,y_{n+1}) \Leftrightarrow \exists(\lambda \neq 0) \in R : x_i = \lambda y_i$$
$$a(x_1,...,x_n) = (ax_1,...,ax_n); a \in K$$

K^n is called the n-dimensional arithmetic vector space if K is a numerical field. K^n has many applications in different fields of sciences, especially when we use linear relationships in K^n to analyze the structure of the projective space.

2.1.2. Subspace of K^n

Definition:

A non-empty subset L of K^n is called the subspace of K^n if it is closed to vector summation and scalar multiplication.

The term subspace includes two aspects: first, L is a part of K^n; second, operations in L are the operations that apply to all vectors of K^n

The word definition is easy to deduce:

- All subspace L contains vectors – zero $O_n = (0,...,0)$

Indeed, $\forall \alpha \in L$ We have: $O_n = 0\alpha \in L$

- All vectors $\alpha \in L$, Its opposite vector also belongs to L

Indeed, $-\alpha = (-1)\alpha \in L$

Example: $L_0 = \{O_n\}, L_1 = K, L_2 = K^2, L_3 = K^3$ are subspaces of K^n $(n \geq 3)$

2.2. The linear relationship

2.2.1. Linear combination and linear representation

In space K^n (fixed n), let m vector: $\alpha_1,...,\alpha_m$ (1)

Take a set of any m numbers $a_1,...,a_m$ and set up the sum: $a_1\alpha_1 + ... + a_m\alpha_m$ (2)

Definition 1:

Each sum (2) is called a linear combination of vectors in the system (1). The numbers α_i (i = 1, ..., m) are called coefficients of that linear combination.

From the vectors of the system (1), we can create a multitude of linear combinations (each set of coefficients $a_1,...,a_m$ corresponds to a linear combination of them) and each linear combination of System (1) is an n-dimensional vector.

A set of all linear combinations of given n-dimensional vectors $\alpha_1,...,\alpha_m$ called linear closures of the $\alpha_1,...,\alpha_m$ vectors

We see now:

The sum of two linear combinations of n-dimensional vectors $\alpha_1,...,\alpha_m$ is a linear combination of those vectors:

$$(a_1\alpha_1 + ... + a_m\alpha_m) + (b_1\alpha_1 + ... + b_m\alpha_m)$$
$$= (a_1 + b_1)\alpha_1 + ... + (a_m + b_m)\alpha_m$$

- The product of any linear combination of dimensional vectors $\alpha_1,...,\alpha_m$ with a number b is also a linear combination of the vectors:

The above two comments show:

$$b(a_1\alpha_1 + ... + a_m\alpha_m) = (ba_1)\alpha_1 + ... + (ba_m)\alpha_m$$

Theorem:

A set of all the linear combinations of the given vector n-dimensions $\alpha_1,...,\alpha_m$ is a subspace of K^n space.

If symbol S = ($\alpha_1,...,\alpha_m$), space of linear combinations of S denotes L_S or $\langle S \rangle$

$L_S = \langle S \rangle = \{a_1\alpha_1 + ... + a_m\alpha_m \,/\, a_i \in K\}$ is also called space generated by S (or S is the linear span of space L_S)

Definition 2:

We say vector α denotes linearly through vectors $\alpha_1,...,\alpha_m$ If and only if there is a linear combination of $\alpha_1,...,\alpha_m$ with vector α. That is, there are numbers $\alpha_1,...,\alpha_m$ such that:

$$\alpha = a_1\alpha_1 + ... + a_m\alpha_m$$

In particular, if vector α represents linearly through a vector β, ie $\alpha = a\beta$ (fixed number a), we say α and β are proportional to each other.

Example:

With $\alpha_1,...,\alpha_m$ any n-dimensional vectors, there are always:

$$O_n = 0\alpha_1 + ... + 0\alpha_m$$

The linear combination in the right side (All coefficients equal to 0) is called trivial linear combination (or trivial constraint in the mechanical sense) of vectors $\alpha_1,...,\alpha_m$.

Thus:

- In zero vector space O_n represent linearly through any system (at least by trivial linear combination)
- In addition to O_n other vectors of space have or do not have represent linearity through the vector $\alpha_1,...,\alpha_m$ system.
- If all vectors of space are represented by the system $\alpha_1,...,\alpha_m$, then this system is called the linear span of space.

2.2.2. The linear dependence

Let the system include m n-dimensional vectors: $\alpha_1,...,\alpha_m$ (1)

When considering the relationship between the vectors, we call them an vector system. The term "vector system" is synonymous with "Set of vector" if the system does not have any two vectors are equal.

Definition 1:

We say vector system (1) is linearly dependent if and only if m number $a_1,...,a_m$ not equal to 0 at the same time so that:

$$a_1\alpha_1 + ... + a_m\alpha_m = O_n \quad (3)$$

Conversely, if the equation (3) is satisfied only when $a_1 = ... = a_m = 0$ then we say that system (1) is linearly independent.

The concept of linear dependence of an vector system can be viewed from the perspective of linear representation of the zero vector system O_n through the vectors of that system.

As mentioned, zero vector represent linearity through any system (at least by mediocre linear combination). The question is: In addition to the trivial linear combination of vectors (1), is there any other linear combinations by O_n vector?

The answer is:

- If so, the system (1) is linearly dependent
- If there is no, ie the mediocre linear combination is the only linear combination equal to O_n, then the system (1) is linearly independent

From concepts: linear representation of a vector through a system and linear independence of the vector system, if S = ($\alpha_1,...,\alpha_m$) is a linear independent vector set and vector α represents linearly through S, then representation is unique.

Moreover, S is linearly independent if and only if S has a vector that is a linear combination of other vectors.

Difinition 2:

The vector set S = ($\alpha_1,...,\alpha_n$) of the K^n space is called the basis of K^n if S is a linear independent linear span in K^n.

Example:

Episode $S = (e_1(1,0,0); e_2(0,1,0); e_3(0,0,1))$ is a base in $K^3 = \{(x_1, x_2, x_3) / x_i \in K\}$

Indeed:

- $(x_1, x_2, x_3) = x_1e_1 + x_2e_2 + x_3e_3$ So S is the linear span.
- Besides: $a_1(1,0,0) + a_2(0,1,0) + a_3(0,0,1) = O_n \Leftrightarrow a_1 = a_2 = a_3 = 0$.

Show that, S is linearly independent

We can easily see:

- Every other space with trivial space has many base. But the force of the base is equal. For the finite linear span, number of vectors in each facility called dimensional numbers (or dimensional), which is the index (integer positive) measured "magnitude" of space. For example, in addition to the aforementioned S facility (also called a natural basis), set $S' = (\alpha_1(1,1,0); \alpha_2(1,0,1); \alpha_3(0,1,1))$ also forms an nternal base in K^3 and dim(K^3) = 3.

- The following statements for an S vector system are equivalent:

S is a linear span and linear independent $\Leftrightarrow$ S is the minimum linear span $\Leftrightarrow$ S is the maximum linear independent system.

The above statements are different but have the same assertion: Episode S is the basis in K^n. Another question arises: With such statements, what is the nature of the concept of "Base"?

Answer: All vectors of space denote sole through S!

That is, if S = ($\alpha_1,...,\alpha_n$) is the base, each vector $\alpha \in K^n$ corresponds to a unique set of numbers $(x_1,...,x_n)$ satisfying the expression:

$$\alpha = x_1\alpha_1 + ... + x_n\alpha_n \quad (4)$$

Thence, the concept of vector coordinates is stated as follows:

Difinition 3:

The set of numbers $(x_1,...,x_n)$ satisfying the system (4) is called the coordinates of the vector α in base S

In the above example:

$$\alpha = x_1e_1 + x_2e_2 + x_3e_3 \Leftrightarrow \alpha = (x_1, x_2, x_3) \mid (S)$$

3. PROJECTIVE SPACE

3.1. Difinitions

Suppose V^{n+1} is the vector space (n + 1) - dimensional $(n \geq 0)$ on field K, arbitrary set $(X \neq \Phi)$. We symbol $\left[V^{n+1}\right]$ as a set of one-dimensional sub spaces of V^{n+1}, meaning that each element of $\left[V^{n+1}\right]$ is a one-dimensional subspace V^1 of V^{n+1}. If there are bijection

At that time the triplet $\mathrm{P^n = (X, \pi, V^{n+1})}$ is called a n-dimensional projective space associated with V^{n+1} and is denoted by: P^n

Depending on V^{n+1} is a real or complex vector space, we have P^n as real or complex projective space.

In this article, only the actual projective space is mentioned

Thus, each point projective $A \in P^n : A = \pi\left[V^1\right]; V^1 = \left\langle \alpha \neq O_{n+1} \right\rangle$.

If $V^{m+1} \subset V^{n+1} (0 \leq m \leq n)$ then set $\left[V^{m+1}\right] \subset X$ is m – plane projective of P^n

Therefore:

- 0 - plane is also called point
- 1 - plane is also called line
- (n-1) - plane is also called hyperplane

Suppose $X' = \pi\left[V^{m+1}\right]$ is m - plane, then the bijection $\pi' : \left[V^{m+1}\right] \to X'$ induced by π. That is: $\pi' = \pi / \left[V^{m+1}\right]$. Then (X', π', V^{m+1}) is also m-dimensional projections space, denoted by P^m. We have: $P^m = (X', \pi', V^{m+1})$

3.2. Models of projective space

3.2.1. Arithmetic model

Consider an ordered real number set of n numbers (a, b, c ...) in which at least one number is different from 0. Two sets of numbers

$$(x_1, ..., x_{n+1}) \sim (y_1, ..., y_{n+1}) \Leftrightarrow \exists (\lambda \neq 0) \in \mathbb{R} : x_i = \lambda y_i \quad ; \quad i = 1, ..., n+1$$

The set of numbers mentioned above will be divided into equivalent classes. We call X the above set of equivalence classes.

$\mathrm{V^{n+1}}$ is the (n + 1) - dimensional vector space, on which the base (S) has been selected. Bijection π is defined as follows:

$$\pi : \left[V^{n+1}\right] \to X$$

Suppose $V^1 \subset V^{n+1}; V^1 = \left\langle \vec{a} \neq O_{n+1} \right\rangle$ and $\vec{a} = (x_1, ..., x_{n+1}) \,|\, \mathrm{S}$. Then $\pi(V^1)$ is the equivalent class represented by $(x_1, ..., x_{n+1})$. Thus (X, π, V^{n+1}) is the projective space called the arithmetic model of P^n

3.2.2. Model bundles

In an afin space A^{n+1} formation of vector space V^{n+1} select an arbitrary O point. Let X be a straight line of center O. If V^1 is a one-dimensional subspace of V^{n+1} then $\pi(V^1)$ is a straight line.

We have bijection:

Then (X,π,V^{n+1}) is called *a bundle model of n-dimensional projective space*. In this model:

- Each line of the bundle represents a point (0 - plane) projective.
- Each afin plane defined by two distinct lines of a bundle denotes for a straight line (1 - plane) projective,
- Each projective plane (2 - plane) is represented by three straight lines of the center of center O that are not in the same afin plane.

Point C is located on the "projective straight line AB". Above "ABD projective plane" with the "projective straight line AB, BD, AD". From this model, the set of projecting points belongs to the same projective line as a "closed" set. Point C is in line AB, if C moves in the direction from A to B and does not change direction, after passing B, it will return to the old position (Figure 3.2.2). That is the difference between straight lines and straight lines afin projective. From the closed nature of the straight lines AB, BD, AD we can imagine the closure of the "ABC plane".

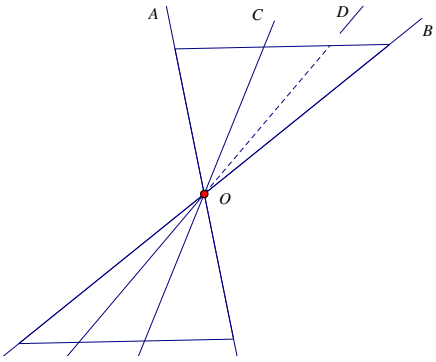

Hình 3.2.1

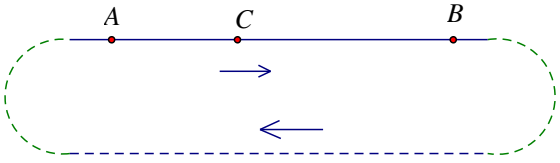

Hình 3.2.2

3.2.3. The afin model after adding endless elements

Let A^{n+1} be the (n + 1) - dimensional afin space associated with vector space V^{n+1}, which is a hyperplane has direction of $V^n \subset V^{n+1}$.We consider the sets:

$$\overline{A}^n = A^n \cup \left[V^n\right]$$

Bijection $\pi : \left[V^{n+1}\right] \to \overline{A}^n$ Defined as follows:

Let the fixed point O in A^{n+1} not belong to A^n. Suppose $V^1 \subset V^{n+1}$

- If $V^1 \not\subset V^n$ then there is only M point, $M \in A^n : \overrightarrow{OM} \in V^1$

We put $\pi(V^1) = M$

- If $V^1 \subset V^n$ we put $\pi(V^1) = M_\infty$ (M_∞ is meeting poit of parallel lines in A^n with the same V^1 direction, often called infinite point)

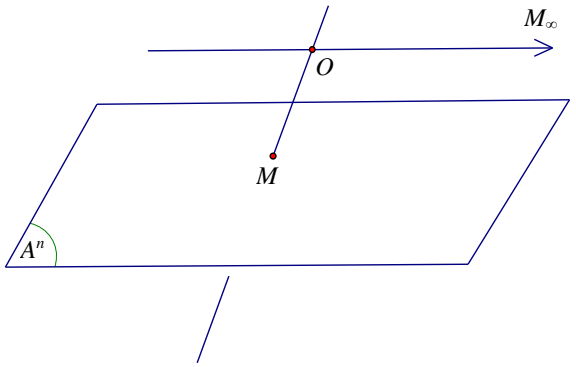

Fig 3.2.3

Thus, π is a 1-1 correspondence between the set of straight lines belonging to bundle the center O with the points of $\overline{A}^n$. So we have n-dimensional projective space $(\overline{A}^n, \pi, V^{n+1})$, called an afin model with additional infinite elements.

3.3. Projective coordinates and projective goal

3.3.1. Vector represents a point

As mentioned in (**3.1**). $P^n = (X, \pi, V^{n+1})$, in V^{n+1} each vector $\alpha \neq O_{n+1}$ will produce a subspace $V^1 = \langle \alpha \rangle$ and $\pi(V^1) = A$. Then, vector α is called vector representing for A point. With number $k \neq 0$: $V^1 = \langle \alpha \rangle = \langle k\alpha \rangle$, Thus, each projecting point has many representative vectors, α and β the same represents for A if and only if $\alpha = k\beta$

A system consists r of points $(M_1, ..., M_r) \subset P^n$ is called independent if their represent vector system is independent of V^{n+1}. Như vậy:

- Independent point system $(M_1, ..., M_r) \subset P^n$ identify a $(r-1)$ - plane
- In P^n, want an independent points r: then $r \leq n+1$

Suppose in V^{n+1} chose a facility $(S) = (e_1, ..., e_{n+1})$, $\alpha = (x_1, ..., x_{n+1}) \,|\, (S)$. Then, the coordinates of $A = (x_1, ..., x_{n+1})$ for establishments (S).

With fixed (S), in P^n we call A_i are the points that receive the vectors $e_i; i = 1, ..., n+1$ is representative.

We have: $A_1 = (1,0,...,0,0)$

……

$A_{n+1} = (0,0,...,0,1)$

Point E, there is vector representing e, in it $e = e_1 + ... + e_{n+1}$ and $E = (1,1,...,1,1)$

A set of n + 2 points in order is constructed as above, called a projective target $(A_i; E), i = 1,...,n+1$

- A_i is called the ith peak of the target
- E is the unit point

If $\alpha = (x_1,...,x_{n+1}) | (S)$, then $A = (x_1,...,x_{n+1})$ for the goal $(A_i; E)$. It should be noted that, in n + 2 points of the target $(A_i; E)$, Any n + 1 points are independent.

Example:

On the P^1 projective straight line, the goal is a set of three distinct points of alignment (A_1, A_2, E). The coordinates of any X point belong to P^1: $X = (x_1, x_2)$ for the given goal.

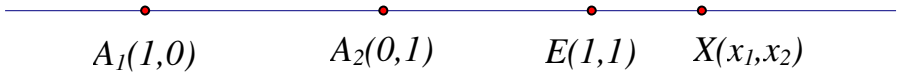

Fig 3.3.1

In the P^2 projective plane:

projective goal is a set of four points, in which any three points are not along a straight line (A_1, A_2, A_3, E).

With any X point of P^2, We have its coordinates for the given target: $X = (x_1, x_2, x_3)$

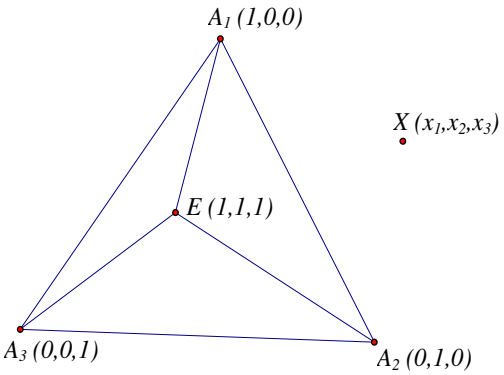

Fig 3.3.2

Theorem:

In $P^n = (X, \pi, V^{n+1})$, each goal $(A_i; E)$ there are many representative bases, those base are homothetic.

That is, $(S)=(e_1,...,e_{n+1})$ and $(S')=(e'_1,...,e'_{n+1})$ together represent $(A_i;E)$ if then only if there is a $k\neq 0$ number such that $e_i=ke'_i;i=1,...,n+1$

4. USE LINEAR RELATIONSHIP TO SOLVE SOME PROBLEMS OF PROJECTIVE GEOMETRY

Problem 1.

In P^2 with projective goal for the last two distinct points A, B coordinates $A=(a_1,a_2,a_3), B=(b_1,b_2,b_3)$ meanwhile, the equation of the line AB will be determined as follows:

Point $X\in P^2$: Suppose $X=(x_1,x_2,x_3)$.

The vectors representing X,A,B in turn are x,a,b

By $A\neq B\rightarrow rank(a,b)=2$

$X\in AB\Leftrightarrow x\in\langle(a,b)\rangle=V^2\Leftrightarrow(x,a,b)$ is linearly dependent

$$\Leftrightarrow\begin{vmatrix}a_1 & b_1 & x_1\\ a_2 & b_2 & x_2\\ a_3 & b_3 & x_3\end{vmatrix}=0\ (*)$$

Developed according to column 3, we have the equation of AB with the form: $u_1x_1+u_2x_2+u_3x_3=0$ with u_1,u_2,u_3 is the determinant of level 2 in the development of $(*)$ and $\sum_{i=1}^{3}u_i^2\neq 0$

Problem 2.

In the P^2 projective space, prove that if two triangles ABC and $A'B'C'$ have straight lines through the corresponding vertices AA',BB',CC' at point S, the intersection of the corresponding pairs of $AB\cap A'B', BC\cap B'C', AC\cap A'C'$ is on the same straight line (Desargues Theorem)

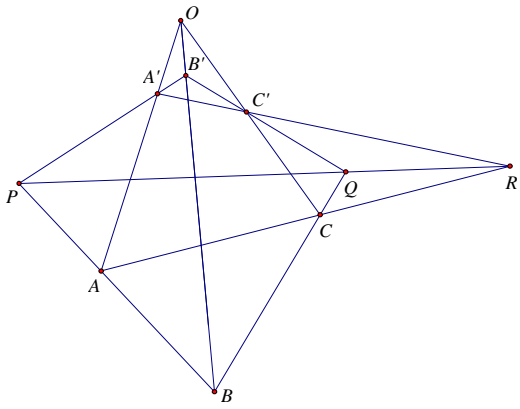

Fig 4.1

- Coordinates methods:

Let P, Q, R be the above corresponding intersections. P, Q, R are on the same line when and only when defining their coordinate matrix:

$$\begin{vmatrix} p_1 & p_2 & p_3 \\ q_1 & q_2 & q_3 \\ r_1 & r_2 & r_3 \end{vmatrix} = 0$$

Choose a projective rational goals, we try to find the coordinates of the intersection P, Q, R. If you choose to target: (A, B, C, O). We have:

O, A, A' are on the same line, $A' = (x_1, x_2, x_3)$ should exist (λ, μ) satisfy: $[A'] = \lambda[O] + \mu[A]$ with $\lambda, \mu \neq 0$

$$\begin{bmatrix} x_1 \\ x_2 \\ x_3 \end{bmatrix} = \lambda \begin{bmatrix} 1 \\ 1 \\ 1 \end{bmatrix} + \mu \begin{bmatrix} 1 \\ 0 \\ 0 \end{bmatrix} \equiv \begin{bmatrix} \lambda + \mu \\ \lambda \\ \lambda \end{bmatrix}$$

Can choose $\lambda = 1; \lambda + \mu = a$; $a \neq 1$. Then, the coordinate A' has the form: $A' = (a, 1, 1)$

The similar: $B' = (1, b, 1)$; $C' = (1, 1, c)$; $b, c \neq 1$

Equations of AB: $x_3 = 0$ should line AB with coordinates: $[0, 0, 1]$

Equations of A'B': $(1-b)x_1 + (1-a)x_2 + (ab-1)x_3 = 0$

should line A'B' with coordinates $[1-b, 1-a, ab-1]$

Because the $\{P\} = AB \cap A'B'$ so coordinate P satisfies the system:

$$\begin{cases} x_3 = 0 \\ (1-b)x_1 + (1-a)x_2 + (ab-1)x_3 = 0 \end{cases}$$

Solve the system of equations we have: $P = (a-1, 1-b, 0)$

The similar: $Q = (0, 1-b, c-1)$ and $R = (1-a, 0, c-1)$

$\det[P, Q, R] = 0 \Rightarrow P, Q, R$ are on the same line.

Reviews:

The solution to problem 1 using the coordinate method is presented briefly and quite simply (if choosing a reasonable goal). However, the calculation volume is quite cumbersome (due to arguments to establish and solve three equations)

We can overcome this disadvantage if we use linear relationships of the set of vectors - representing the set of points to have a simple and concise solution. This idea comes from an "equal" relationship that is different from an isomorphism between V^{n+1} and P^n.

- Call the representative vectors of O, A, B, C, A', B', C' respectively: s, a, b, c, a', b', c'

$(a,a');(b,b');(c,c')$ pairs are linearly independent in V^3

According to the beginning of the post, because $\{O\} = AA' \cap BB' \cap CC' \Rightarrow \langle s \rangle = \langle (a,a') \rangle \cap \langle (b,b') \rangle \cap \langle (c,c') \rangle$ (intersection of super plane produces 1-plane).

Therefore: $s = \alpha a + \alpha' a' = \beta b + \beta' b' = \gamma c + \gamma' c'$

From the above linear representations we deduce:

$\alpha a - \beta b = \beta' b' - \alpha' a' = p$ (representing P intersection point)

$\beta b - \gamma c = \gamma' c' - \beta' b' = q$ (representing Q intersection point)

$\gamma c - \alpha a = -\gamma' c' + \alpha' a' = r$ (representing R intersection point)

On the other hand, because: $p + q + r = O_3$, three vectors are linear, so $(p,q,r) \subset V^2$

That is, P, Q, R are on the same line.

Problem 3.

In a full four peaks, two crossover points located on a diagonal split conditioning intersection of diagonal pairs that with a pair of edge passing third cross point.

Suppose ABCD is a shape with four total vertices. Three cross points: P, Q and R

$\Leftrightarrow [P,Q,M,N] = -1$.

The two crossover points P and Q divide the conditioning point of the intersection of the PQ diagonal with the pair of edges passing through the third cross point R $\Leftrightarrow [P,Q,M,N] = -1$

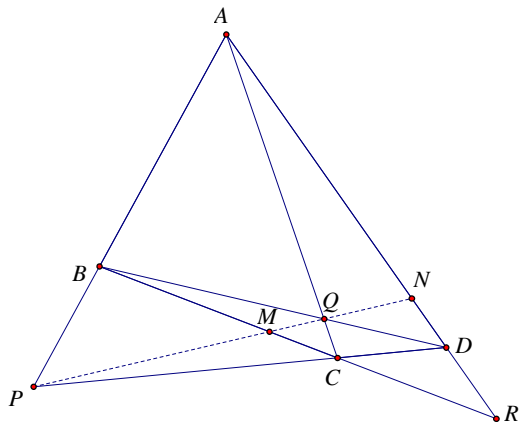

Fig 4.5

In $P^2 = \langle A, B, C, D \rangle$ We choose the target (A, B, C, D).

Then: the base represents the selected target $(e_1, e_2, e_3) \subset V^3$ links and $e_1 = (1;0;0), e_2 = (0;1;0), e_3 = (0;0;1), e = (1;1;1)$ represents A, B, C, D respectively

The straight line AB has an $x_3 = 0$ equation so $P = (x_1, x_2, 0)$

On the other hand, P, D, C are collinear so their vectors are all in the same space V^2. That is, they establish a linear dependency in V^2

Thus: $\det \begin{bmatrix} x_1 & x_2 & 0 \\ 1 & 1 & 1 \\ 0 & 0 & 1 \end{bmatrix} = 0$ or $x_1 = x_2$ should $P = (1,1,0)$

Similarly, we can calculate $Q = (1,0,1)$; $M = (2,1,1)$ and $N = (0,1,-1)$

Since then the linear representations of the representative vectors in V^3 are:

$$\begin{matrix} m = p + q \\ n = p - q \end{matrix} \text{ or } [P, Q, M, N] = -1$$

5. CONCLUSION

The article concerns the relationship between two vector space objects of Algebra and the projective space in Geometry. Exploiting some results from the relationship between the elements of vector space as the basis for the corresponding relationship between flats in the projective space because of a strong connection tight: Each projective space P^n has a space of vector V^{n+1} as a background and they are bound together by the bijection π. The corresponding term is an isomorphism between two sets of X and $[V^{n+1}]$ - the set of one-dimensional subspace of V^{n+1}

REFERENCES

1. Nguyễn Hữu Việt Hưng (2001), *Đại số tuyến tính,* - Nxb Đại học Quốc gia Hà Nội.
2. Lê Tuấn Hoa (2001), *Đại số hiện đại,* - Nxb Đại học Quốc gia Hà Nội.
3. Văn Như Cương (2005), *Hình học xạ ảnh*, - Nxb Đại học Sư phạm.
4. Nguyễn Mộng Hy (2003), *Hình học cao cấp*, - Nxb Giáo dục.

MỐI LIÊN HỆ TUYẾN TÍNH TRONG KHÔNG GIAN VÉC TƠ ỨNG DỤNG GIẢI CÁC BÀI TOÁN VỀ SỰ LIÊN THUỘC TRONG KHÔNG GIAN XẠ ẢNH

Tóm tắt: *Bài viết này đề cập tới một số khái niệm cùng những kết quả quan trọng của Đại số tuyến tính như Tổ hợp tuyến tính, hệ sinh, sự phụ thuộc tuyến tính... trong Không gian véc tơ và sử dụng chúng như một công cụ hữu hiệu để giải một lớp các bài toán "Xác định sự liên thuộc" nhằm khẳng định mối quan hệ giữa các m - phẳng trong Không gian xạ ảnh* P^n *của Hình học xạ ảnh.*

Từ khóa: *Không gian, m - phẳng, tổ hợp tuyến tính, hệ sinh...*

SEPTIC B – SPLINE COLLOCATION METHOD FOR NUMERICAL SOLUTION OF THE mGRLW EQUATION

Nguyen Van Tuan
Hanoi Metropolitan University

Abstract: *In this paper, numerical solution of a modified generalized regularized long wave (mGRLW) equation are obtained by a new method based on collocation of septic B – splines. Applying the von – Neumann stability analysis, the proposed method is shown to be unconditionally stable. The numerical result shows that the present method is a successful numerical technique for solving the GRLW equations and the mGRLW equations.*

Keyword: *mGRLW equation; septic B-spline; collocation method; finite difference.*

Email: nvtuan@hnmu.edu.vn
Received 27 March 2019
Accepted for publication 25 May 2019

1. INTRODUCTION

In this work, we consider the solution of the mGRLW equation

$$u_t + u_x + \varepsilon u^p u_x - \mu u_{xx} - \beta u_{xxt} = 0, \tag{1}$$

$x \in [a, b], t \in [0, T]$, with the initial condition

$$u(x, 0) = f(x), x \in [a, b], \tag{2}$$

and the boundary condition

$$\begin{cases} u_x(a, t) = 0, u_x(b, t) = 0 \\ u_{xx}(a, t) = u_{xx}(b, t) = 0 \\ u_{xxx}(a, t) = u_{xxx}(b, t) = 0, \end{cases} \tag{3}$$

where $\varepsilon, \mu, \beta, p$ are constants, $\mu > 0, \beta > 0, p$ is a positive integer.

The equation (1) is called the modified generalized regularized long wave (mGRLW) equation. If $\mu = 0$, the equation (1) is called the generalized regularized long wave (GRLW).

Equation (1) describes the mathematical model of wave formation and propagation in fluid dynamics, turbulence, acoustics, plasma dynamics, ect. So in recent years,

researchers solve the GRLW and mGRLW equation by both analytic and numerical methods.

In this present work, we have applied the septic B – spline collocation method to the mGRLW equations and GRLW equations. This work is built as follow: in Section 2, numerical scheme is presented. The stability analysis of the method is established in Section 3. The numerical results are discussed in Section 4. In the last Section, Section 5, conclusion is presented.

2. SEPTIC B – SPLINE COLLOCATION METHOD

The interval $[a, b]$ is partitioned in to a mesh of uniform length $\mathrm{h} = \mathrm{x_{i+1}} - \mathrm{x_i}$ by the knots $\mathrm{x_i}, \mathrm{i} = \overline{0, \mathrm{N}}$ such that

$$\mathrm{a} = \mathrm{x_0} < \mathrm{x_1} < \cdots < \mathrm{x_{N-1}} < \mathrm{x_N} = \mathrm{b}.$$

Our numerical study for mGRLW equation using the collocation method with septic B-spline is to find an approximate solution $\mathrm{U(x,t)}$ to exact solution $\mathrm{u(x,t)}$ in the form

$$\mathrm{U(x,t)} = \sum_{\mathrm{i=-3}}^{\mathrm{N+3}} \delta_\mathrm{i}(\mathrm{t})\mathrm{B_i(x)}, \tag{4}$$

$\mathrm{B_i(x)}$ are the septic B-spline basis functions at knots, given by [4].

$$\mathrm{B_i(x)} = \frac{1}{\mathrm{h^7}} \begin{cases} (\mathrm{x} - \mathrm{x_{i-4}})^7, & \mathrm{x_{i-4}} \le \mathrm{x} \le \mathrm{x_{i-3}} \\ (\mathrm{x} - \mathrm{x_{i-4}})^7 - 8(\mathrm{x} - \mathrm{x_{i-3}})^7, & \mathrm{x_{i-3}} \le \mathrm{x} \le \mathrm{x_{i-2}} \\ (\mathrm{x} - \mathrm{x_{i-4}})^7 - 8(\mathrm{x} - \mathrm{x_{i-3}})^7 + 28(\mathrm{x} - \mathrm{x_{i-2}})^7, & \mathrm{x_{i-2}} \le \mathrm{x} \le \mathrm{x_{i-1}} \\ (\mathrm{x} - \mathrm{x_{i-4}})^7 - 8(\mathrm{x} - \mathrm{x_{i-3}})^7 + 28(\mathrm{x} - \mathrm{x_{i-2}})^7 - & \\ -56(\mathrm{x} - \mathrm{x_i})^5, & \mathrm{x_{i-1}} \le \mathrm{x} \le \mathrm{x_i} \\ (\mathrm{x_{i+4}} - \mathrm{x})^7 - 8(\mathrm{x_{i+3}} - \mathrm{x})^7 + 28(\mathrm{x_{i+2}} - \mathrm{x})^7 - 56(\mathrm{x_{i+1}} - \mathrm{x})^7, & \\ \mathrm{x_i} \le \mathrm{x} \le \mathrm{x_{i+1}} & \\ (\mathrm{x_{i+4}} - \mathrm{x})^7 - 8(\mathrm{x_{i+3}} - \mathrm{x})^7 + 28(\mathrm{x_{i+2}} - \mathrm{x})^7, & \mathrm{x_{i+1}} \le \mathrm{x} \le \mathrm{x_{i+2}} \\ (\mathrm{x_{i+4}} - \mathrm{x})^7 - 8(\mathrm{x_{i+3}} - \mathrm{x})^7, & \mathrm{x_{i+2}} \le \mathrm{x} \le \mathrm{x_{i+3}} \\ (\mathrm{x_{i+4}} - \mathrm{x})^7, & \mathrm{x_{i+3}} \le \mathrm{x} \le \mathrm{x_{i+4}} \\ 0, & \mathrm{x} < \mathrm{x_{i-4}} \cup \mathrm{x} > \mathrm{x_{i+4}}. \end{cases} \tag{5}$$

Using (4) and (5) we have

$$\begin{cases} \mathrm{U(x_i,t)} = \mathrm{U_i} = \delta_{\mathrm{i-3}} + 120\delta_{\mathrm{i-2}} + 1191\delta_{\mathrm{i-1}} + 2416\delta_\mathrm{i} + 1191\delta_{\mathrm{i+1}} + 120\delta_{\mathrm{i+2}} + \delta_{\mathrm{i+3}} \\ \mathrm{U'_i} = \frac{7}{\mathrm{h}}(-\delta_{\mathrm{i-3}} - 56\delta_{\mathrm{i-2}} - 245\delta_{\mathrm{i-1}} + 245\delta_{\mathrm{i+1}} + 56\delta_{\mathrm{i+2}} + \delta_{\mathrm{i+3}}) \\ \mathrm{U''_i} = \frac{42}{\mathrm{h^2}}(\delta_{\mathrm{i-3}} + 24\delta_{\mathrm{i-2}} + 15\delta_{\mathrm{i-1}} - 80\delta_\mathrm{i} + 15\delta_{\mathrm{i+1}} + 24\delta_{\mathrm{i+2}} + \delta_{\mathrm{i+3}}). \end{cases} \tag{6}$$

Using the finite difference method, from the equation (1), we get

$$\frac{(u-\beta u_{xx})^{n+1}-(u-\beta u_{xx})^{n}}{\Delta t}+\varepsilon(u^{p-1})^{n}(u_x)^{n}\frac{u^{n+1}+u^{n}}{2}+\frac{(u_x)^{n+1}+(u_x)^{n}}{2}-\mu\frac{u_{xx}^{n+1}+u_{xx}^{n}}{2}=0. \tag{7}$$

We take the collocations points with the knots and use equation (6) to evaluate U_i, U_i', U_i'' and substitute into equation (1). Equation (7) reduces to

$$a_{m1}\delta_{m-3}^{n+1}+a_{m2}\delta_{m-2}^{n+1}+a_{m3}\delta_{m-1}^{n+1}+a_{m4}\delta_{m}^{n+1}+a_{m5}\delta_{m+1}^{n+1}+a_{m6}\delta_{m+2}^{n+1}+a_{m7}\delta_{m+3}^{n+1}=b_{m1}\delta_{m-3}^{n}+b_{m2}\delta_{m-2}^{n}+b_{m3}\delta_{m-1}^{n}+b_{m4}\delta_{m}^{n}+b_{m5}\delta_{m+1}^{n}+b_{m6}\delta_{m+2}^{n}+b_{m7}\delta_{m+3}^{n}, \tag{8}$$

where

$$\begin{aligned}
a_{m1}&=A_1+KQ_m\\
a_{m2}&=A_2+120KQ_m\\
a_{m3}&=A_3+1191KQ_m\\
a_{m4}&=A_4+2416KQ_m\\
a_{m5}&=A_5+1191KQ_m\\
a_{m5}&=A_6+120KQ_m\\
a_{m5}&=A_7+KQ_m\\
b_{m1}&=B_1-KQ_m\\
b_{m2}&=B_2-120KQ_m\\
b_{m3}&=B_3-1191KQ_m\\
b_{m4}&=B_4-2416KQ_m\\
b_{m5}&=B_5-1191KQ_m\\
b_{m6}&=B_6-120KQ_m\\
b_{m7}&=B_7-KQ_m,
\end{aligned}$$

with

$$\begin{cases}
A_1=1-M-L_1L_2\\
A_2=120-56M-24L_1L_2\\
A_3=1191-245M-15L_1L_2\\
A_4=2416+80L_1L_2\\
A_5=1191+245M-15L_1L_2\\
A_6=120+56M-24L_1L_2\\
A_7=1+M-L_1L_2,
\end{cases}
\qquad
\begin{cases}
B_1=1+M+L_1L_3\\
B_2=120+56M+24L_1L_3\\
B_3=1191+245M+15L_1L_3\\
B_4=2416-80L_1L_3\\
B_5=1191-245M+15L_1L_3\\
B_6=120-56M+24L_1L_3\\
B_7=1-M+L_1L_3,
\end{cases}$$

and

$$\begin{cases}
M=\frac{7\Delta t}{2h}, K=\frac{\varepsilon\Delta t}{2}, Q_m=(U_m)^{p-1}(U_m)_x\\
L_1=\frac{42}{h^2}, L_2=\frac{\mu\Delta t}{2}+\beta, L_3=\frac{\mu\Delta t}{2}-\beta.
\end{cases}$$

The system (8) consists of $N+1$ equations in the $N+7$ knowns $(\delta_{-3}, \delta_{-2}, \dots, \delta_{N+2}, \delta_{N+3})^T$.

To get a solution to this system, we need six additional constraints. These constraints are obtained from the boundary conditions (3) and can be used to eliminate from the system (8). Then, we get the matrix system equation

$$A(\delta^n)\delta^{n+1} = B(\delta^n)\delta^n + r, \tag{9}$$

where the matrix $A(\delta^n), B(\delta^n)$ are septa-diagonal $(N+1)\times(N+1)$ matrices and r is the $N+1$ dimensional colum vector. The algorithm is then used to solve the system (9). We apply first the intial condition

$$U(x,0) = \sum_{i=-3}^{N+3} \delta_i^0 B_i(x), \quad (10)$$

then we need that the approximately solution is satisfied folowing conditions

$$\begin{cases} U(x_i,0) = f(x_i) \\ U_x(x_0,0) = U_x(a,0) = 0 \\ U_x(x_N,0) = U_x(b,0) = 0 \\ U_{xx}(x_0,0) = U_{xx}(a,0) = 0 \\ U_{xx}(x_N,0) = U_{xx}(b,0) = 0 \\ U_{xxx}(x_0,0) = U_{xxx}(a,0) = 0 \\ U_{xxx}(x_0,0) = U_{xxx}(a,0) = 0 \\ i = 0,1,\dots,N. \end{cases} \tag{11}$$

Eliminating $\delta_{-3}^0, \delta_{-2}^0, \delta_{-1}^0, \delta_{N+1}^0, \delta_{N+2}^0$ and δ_{N+3}^0 from the system (11), we get $A\delta^0 = r$ where A is the penta-diagonal matrix given by

$$A = \begin{pmatrix} 1536 & 2712 & 768 & 24 & 0 & \dots & & & & 0 \\ \frac{82731}{81} & \frac{210568.5}{81} & \frac{104796}{81} & \frac{10063.5}{81} & 1 & 0 & \dots & & & 0 \\ \frac{9600}{81} & \frac{96597}{81} & \frac{195768}{81} & \frac{96474}{81} & 120 & 1 & 0 & \dots & & 0 \\ 1 & 120 & 1191 & 2416 & 1191 & 120 & 1 & 0 & \dots & 0 \\ \dots & & & \dots & & & & & & \\ \dots & & & \dots & & & & & & \\ 0 & \dots & 0 & 1 & 120 & 1191 & 2416 & 1191 & 120 & 1 \\ 0 & \dots & & 0 & 1 & 120 & \frac{96474}{81} & \frac{195768}{81} & \frac{96597}{81} & \frac{9600}{81} \\ 0 & \dots & & & 0 & 1 & \frac{10063.5}{81} & \frac{104796}{81} & \frac{210568.5}{81} & \frac{82731}{81} \\ 0 & \dots & & & & 0 & 24 & 768 & 2712 & 1536 \end{pmatrix}$$

and $\delta^0 = (\delta_0^0, \delta_1^0, \dots, \delta_N^0)^T, r = (f(x_0), f(x_1), \dots, f(x_N))^T$.

3. STABILITY ANALYSIS

To apply the Von-Neumann stability for the system (6), we must first linearize this system.

We have

$$\delta_j^n = \xi^n \exp(i\gamma jh), i = \sqrt{-1}, \tag{12}$$

where γ is the mode number and h is the element size.

Being applicable to only linear schemes the nonlinear term U^pU_x is linearized by taking U as a locally constant value c. The linearized form of proposed scheme is given as

$$\begin{aligned} &p_1\delta_{i-3}^{n+1} + p_2\delta_{i-2}^{n+1} + p_3\delta_{i-1}^{n+1} + p_4\delta_i^{n+1} + p_5\delta_{i+1}^{n+1} + p_6\delta_{i+2}^{n+1} + p_7\delta_{i+3}^{n+1} = \\ &p'_1\delta_{i-3}^{n} + p'_2\delta_{i-2}^{n} + p'_3\delta_{i-1}^{n} + p'_4\delta_i^{n} + p'_5\delta_{i+1}^{n} + p'_6\delta_{i+2}^{n} + p'_7\delta_{i+3}^{n} \end{aligned} \tag{13}$$

where

$$p_1 = 1 - L_5 + L_6,\ p_2 = 120 - 56L_5 - 24L_6,\ p_3 = 1191 - 245L_5 - 16L_6,$$
$$p_4 = 2416 + 80L_6, p_5 = 1191 + 245L_5 - 15L_6,\ p_6 = 120 + 56L_5 - 24L_6,$$
$$p_7 = 1 + L_5 - L_6,$$
$$p'_1 = 1 + L_5 + L_7, p'_2 = 120 + 56L_5 + 24L_7, p'_3 = 1191 + 245L_5 + 15L_7,$$
$$p'_4 = 2416 - 80L_7, p'_5 = 1191 - 245L_5 + 15L_7,$$
$$p'_6 = 120 - 56L_5 + 24L_7, p'_7 = 1 - L_5 + L_7,$$
$$L_5 = \frac{7(1+\varepsilon c^p)\Delta t}{2h}, L_6 = \frac{42}{h^2}\left(\frac{\mu\Delta t}{2} + \beta\right), L_7 = \frac{42}{h^2}\left(\frac{\mu\Delta t}{2} - \beta\right).$$

Substitretion of $\delta_j^n = \exp(i\gamma jh)\xi^n$, into equation (13) leads to

$$\begin{aligned} \xi[&p_1\exp(-3ih\gamma) + p_2\exp(-2i\gamma h) + p_3\exp(-i\gamma h) + p_4 \\ &+ p_5\exp(3i\gamma h) + p_6\exp(2i\gamma h) + p_7\exp(i\gamma h)] \\ = &\ p'_1\exp(-3ih\gamma) + p'_2\exp(-2i\gamma h) + p'_3\exp(-i\gamma h) + p'_4 \\ &+ p'_5\exp(3i\gamma h) + p'_6\exp(2i\gamma h) + p'_7\exp(i\gamma h). \end{aligned} \tag{14}$$

Simplifying equation (14), we get

$$\xi = \frac{A_1 - iB}{C + iB}.$$

It is clear that $C^2 \geq A_1^2$. So $|\xi| \leq 1$.

Therefore, the linearized numerical scheme for the mGRLW equation is unconditionally stable.

4. NUMERICAL EXAMPLE

We now obtain the numerical solution of the mGRLW equation for some problems. To show the efficiency of the present method for our problem in comparison with the exact solution, we report L_∞ and L_2 using formula

$$L_\infty = \max_i |U(x_i, t) - u(x_i, t)|,$$

$$L_2 = \left(h \sum_i |U(x_i, t) - u(x_i, t)|^2 \right)^{\frac{1}{2}},$$

where U is numerical solution and u denotes exact solution.

Three invariants of motion which correspond to the conservation of mass, momentum, and energy are given as

$$I_1 = \int_a^b u dx,\ I_2 = \int_a^b (u^2 + \beta u_x^2) dx,\ I_3 = \int_a^b u^{p+2} dx.$$

When $\mu = 0, \varepsilon = p(p+1)$ we get the exact of the GRLW is

$$u(x,t) = \sqrt[p]{\frac{c(p+2)}{2p} \operatorname{sech}^2 \left[\frac{p}{2} \sqrt{\frac{c}{\beta(c+1)}} (x - (c+1)t) - x_0 \right]}.$$

Using the method [8], we find the exact solution of the mGRLW is

$$u(x,t) = \left\{ \rho \left[1 + \frac{3\sinh(kx + \omega t + x_0) + 5\cosh(kx + \omega t + x_0)}{3\cosh(kx + \omega t + x_0) + 5\sinh(kx + \omega t + x_0)} \right] \right\}^{\frac{2}{p}},$$

where $\rho = \frac{1}{8\beta\varepsilon(p+4)} \left(\alpha\beta(p^2 + 5p + 4 + (p+1)A_2) \right), k = \frac{1}{8\beta\mu(p+2)} (-\alpha\beta(p+4) + A_2),$

$$\omega = \frac{-p\mu}{2\beta(p+4)}, A_2 = \sqrt{\beta(p+4)[\alpha^2\beta(p+4) - 8\mu^2]}.$$

The initial condition of equation (1) given by

$$f(x) = \left\{ \rho \left[1 + \frac{3\sinh(kx + x_0) + 5\cosh(kx + x_0)}{3\cosh(kx + x_0) + 5\sinh(kx + x_0)} \right] \right\}^{\frac{2}{p}}.$$

We take $p = 4, \varepsilon = p(p+1), \mu = 0, \beta = 1, a = 0, b = 100, x_0 = 40, \Delta t = 0.01$ and $\Delta t = 0.01, h = 0.1$ and $h = 0.2$, $t \in [0, 20]$. The values of the variants and the error norms at several times are listed in Table 1 and Table 2.

In Table 1, changes changes of variants $I_1 \times 10^4, I_2 \times 10^5$ and $I_3 \times 10^4$ from their initial value are less than 0.3, 0.5 and 0.7, respectively. The error nomrs L_2, L_∞ are less than 1.096651×10^{-3} and 0.638539×10^{-3}, respectively. The plot of the estimated solution at time t = 0, 10, 20 in Figure 1

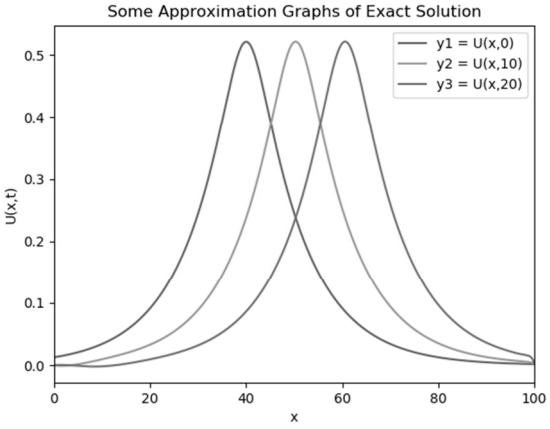

Figure 1. *Single solitary wave with $p = 4$, $c = 0.03$, $x_0 = 40$, $t = 0, 10, 20$.*

From Table 2, we see that, changes of variants $I_1 \times 10^2, I_2 \times 10^3$ and $I_3 \times 10^4$ from their initial value are less than 0.3, 0.9 and 0.7, respectively. The error nomrs L_2, L_∞ are less than 1.064872×10^{-3} and 0.638539×10^{-3}, respectively.

Table 1. *Variants and error norms of the GRLW equation with $p = 4$, $\varepsilon = p(p+1), \mu = 0, \beta = 1, a = 0, b = 100, x_0 = 40, \Delta t = 0.01, h = 0.1, t \in [0, 20]$*

t	0	5	10	15	20
I_1	5.946800	5.947515	5.947215	5.946512	5.944454
I_2	1.400709	1.400942	1.401176	1.401410	1.401647
I_3	0.015532	0.015550	0.015566	0.015581	0.015596
$L_2 \times 10^3$	0	0.574290	0.805070	0.938071	1.096651
$L_\infty \times 10^3$	0	0.282476	0.274554	0.308184	0.638539

Table 2. *Variants and error norms of the GRLW equation with $p = 4$, $\varepsilon = p(p+1), \mu = 0, \beta = 1, a = 0, b = 100, x_0 = 40, \Delta t = 0.01, h = 0.2, t \in [0, 20]$*

t	0	5	10	15	20
I_1	5.946800	5.947856	5.947540	5.946768	5.944769
I_2	1.400709	1.400942	1.401176	1.401411	1.401649
I_3	0.015532	0.015550	0.015566	0.015581	0.015596
$L_2 \times 10^3$	0	0.471979	0.738460	0.888661	1.064872
$L_\infty \times 10^3$	0	0.237987	0.239144	0.308184	0.638539

To get more the variants and error norms, we choose set of parameters with p = 3, $\beta = 1, a = 0, b = 100, x_0 = 40, \Delta t = 0.01, h = 0.1$ The variants and error norms are calculated from time t = 0 to t = 10. The variants and error norms are listed in Table 3.

Table 3. *Variants and error norms of the GRLW equation with* $p = 3$, $\varepsilon = p(p+1), \mu = 0, \beta = 1, a = 0, b = 100, x_0 = 40, \Delta t = 0.01, h = 0.1, t \in [0, 10]$

t	0	2	4	6	8	10
I_1	3.677552	3.681204	3.684933	3.688736	3.692620	3.696589
I_2	1.565741	1.572597	1.579622	1.586813	1.594182	1.601743
I_3	0.203546	0.206558	0.209518	0.212565	0.215760	0.219117
$L_2 \times 10^2$	0	0.348156	0.836246	1.569786	2.596696	3.938000
$L_\infty \times 10^2$	0	0.245211	0.515165	0.931261	1.498778	2.215615

In this table, we get, the changes of variants I_1, I_2 and I_3 from their initial values are less than 0.02; 0.04 and 0.006, respectively. The error nomrs L_2 and L_∞ are less than 5.242345×10^{-4} and 0.602344×10^{-4}, respectively.

Now we consider the mGRLW equation (1).

We take $p = 2, \varepsilon = 3000, \beta = 2, \mu = 1, a = 0, b = 100, x_0 = 40, \Delta t = 0.01, h = 0.1$ and 0.2. The variants and error norms are calculated from time t = 0 to t = 20. The variants and error norms are listed in Table 4 and Table 5. In this Table 4, we get, the changes of variants $I_1 \times 10^2$ from their initial values are less than 0.8. The error nomrs L_2 and L_∞ are less than 0.160044×10^{-2} and 0.039648×10^{-2}, respectively. The plot of the estimated solution at time t = 0, 10, 20 in Figure 2.

Table 4*. Variants and error norms of the mGRLW equation with* $p = 2$, $\varepsilon = 3000, \mu = 1, \beta = 2, a = 0, b = 100, x_0 = 40, \Delta t = 0.01, h = 0.1, t \in [0, 20]$

t	0	5	10	15	20
I_1	0.039434	0.037359	0.035418	0.033446	0.031473
I_2	1.555021	0	0	0	0
I_3	2.418091	0	0	0	0
$L_2 \times 10^2$	0	0.064293	0.107546	0.136128	0.160044
$L_\infty \times 10^2$	0	0.037985	0.039514	0.039643	0.039648

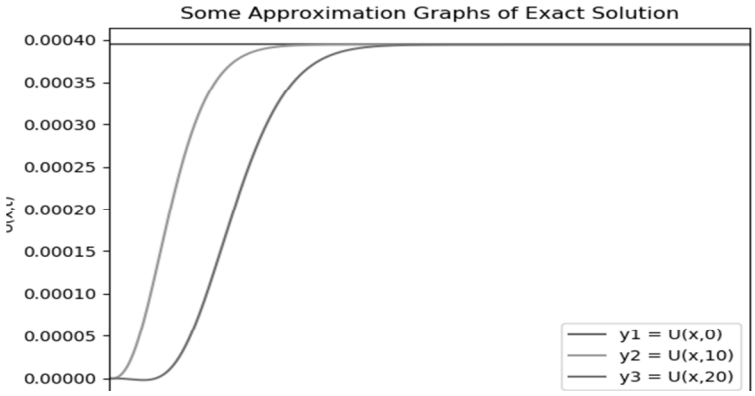

Figure 2. *Single solitary wave with*
$p = 2, \varepsilon = 3000, \beta = 2, \mu = 1, a = 0,$
$b = 100, x_0 = 40, \Delta t = 0.01, h = 0.1$

Table 5. *Variants and error norms of the mGRLW equation with* $p = 3, \alpha = 2,$
Table 5. Variants and error norms of the mGRLW equation with $p = 2, \varepsilon = 3000, \mu = 1,$
$\beta = 2, a = 0, b = 100, x_0 = 40, \Delta t = 0.01, h = 0.2, t \in [0, 20]$

t	0	5	10	15	20
I_1	0.039434	0.037597	0.035693	0.033726	0.031752
I_2	1.555021	0	0	0	0
I_3	2.418091	0	0	0	0
$L_2 \times 10^2$	0	0.064293	0.102215	0.131923	0.156537
$L_\infty \times 10^2$	0	0.035594	0.039155	0.039531	0.039578

In this Table 5, we get, the changes of variants $I_1 \times 10^2$ from their initial values are less than 0.8. The error nomrs L_2 and L_∞ are less than 0.156537×10^{-2} and 0.039578×10^{-2}, respectively.

For the purpose of illustration of the presented method for solving the mGRLW equation, we use parameters $p = 3$ with $\varepsilon = 3000, \beta = 2, a = 0, b = 100, x_0 = 40, \Delta t = 0.01, h = 0.2$. The results are listed in Table 6.

The plot of the estimated solution at time t = 0, 10, 20 in Figure 3.

From from these tables, we see that, the error norms L_2, L_∞ are quite small for present method.

Table 6. *Variants and error norms of the mGRLW equation with* $p = 3$, $\varepsilon = 3000, \mu = 1, \beta = 2, a = 0, b = 100, x_0 = 40, \Delta t = 0.01, h = 0.2, t \in [0, 20]$

t	0	5	10	15	20
I_1	0.672549	0.641225	0.608753	0.575188	0.541528
I_2	0.004523	0.004225	0.003970	0.003720	0.003473
I_3	0	0	0	0	0
L_2	0	0.010966	0.017433	0.022500	0.026698
L_∞	0	0.006071	0.006678	0.006742	0.006750

5. CONCLUSION

In this work, we have used the septic B - spline collocation method for solution of the mGRLW equation. We tasted our scheme through single solitary wave and the obtained results are tabulaces. These tables show that, the changes of variants are quite small. So the present method is more capable for solving these equations.

REFERENCES

1. S. S. Askar and A. A. Karawia (2015), "On solving pentadiagonal linear systems via transformations", *Mathematical Problems in Engineering*, Vol. **2015**, pp. 1 - 9.
2. S. Battal Gazi Karakoça, Halil Zeybek (2016), "Solitary - wave solutions of the GRLW equation using septic B - spline collocation method", *Applied Mathematics and Computation*, Vol. **289**, pp. 159 - 171.
3. H. Che, X. Pan, L. Zhang and Y. Wang (2012), "Numerical analysis of a linear - implicit average scheme for generalized Benjamin - Bona - Mahony - Burgers equation", J. *Applied Mathematics*, Vol. **2012**, pp. 1 - 14.
4. D. J. Evans and K. R. Raslan (2005), "Solitary waves for the generalized equal width (GEW) equation", *International J. of Computer Mathematics*, Vol. **82(4)**, pp. 445 - 455.
5. C. M. García - Lospez, J. I. Ramos (2012), "Effects of convection on a modified GRLW equation", *Applied Mathematics and Computation*, Vol. **219**, pp. 4118 - 4132.
6. C. M. García - Lospez, J. I. Ramos (2015), "Solitari waves generated by bell - shaped initial conditions in the invicis and viscous GRLW equations", *Applied Mathematical Modelling*, Vol. **39 (21)**, pp. 6645 - 6668.
7. P. A. Hammad, M. S. EI – Azab (2015), "A 2N order compact finite difference method for solving the generalized regularized long wave (GRLW) equation", *Applied Mathematics and Computation*, Vol. **253**, pp. 248 - 261.
8. B. Hong, D. Lu (2008), "New exact solutions for the generalized BBM and Burgers - BBM equations", *World Journal of Modelling and Simulation*, Vol. **4(4)**, pp. 243-249.

9. S. Islam, F. Haq and I. A. Tirmizi (2010), "Collocation method using quartic B-spline for numerical solution of the modified equal width wave equation", *J. Appl. Math. Inform*., Vol. **28(3 - 4)**, pp. 611–624.
10. A. G. Kaplan, Y. Dereli (2017), "Numerical solutions of the GEW equation using MLS collocation method", *International Journal of Modern Physics C*, Vol. **28(1), 1750011**, pp. 1 - 23.
11. M. Mohammadi, R. Mokhtari (2011), "Solving the generalized regularized long wave equation on the basis of a reproducing kernel space", *J. of Computation and Applied Mathematics*, Vol. **235**, pp. 4003 - 4014.
12. R. Mokhtari, M. Mohammadi (2010), "Numerical solution of GRLW equation using sinc - collocation method", *Computer Physics Communications*, Vol. **181**, pp. 1266 - 1274.
13. E. Pindza and E. Maré (2014), "Solving the generalized regularized long wave equation using a distributed approximating functional method", *International Journal of Computational Mathematics*, Vol. **2014**, pp. 1 - 12.
14. P. M. Prenter (1975), "Splines and Variational Methods", *Wiley, New York*.
15. T. Roshan (2011), "A Petrov – Galerkin method for solving the generalized equal width (GEW) equation", *J. Comput. Appl. Math*., Vol. **235**, pp. 1641–1652.
16. T. Roshan (2012), "A Petrov – Galerkin method for solving the generalized regularized long wave (GRLW) equation", *Computers and Mathematics with Applications*, Vol. **63**, pp. 943 - 956.
17. M. Zarebnia and R. Parvaz (2013), "Cubic B-spline collocation method for numerical solution of the Benjamin - Bona - Mahony - Burgers equation", *International Journal of Mathematical, Computational, Physical, Electrical and Computer Engineering*, Vol. **7 (3)**, pp. 540 - 543.
18. H. Zeybek and S. Battal Gazi Karakoça (2017), "Application of the collocation method with B - spline to the GEW equation", *Electronic Transactions on Numerical Analysis*, Vol. **46**, pp. 71 - 88.
19. L. Zhang (2005), "A finite difference scheme for generalized regularized long wave equation", *Applied Mathematics and Computation*, Vol. **168**, pp. 962 - 972.
20. J. Wang, F. Bai and Y. Cheng (2011), "A meshless method for the nonlinear generalized regularized long wave equation", *Chin. Phys. B,* Vol. **20(3), 030206**, pp. 1 - 8.

PHƯƠNG PHÁP COLLOCATION VỚI B – SPLINE BẬC 7 GIẢI PHƯƠNG TRÌNH mGRLW

Tóm tắt: *Trong bài báo này, nghiệm số của phương trình mGRLW sẽ tìm được dựa trên cơ sở phương pháp mới sử dụng cơ sở B – spline bậc 7. Sử dụng phương pháp Von – Neumann hệ phương trình sai phân ổn định vô điều kiện. Thuật toán được với sóng đơn được áp dụng giải một số ví dụ. Kết quả số chứng tỏ phương pháp đưa ra hữu hiệu để giải phương trình trên.*

Từ khóa: *Phương trình mGRLW, spline bậc 7, phương pháp collocation, phương pháp sai phân hữu hạn.*

APPLICATIONS COMBINATORIAL THEORY IN TEACHING MATHS AT PRIMARY SCHOOLS

Dao Thi To Uyen[1], Nguyen Van Hao[2],
[1]*Department of Primary Education, Hanoi Pedagogical University*
[2]*Department of Mathematics, Hanoi Pedagogical University*

Abstract: *In this paper, we would like to present some applications combinatorial theory in teaching some elementary math form. Through this, teachers can guide students how to solve and how to present the solution in accordance with the characteristics and thinking of elementary students contributing to improve the quality of teaching and learning.*

Keywords*: Combinations, applications combinatorial theory.*

Email: nguyenvanhaodhsphn2@gmail.com
Received 11 April 2019
Accepted for publication 25 May 2019

1. INTRODUCTION AND PROBLEM

The level of elementary students is the beginning of intellectual development for children. At this level of schooling, students have been familiarized with mathematical concepts through simple math problems. In fact, these concepts are taken from the theory, the rules at the higher education levels. In some of that knowledge, we want to introduce the theory of combinations. Combination is an area that has been studied quite early and is interested in many fields of science. In this paper, we illustrate a deep understanding of this theory which is important in teaching some elementary math form.

2. CONTENTS

2.1. Preparation

To present some applications combinatorial theory to teach maths for primary teacher, we repeat some of the most basic knowledge about this concept.

2.1.1. Permutation of a combination

Give set A has n elements $(n \geq 1)$. When arranging this n elements in a certain order, we get an element of a new set and is called a permutation of set A.

The number of elements of the set A has n elements are denoted and defined by the formula

$$P_n = 1 \times 2 \times 3 \times ... \times n = n!$$

Example 1.1. A table has 5 students, changing their seat position arbitrarily, the number of arrangements is the permutation number of 5 children. So, we can calculate

$$P_5 = 5! = 120.$$

2.1.2. Concept of combination

Give set A has n elements and integer k with $1 \le k \le n$. Each subset of A has k elements called a convolution combination k of the set A

Thus, a convolution combination k of the set A is the taking of the k elements of this set regardless about the arrangement of the order of elements in it.

The number convolution combination k of the set A has n are denoted and defined by the formula

$$C_n^k = \frac{n!}{k!\left(n-k\right)!}$$

Example 1.2. Give set $A = \left\{x_1, x_2, x_3\right\}$. Then, the convolution combination 2 of 3 elements of the set A are

$$\left\{x_1, x_2\right\}; \left\{x_1, x_3\right\}; \left\{x_2, x_3\right\}$$

So, the number of element of this set corresponds to the formula

$$C_3^2 = \frac{3!}{2!(3-2)!} = 3$$

2.2. Some applications theory of combinations in teaching maths at primary schools

One of the weaknesses of students who are trained to teach maths at primary school often does not fully understand how to use advanced mathematical knowledge in solving elementary problems. The following section below, we would like to illustrate the use of combinatorial theory to find solutions and ways to present solutions to some problems of this type in accordance with perceptions of students

2.2.1. Analysing some geometry problems are applied combinatorial theory

Problem 1 $[2, \text{Problem } 5 \text{ - page } 42]$. How many triangles below?

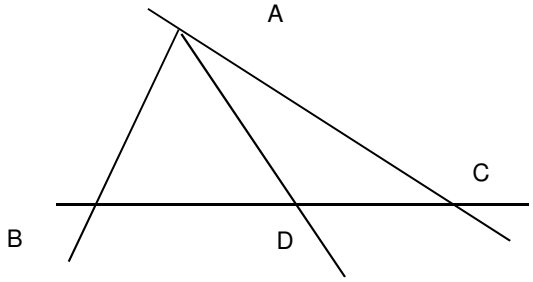

We present the solution of this problem by solving the problem at a higher level corresponding to the level of the students class 3 below.

Problem 2. How many triangles below ?

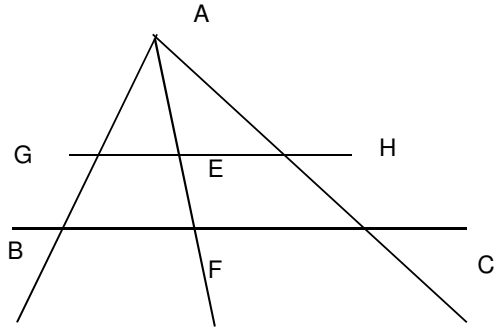

This is a problem for students class 3. Their perception is only intuitive, so counting the triangles can result in missing triangles.

Understanding from advanced math, we can analyze the problem as follows

$1.$ The straight line crosses GH or BC cuts two straight lines in a straight centerline A forming a triangle. Thus, the number of triangles created by two straight lines passing GH and BC cuts the straight lines through point A are equality. Therefore, we only need to count the triangles created by the line passing through BC and multiply by 2.

$2.$ From the straight line of centerline A, two straight lines with the straight line passing through BC create a triangle. So the number of triangles created here is the convolution combination 2 of 3 straight lines in the beam, it means $C_3^2 = 3$

3. The number of triangles are $2 \times C_3^2 = 6$

The guide for students class 3

1. The straight line crosses GH or BC cuts two straight lines from A forming a triangle. Thus, the number of triangles created by two straight lines passing GH and BC are equality. Therefore, we only need to count the triangles created by the line passing through BC and multiply by 2.

2. Matches point B in turn with point F and point C we get two triangles. Then we match F with C to get a triangle. Thus, the straight line passing through BC creates three triangles and so the number of triangles in the picture will be $2 \times 3 = 6$ triangles.

Problem 3. In the plane give 2018 distinguishing points, in which there are no three points in line. How many straight lines does we get from those points ?

Understanding from advanced math. Through two distinguishing points we get a straight line. So, the number of straight lines are created by 2018 points is the convolution combination 2 of 2018, it means C_{2018}^2

The guide for students

1. Numbering points in order from 1 to 2018.

2. Point 1 connects with the remaining 2017 points we get 2017 straight lines.

3. Point 2 connects with the remaining 2016 points we get 2016 straight lines.

4. The same as above point 2017 connects with final point 2018 we get 1 straight lines.

5. So, the number of the straight lines are

$$2017 + 2016 + ... + 2 + 1 = \frac{2017 \times 2018}{2} = 2\,035\,153$$

Problem 4 *(Exams for National Violympic Math 5 in 2013).* Teacher paints quadrangle $ABCD$. Then, teacher takes point E outside quadrangle $ABCD$. When we connect five points $A; B; C; D; E$ together, we get three quadrangles get four in five points $A; B; C; D; E$ to do the top. How many triangles does get three in five points $A; B; C; D; E$ to do the top ?

2.2.2 Analysing some arithmetic problems are applied combinatorial

In this section, we introduce some of the applied problems of combinatorial theory in finding solutions.

Problem 5 $[1,$ Example 1.1 - page $7]$. Give four numbers $0,1,2,3$. How many different four digit numbers from these four numbers ?

Problem 6 $[1,$ Example 1.2 - page $9]$. Give numbers $0,1,2,3,4$. From these five numbers

$a)$ How many four digit numbers ?

$b)$ How many four digit even numbers are there in which the hundreds digit is 2?

Problem 7 $[1,$ Problem 1 - page $20]$. Give five numbers $0,1,2,3,4$. How many different four digit numbers from these five numbers ?

Problem 8 $[1,$ Problem 2 – page $20]$. How many different three digit numbers ? Know that

$a)$ Digits is odd number ?

$b)$ Digits is even number ?

3. CONCLUSION

In this paper we present some applications of combinatorial theory in finding solutions and methods of presenting solutions in accordance with the level of elementary students.

4. THE PROPOSED

For pedagogical students they do not understand the meaning of combinatorial theory in teaching some elementary problems. Therefore, we need to apply the above research results so that teachers can guide students have appropriate solutions.

REFERENCES

1. Trần Diên Hiển (2016), *Bồi dưỡng học sinh giỏi toán tiểu học,* - Nxb Đại học Sư phạm.
2. Đỗ Đình Hoan (chủ biên), Nguyễn Ánh, Đỗ Trung Hiệu, Phạm Thanh Tâm (2009), *Toán 1*, - Nxb Giáo dục.
3. Nguyễn Đình Trí, Tạ Văn Đĩnh, Nguyễn Hồ Quỳnh (2009), *Toán cao cấp tập 1,*- Nxb Giáo dục.

ỨNG DỤNG LÍ THUYẾT TỔ HỢP TRONG DẠY HỌC TOÁN TIỂU HỌC

Tóm tắt: *Trong bài báo này, chúng tôi trình bày ứng dụng lý thuyết tổ hợp trong việc giải một số bài toán bậc tiểu học. Thông qua đó, giáo viên có thể định hướng cho học sinh cách giải và cách trình bày lời giải phù hợp với đặc điểm và tư duy của học sinh tiểu học, góp phần nâng cao chất lượng dạy và học.*

Từ khóa: *Tổ hợp, ứng dụng lý thuyết tổ hợp.*

RADION EFFECTS ON BHABHA SCATTERING

Ha Huy Bang, Pham Que Duong,
Nguyen Thi Thu Huyen, Nguyen Thi Thuy Linh
Ha Noi University of Sciences

Abstract: *In this article, we have considered the possible signatures of radion through Bhabha scattering. The numerical results show that the total cross section with radion effects are abont 0.62-0.65 pb.*

This could have inportant implications for radion searches and for the measurement of the cross – section of the Bhabha scattering.

PACS number: 12.60.Cn, 12.20.-m, 42.55.-f.

Keywords*: radion, Bhabha scattering.*

Email: hahuybang@hus.edu.vn
Received 24 March 2019
Accepted for publication 25 May 2019

1. INTRODUCTION

As well known, there are many convincing evidences that 80% of the matters in the universe is composed of dark matters (DM).

In several extensions of the Standard Model, radion or u-boson is postulated [1-5].

On the other hand, the Randall – Sundrum (RS) Model is one of the attractive condidates to solve the gauge hierarchy problem in the standard Model Many works have been done on the phenomenological aspects of radion in various colliders [6-9].

As we well known, Bhabha scattering is among the key processes in particle physics. Recently, the authors have presented the results of the SANC group on the complete one-loop calculation of the electroweak rediative corrections to Bhabha scattering with polarized beams [10].

Very recently, we have investigated unparticle effects on Bhabha scattering [11] and on axion-like particles production in e^+e^- collisions [12]. In this paper, we investigate virtual radion effects via Bhabha scattering.

2. RADION EXCHANGE AND CROSS SECTION

In this cestion, we will derive a formula for the cross-section of the process presented in Figure.2, which shows on of the possible processes, where a radion may intermediate a creation of e^+e^- in the e^+e^- scattering.

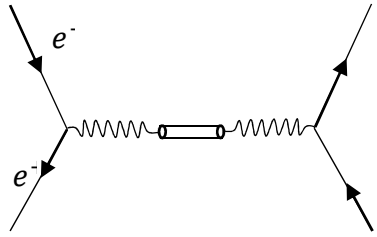

Fig 1. *Feynman diagram for Bhabha scattering via radion and photon*

The amplitude for this process is given by

$$M = \bar{v}(k_2) ie\gamma^\mu u(k_1) \frac{-ie^2(g_{\mu\nu} - q_\mu q_\nu / m_u^2)}{q^2 - m_u^2} \bar{u}(p_1) ie\gamma^\nu v(p_2)$$
$$= ie^2\varepsilon^2 \frac{(g_{\mu\nu} - q_\mu q_\nu / m_u^2)}{q^2 - m_u^2} \bar{v}(k_2)\gamma^\mu u(k_1)\bar{u}(p_1)\gamma^\mu v(p_2), \quad (1)$$

From this, we get

$$|M|^2 = \frac{16e^4\varepsilon^4}{(q^2 - m_u^2)^2} \{ 2(p_1k_1)(p_2k_2) + 2(p_1k_2)(p_2k_1)$$
$$- \frac{qk_2}{m_u^2}\left[(p_1k_1)(qp_2) + (qp_1)(p_2k_1) - 2(p_1p_2)(qk_1)\right]$$
$$- \frac{qk_1}{m_u^2}\left[(p_1k_2)(qp_2) + (qp_1)(p_2k_2) - 2(p_1p_2)(qk_2)\right]$$
$$+ 2\frac{k_1k_2}{m_u^2}\left[2(qp_1)(qp_2) - (p_1p_2)q^2\right] + 2\frac{(qk_1)(qk_2)}{m_u^4}\left[2(qp_1)(qp_2) - (p_1p_2)q^2\right]$$
$$- \frac{q^2(k_1k_2)}{m_u^4}\left[2(qp_1)(qp_2) - (p_1p_2)q^2\right] \} \quad (2)$$

In center of mass frame, four-moments of particles are defined

$$k_1 = (E, k), k_2 = (E, -k), p_1 = (E, p), p_2 = (E, -p)$$

and $$S = (k_1 + k_2)^2 = (p_1 + p_2)^2 = q^2 = 4E^2.$$

Where S is the center of mass energy.The differential cross-section can be obtained as follows.Neglecting the mass of electron, we have

$$|M|^2 = \frac{4e^4\varepsilon^4 s^2}{(q^2 - m_u^2)^2}\left(1+\cos^2\theta + \frac{s}{m_u^2}\right), \tag{3}$$

So, the differential cross section can be obtained as follows

$$\frac{d\sigma}{d\Omega} = \frac{\alpha^2\varepsilon^4 s}{4(q^2 - m_u^2)^2}\left(1+\cos^2\theta + \frac{s}{m_u^2}\right), \tag{4}$$

where

Therefore, the total cross section is

$$\sigma = \frac{\alpha^2\pi\varepsilon^4 s}{(q^2 - m_u^2)^2}\left(\frac{4}{3} + \frac{s}{m_u^2}\right). \tag{5}$$

Finally, from (4) and (5) we get

$$\frac{d\sigma}{\sigma d\Omega} = \frac{\left(1+\cos^2\theta + \frac{s}{m_u^2}\right)}{4\pi\left(\frac{4}{3} + \frac{s}{m_u^2}\right)} \tag{6}$$

Numerical results and discussions

Let us now turn to the numerical analysis. We take $\varepsilon = 10^{-2}, m_n = 10\,\text{GeV}$

As input parameters.

In Fig.2 we plot the $\frac{d\sigma}{\sigma d\Omega}$ with respect to $\cos\theta$. As we can observer from Fig.2 the $\frac{d\sigma}{\sigma d\Omega}$ has a minimum for $\cos\theta = 0$.

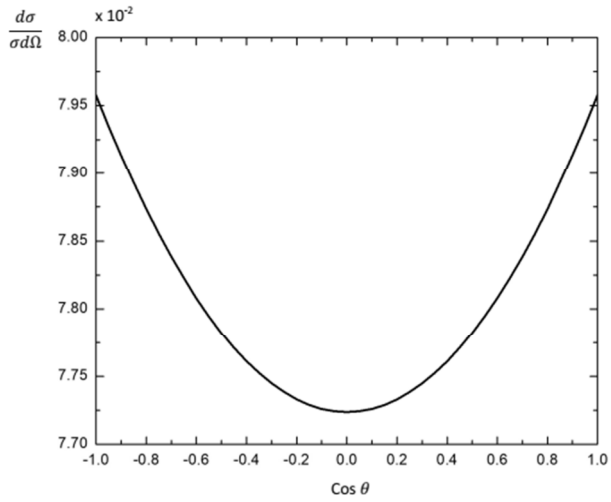

Fig 2. *The* $\frac{d\sigma}{\sigma d\Omega}$ *with respect to* $\cos\theta$.

Table 1. *The* $\frac{d\sigma}{\sigma d\Omega}$ *at different* $\cos\theta$

$\cos\theta$	-1.0	-0.8	-0.6	-0.4	-0.2	0.0	0.2	0.4	0.6	0.8	1.0
$\frac{d\sigma}{\sigma d\Omega}(\times 10^2)$	7.959	7.958	7.957	7.957	7.956	7.956	7.956	7.957	7.957	7.958	7.959

In the figure 3, we plot the differential cross sections and the toatal cross sections as a function of $\sqrt{s}$ for $\cos\theta = 1$

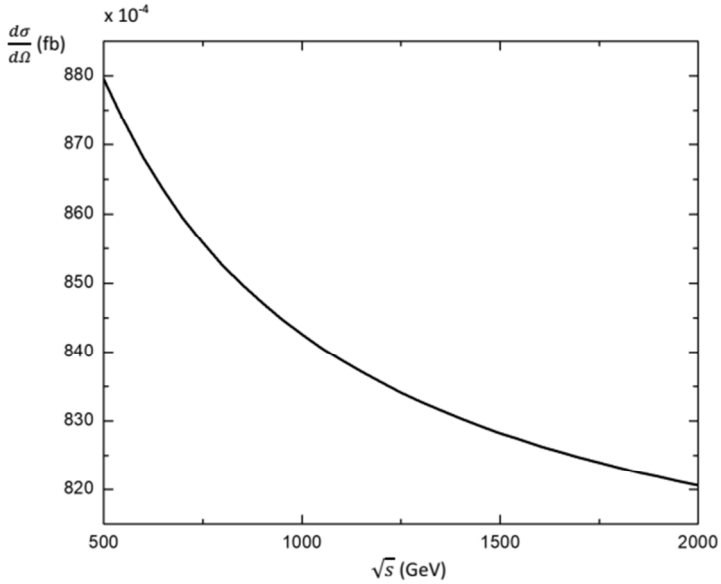

Fig 3. *The variation of* $\frac{d\sigma}{d\Omega}$ *as a function of* $\sqrt{s}$ *for* $\cos\theta = 1$

As we see from the Figure 3 that the radion effects quickly go down as $\sqrt{s}$ becomes larger.

In the following, we give the numerical values of the differential cross section with radion effects in Table 2.

Table 2. *The differential cross sections with radion effects for* $\cos\theta = 1$ *at different energies*

$\sqrt{s}$ GeV	500	650	800	950	1100	1250	1400	1550	1700	1850	2000
$\frac{d\sigma}{\sigma d\Omega}(\times 10^2)$	5.195	5.191	5.190	5.189	5.188	5.188	5.187	5.187	5.187	5.187	5.187

For the next step, we give the numerical values of the total cross-sections with radion effects at different energies in Figure 4 and Table 3.

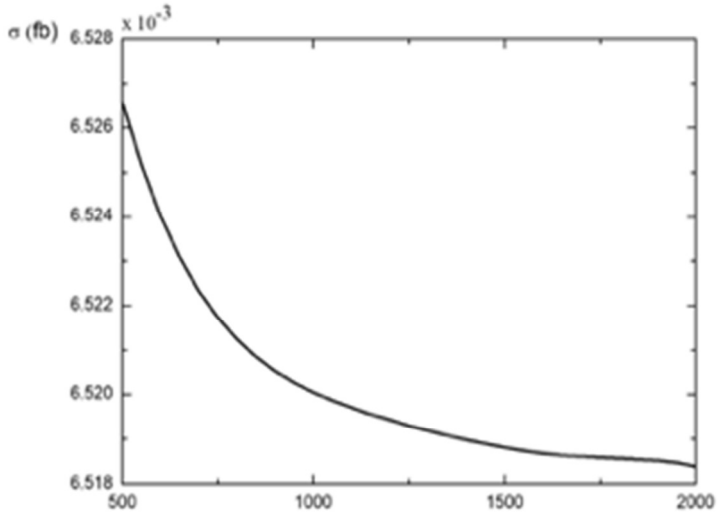

Fig 4. *The variation of* σ *as a function of* $\sqrt{s}$.

So, direct computations have showed that the total cross-sections should be about 0.006-0.007 fem to barn.

Therefore, in the range $\sqrt{s}$ =500GeV to 2000GeV the total cross-sections are slightly different.

Table 3. *The total cross sections with radion effects at different energies*

$\sqrt{s}$ GeV	500	650	800	950	1100	1250	1400	1550	1700	1850	2000
$\sigma \times 10^3 (fb)$	6.5266	6.5230	6.5213	6.5203	6.5197	6.5192	6.5190	6.5188	6.5186	6.5185	6.5184

3. CONCLUSION

Our results are attractive because of possible connection to radion. We hope that future experiments will confirm the existence of radion.

REFERENCES

1. R.Foot, X. G. He (1991), *Phys.Lett*. B 267, 509.
2. J. D. Bjorken, R. Essig, P. Schuster, and N. Toro (2009), *Phys. Rev.* D 80, 075018.
3. Davoudiasl, H. S. Lee and W. J. Marciano (2012), *Phys. Rev. Lett*. 109, 031802.
4. M.Anelli et al. [SHiP Collaboration], *arXiv:*1504.04956[physics.ins-det].
5. P. Ilten, Y. Soreq, J. Thaler, M. Williams and W. Xue, *Phys. Rev. Lett*. 116, no. 25, (2016) 251803 [arXiv:1603.08926 [help-ph]].
6. D.V. Soa, D.T.L. Thuy, N.H. Thao and T.D. Tham, Mod. *Phys. Lett*. A27 (2012) 1250126.

7. N. Desai, U. Maitra and B. Mukhopadhyay, *ar XIV*: 1307.3765.
8. Y. Ohno, *ar XIV*: 1402.7159.
9. G.C. Cho, Y. Ohno, *ar XIV*: 1404.1200.
10. Andrey Arubuzov, wt al. (LL2018), *proceedings of Science*, POS 010.
11. S.T.L. Anh, H.H. Bang et al (2018) , *Can. J. Phys*. 96:3 268.
12. S.T.L. Anh, H.H. Bang et al (2018), *Int. J. Theor. Phys* 149.

ẢNH HƯỞNG CỦA RADION LÊN TÁN XẠ BHABHA

Tóm tắt: *Trong bài báo này chúng tôi xem xét các tín hiệu của hạt radion qua tán xạ Bhabha. Các kết quả đánh giá số chỉ ra tiết diện tán dạ toàn phần với ảnh hưởng của radion là khoảng 0.62-0.65 pb. Điều này là quan trọng cho việc tìm kiếm radion và cho việc đo tiết diện tán xạ của tán xạ Bhabha.*

Từ khóa: *radion, tán xạ Bhabha*

INTERACTION ENERGY BETWEEN ELECTRONS AND LONGITUDINAL OPTICAL PHONON IN POLARIZED SEMICONDUCTOR QUANTUM WIRES

Dang Tran Chien
Hanoi University of Natural Resources & Environment

Abtract: *In this work we calculated the displacement of the lattice nodes in the quantum wire. Then building Hamilton's interaction between electrons and phonons in quantum wires and calculating dispersion expressions. Draw dispersion curves for modes p = 0 and wire with radius of 100 Å and 150 Å. Built an energy expression that interacts between the electron and the longitudinal optical phonon in polarized semiconductor quantum wires.*

Keywords: *Longitudinal optical phonon, dispersion expression, quantum wires, Hamilton*

Email: dtchien@hunre.edu.vn
Received 27 April 2019
Accepted for publication 25 May 2019

1. INTRODUCTION

Nowadays, with modern techniques in crystal culture, many material systems have been created with nanostructures. Low-dimensional system structure not only significantly changes many properties of materials, but also appears many new physical properties superior compared to conventional three-dimensional electron systems. Electrons and their vibrations are distorted because they become low-dimensional and low symmetry.

One of the methods for making quantum wires is to create alternating thin semiconductor layers. These semiconductor classes have different band gaps. Then by etching such as chemical corrosion, corrosion of plasma, we have a quantum wire.

There have been many authors studying on quantum wires in the world. Longitudinal optical oscillations (LO) and electron transfer rate are calculated in [5, 6], the electron scattering rate in rectangular quantum wire in [1-4] etc… In semi-conductive material polarized conductors (Polar-semiconductor), electrons mainly interact with longitudinal optical phonons. But the energy interaction between electrons and phonons in quantum wires has not been studied much.

So this paper will focus on calculation of energy interaction between electrons and longitudinal optical phonons in GaAs/AlGaAs polarized semiconductor quantum wires.

2. CALCULATIONS

2.1. Oscillations in a quantum wire

Here the cylindrical coordinate system was applied

$$[\nabla^2 + k_i^2]\mathbf{u}^L = 0 \tag{1}$$

Where $\mathbf{u}^L$ was denoted as longituadinal oscillation

$$\left(\frac{1}{r}\frac{\partial}{\partial r} + \frac{\partial^2}{\partial r^2} + \frac{1}{r^2}\frac{\partial^2}{\partial \varphi^2} + \frac{\partial^2}{\partial z^2} + \mathbf{k}_i^2\right)\mathbf{u}^{\mathbf{L}} = 0 \tag{2}$$

The solution of the equation (2) was written as follows:

$$\mathbf{u}^{(L)}(r,\varphi,z) = \mathbf{A}.\mathrm{u}^{(L)}(r).e^{ip\varphi}.e^{i\mathbf{q}_z z}e^{-i\omega t} \tag{3}$$

Put (3) into (2) we have:

$$\frac{\partial^2}{\partial r^2}\mathrm{u}^{(L)}(r) + \frac{1}{r}\frac{\partial}{\partial r}\mathrm{u}^{(L)}(r) - \frac{p^2}{r^2}\mathrm{u}^{(L)}(r) - \mathbf{q}_z{}^2\mathrm{u}^{(L)}(r) + \mathbf{k}_i{}^2\mathrm{u}^{(L)}(r) = 0 \tag{4}$$

Due to differential equation (4) has only *r* variable so we have:

$$\frac{d^2}{dr^2}\mathrm{u}^{(L)}(r) + \frac{1}{r}\frac{d}{dr}\mathrm{u}^{(L)}(r) + \left(-\frac{p^2}{r^2} - \mathbf{q}_\mathbf{z}^2 + \mathbf{k}_i^2\right)\mathrm{u}^{(L)}(r) = 0$$

$$\mathbf{q}_i^2 = \mathbf{k}_i^2 - \mathbf{q}_\mathbf{z}{}^2 = (\omega_L^2 - \omega^2)\beta^{-2} - \mathbf{q}_\mathbf{z}{}^2$$

$$\frac{d^2}{dr^2}\mathrm{u}^{(L)}(r) + \frac{1}{r}\frac{d}{dr}\mathrm{u}^{(L)}(r) + \left(\mathbf{q}_i^2 - \frac{p^2}{r^2}\right)\mathrm{u}^{(L)}(r) = 0 \tag{5}$$

Put $\boldsymbol{\chi}_{ps} = \mathbf{q}_\mathbf{i} r$, equantion (5) changes into

$$\frac{d^2}{d\boldsymbol{\chi}_{ps}^2}\mathrm{u}^{(L)}(r) + \frac{1}{\boldsymbol{\chi}_{ps}}\frac{d}{d\boldsymbol{\chi}_{ps}}\mathrm{u}^{(L)}(r) + (1 - \frac{p^2}{\boldsymbol{\chi}_{ps}^2})\mathrm{u}^{(L)}(r) = 0 \tag{6}$$

$J_p(\chi_{p\mathbf{s}})$ in the solution to the modified Bessel's equation is referred to as a modified Bessel function of the first kind.

The second material area, the solution of the second region is Hankel function

$$H_p\left(\boldsymbol{\chi}_{ps}\right) = J_p\left(\boldsymbol{\chi}_{ps}\right) + iN_p\left(\boldsymbol{\chi}_{ps}\right)$$

For the first material area, the solution was:

$$\mathbf{u}^{(L)}(r,\varphi,z)=\mathbf{A}J_p\left(\chi_{ps}\right)e^{ip\varphi}e^{i\mathbf{q}_z z}e^{-i\omega t}$$

Longituadinal Optical (LO) mode satisfies the condition:

$$\left[\nabla.\mathbf{u}\right]=0$$

In cylindrical coordinate system

$$\left[\nabla.\mathbf{u}\right]=\frac{1}{r}\left[\frac{\partial}{\partial\varphi}\mathrm{u}_z^{(L)}(r,\varphi,z)-\frac{\partial}{\partial z}\left(r\mathrm{u}_\varphi^{(L)}(r,\varphi,z)\right)\right].\mathbf{e}_r+\left[\frac{\partial}{\partial z}\mathrm{u}_r^{(L)}(r,\varphi,z)-\frac{\partial}{\partial r}\mathrm{u}_z^{(L)}(r,\varphi,z)\right].\mathbf{e}_\varphi+$$
$$+\frac{1}{r}\left[\frac{\partial}{\partial r}\left(r\mathrm{u}_\varphi^{(L)}(r,\varphi,z)\right)-\frac{\partial}{\partial\varphi}\mathrm{u}_r^{(L)}(r,\varphi,z)\right].\mathbf{e}_z=0 \quad (7)$$

The axial unit vectors are linearly independent for each other so from (7), we obtain the following system of equations:

$$\begin{cases}\dfrac{\partial}{\partial\varphi}\mathrm{u}_z^{(L)}(r,\varphi,z)-r\dfrac{\partial}{\partial z}\mathrm{u}_\varphi^{(L)}(r,\varphi,z)=0\\ \dfrac{\partial}{\partial z}\mathrm{u}_r^{(L)}(r,\varphi,z)-\dfrac{\partial}{\partial r}\mathrm{u}_z^{(L)}(r,\varphi,z)=0\\ \mathrm{u}_\varphi^{(L)}(r,\varphi,z)+r\dfrac{\partial}{\partial r}\mathrm{u}_\varphi^{(L)}(r,\varphi,z)-\dfrac{\partial}{\partial\varphi}\mathrm{u}_r^{(L)}(r,\varphi,z)=0\end{cases} \quad (8)$$

With some calcultion we obtained the equation for the ion displacement of the LO mode in the quantum wire as follows:

$$\begin{cases}\mathrm{u}_r^{1L}=\dfrac{-i\mathbf{q}_1}{\mathbf{q}_z}\mathrm{A}_z J_p'\left(\mathbf{q}_1 r\right)e^{ip\varphi}e^{i\mathbf{q}_z z}e^{-i\omega t}\\ \mathrm{u}_\varphi^{1L}=\dfrac{p}{r\mathbf{q}_z}\mathrm{A}_z J_p\left(\mathbf{q}_1 r\right)e^{ip\varphi}e^{i\mathbf{q}_z z}e^{-i\omega t}\\ \mathrm{u}_z^{1L}=\mathrm{A}_z J_p\left(\mathbf{q}_1 r\right)e^{ip\varphi}e^{i\mathbf{q}_z z}e^{-i\omega t}\end{cases} \quad (9)$$

For the second material area, the motion equation for the node is also satisfied as for region 1. At the same time, the Hankel function with the derivative is completely similar to the Bessel function, so we have:

$$\begin{cases}\mathrm{u}_r^{2L}=\dfrac{-i\mathbf{q}_2}{\mathbf{q}_z}\mathrm{A}_{2z}H_p'\left(\mathbf{q}_2 r\right)e^{ip\varphi}e^{i\mathbf{q}_z z}e^{-i\omega t}\\ \mathrm{u}_\varphi^{2L}=\dfrac{p}{r\mathbf{q}_z}\mathrm{A}_{2z}H_p\left(\mathbf{q}_2 r\right)e^{ip\varphi}e^{i\mathbf{q}_z z}e^{-i\omega t}\\ \mathrm{u}_z^{2L}=\mathrm{A}_{2z}H_p\left(\mathbf{q}_2 r\right)e^{ip\varphi}e^{i\mathbf{q}_z z}e^{-i\omega t}\end{cases} \quad (10)$$

2.2. The dispersion equations

Applying continuous boundary conditions that is the perpendicular velocity component ie the direction of r continuously and the pressure at the interface is continuous.

Let $\beta = \frac{\beta_1^2}{\beta_2^2}$ where β_1, β_2 sound velocity parameters in the material area 1, 2. ρ_1 , ρ_2 denote mass density in the area of material 1,2. If we let:

$$A_{1z} = A^{(1)}, \quad A_{2z} = A^{(2)}; \overline{\rho} = \frac{\rho_1}{\rho_2}$$

Applied the continuous conditions of pressure at the interface, we have

$$\beta^2 \sqrt{\overline{\rho}} \nabla . \mathbf{u}^{1L}\Big|_{r=R_0} = \nabla . \mathbf{u}^{2L}\Big|_{r=R_0} \tag{11}$$

Put equations (9), (10) into (11), we obtained:

$$\nabla . \mathbf{u}^{1L} = \frac{1}{r} \mathrm{u}_r^{1L}(r,\varphi,z) + \frac{\partial}{\partial r} \mathrm{u}_r^{1L}(r,\varphi,z) + \frac{1}{r}\frac{\partial}{\partial \varphi} \mathrm{u}_\varphi^{1L}(r,\varphi,z) + \frac{\partial}{\partial z} \mathrm{u}_z^{1L}(r,\varphi,z)$$

$$\nabla . \mathbf{u}^{1L}\Big|_{r=R_0} = -iA^{(1)} \left\{ \frac{\mathbf{q_1^2}}{\mathbf{q_z}} J_p^{''}(\mathbf{q_1}R_0) + \frac{\mathbf{q_1}}{\mathbf{q_z}R_0} J_p^{'}(\mathbf{q_1}R_0) - \left[\frac{p^2}{\mathbf{q_z}R_0^{\,2}} + \mathbf{q_z} \right] J_p(\mathbf{q_1}R_0) \right\} e^{ip\varphi} e^{i\mathbf{q_z}z}\, e^{-i\omega t}$$

Do the same for the second area we have:

$$\nabla . \mathbf{u}^{2L}\Big|_{r=R_0} = -iA^{(2)} \left\{ \frac{\mathbf{q_2}^{\,2}}{\mathbf{q_z}} H_p^{''}(\mathbf{q_2}R_0) + \frac{\mathbf{q_2}}{\mathbf{q_z}R_0} H_p^{'}(\mathbf{q_2}R_0) - \left[\frac{p^2}{\mathbf{q_z}R_0^{\,2}} + \mathbf{q_z} \right] H_p(\mathbf{q_2}R_0) \right\} e^{ip\varphi} e^{i\mathbf{q_z}z} e^{-i\omega t}$$

from (11) one gets

$$\begin{aligned}
&\beta^2 \sqrt{\overline{\rho}} A^{(1)} \left\{ \frac{\mathbf{q_1^2}}{\mathbf{q_z}} J_p^{''}(\mathbf{q_1}R_0) + \frac{\mathbf{q_1}}{\mathbf{q_z}R_0} J_p^{'}(\mathbf{q_1}R_0) - \left[\frac{p^2}{\mathbf{q_z}R_0^{\,2}} + \mathbf{q_z} \right] J_p(\mathbf{q_1}R_0) \right\} = \\
&\quad = A^{(2)} \left\{ \frac{\mathbf{q_2}^{\,2}}{\mathbf{q_z}} H_p^{''}(\mathbf{q_2}R_0) + \frac{\mathbf{q_2}}{\mathbf{q_z}R_0} H_p^{'}(\mathbf{q_2}R_0) - \left[\frac{p^2}{\mathbf{q_z}R_0^{\,2}} + \mathbf{q_z} \right] H_p(\mathbf{q_2}R_0) \right\} \\
&\beta^2 \sqrt{\overline{\rho}} A^{(1)} \left\{ \frac{\mathbf{q_1^2}}{\mathbf{q_z}} J_p^{''}(\mathbf{q_1}R_0) + \frac{\mathbf{q_1}}{\mathbf{q_z}R_0} J_p^{'}(\mathbf{q_1}R_0) - \left[\frac{p^2}{\mathbf{q_z}R_0^{\,2}} + \mathbf{q_z} \right] J_p(\mathbf{q_1}R_0) \right\} = \\
&\quad = A^{(2)} \left\{ \frac{\mathbf{q_2}^{\,2}}{\mathbf{q_z}} H_p^{''}(\mathbf{q_2}R_0) + \frac{\mathbf{q_2}}{\mathbf{q_z}R_0} H_p^{'}(\mathbf{q_2}R_0) - \left[\frac{p^2}{\mathbf{q_z}R_0^{\,2}} + \mathbf{q_z} \right] H_p(\mathbf{q_2}R_0) \right\}
\end{aligned} \tag{12}$$

From the continuous velocity conditions, we put the expressions (9) and (10) into

$$\rho_1^{-1/2} \dot{\mathbf{u}}_r^{1L}\Big|_{r=R_0} = \rho_2^{-1/2} \dot{\mathbf{u}}_r^{2L}\Big|_{r=R_0} \tag{13}$$

Then taking the simple derivative and transformation, we have:

$$\frac{1}{\sqrt{\rho}} A^{(1)} \mathbf{q}_1 J_p^{'}(\mathbf{q}_1 R_0) - A^{(2)} \mathbf{q}_2 H_p^{'}(\mathbf{q}_2 R_0) = 0 \tag{14}$$

from (12) and (14), we have a equation system as below:

$$\begin{cases} \beta^2 \sqrt{\rho} A^{(1)} \left(\frac{\mathbf{q}_1^2}{\mathbf{q}_z} J_p^{''}(\mathbf{q}_1 R_0) + \frac{\mathbf{q}_1}{\mathbf{q}_z R_0} J_p^{'}(\mathbf{q}_1 R_0) - \left[\frac{p^2}{\mathbf{q}_z R_0^{\,2}} + \mathbf{q}_z \right] J_p(\mathbf{q}_1 R_0) \right) - \\ -A^{(2)} \left(\frac{\mathbf{q}_2^{\,2}}{\mathbf{q}_z} H_p^{''}(\mathbf{q}_2 R_0) + \frac{\mathbf{q}_2}{\mathbf{q}_z R_0} H_p^{'}(\mathbf{q}_2 R_0) - \left[\frac{p^2}{\mathbf{q}_z R_0^{\,2}} + \mathbf{q}_z \right] H_p(\mathbf{q}_2 R_0) \right) = 0 \\ \frac{1}{\sqrt{\rho}} A^{(1)} \mathbf{q}_1 J_p^{'}(\mathbf{q}_1 R_0) - A^{(2)} \mathbf{q}_2 H_p^{'}(\mathbf{q}_2 R_0) = 0 \end{cases} \tag{15}$$

From equation (14), we have:

$$A^{(2)} = \frac{A^{(1)} \mathbf{q}_1 J_p^{'}(\mathbf{q}_1 R_0)}{\mathbf{q}_2 H_p^{'}(\mathbf{q}_2 R_0) \sqrt{\rho}}$$

$$\tau = \frac{\mathbf{q}_1 J_p^{'}(\mathbf{q}_1 R_0)}{\mathbf{q}_2 H_p^{'}(\mathbf{q}_2 R_0) \sqrt{\rho}}$$

It leads to

$$A^{(2)} = A^{(1)} \tau$$

For the equation (15) to have a non-trivial solution, its determinant must be zero ie:

$$\begin{vmatrix} \beta^2 \sqrt{\rho} \left(\frac{\mathbf{q}_1^2}{\mathbf{q}_z} J_p^{''}(\mathbf{q}_1 R_0) + \right. & - \left(\frac{\mathbf{q}_2^{\,2}}{\mathbf{q}_z} H_p^{''}(\mathbf{q}_2 R_0) + \frac{\mathbf{q}_2}{\mathbf{q}_z R_0} H_p^{'}(\mathbf{q}_2 R_0) - \right. \\ \left. + \frac{\mathbf{q}_1}{\mathbf{q}_z R_0} J_p^{'}(\mathbf{q}_1 R_0) - \left[\frac{p^2}{\mathbf{q}_z R_0^{\,2}} + \mathbf{q}_z \right] J_p(\mathbf{q}_1 R_0) \right) & \left. - \left[\frac{p^2}{\mathbf{q}_z R_0^{\,2}} + \mathbf{q}_z \right] H_p(\mathbf{q}_2 R_0) \right) \\ \frac{1}{\sqrt{\rho}} \mathbf{q}_1 J_p^{'}(\mathbf{q}_1 R_0) & -\mathbf{q}_2 H_p^{'}(\mathbf{q}_2 R_0) \end{vmatrix} = 0$$

Use the properties of the Bessel function and transform, we have the dispersion expression for the (LO) mode as follows:

$$\overline{\rho} \mathbf{q}_2 (\omega_1^2 - \omega^2) J_p(\mathbf{q}_1 R_0) H_p^{'}(\mathbf{q}_2 R_0) = \mathbf{q}_1 (\omega_2^2 - \omega^2) H_p(\mathbf{q}_2 R_0) J_p^{'}(\mathbf{q}_1 R_0) \tag{16}$$

Applied (16) for a quantum wire $Ga\mathrm{As}/\mathrm{Al}_{0.3}Ga_{0.7}\mathrm{As}$ with parameters as followings:

$$\omega_1 = 292.8 cm^{-1}; \quad \omega_2 = 0.95\omega_1; \; \beta_1 = 4.73 \times 10^3 ms^{-1}; \quad \beta_2 = 1.06\beta_1; \; \overline{\rho} = 1.11$$

For mode p=0, the quantum wire with radius R_o=100 Å, 150 Å, the dispersion curves were shown in **Fig**.1a and **Fig**. 1b, respectively.

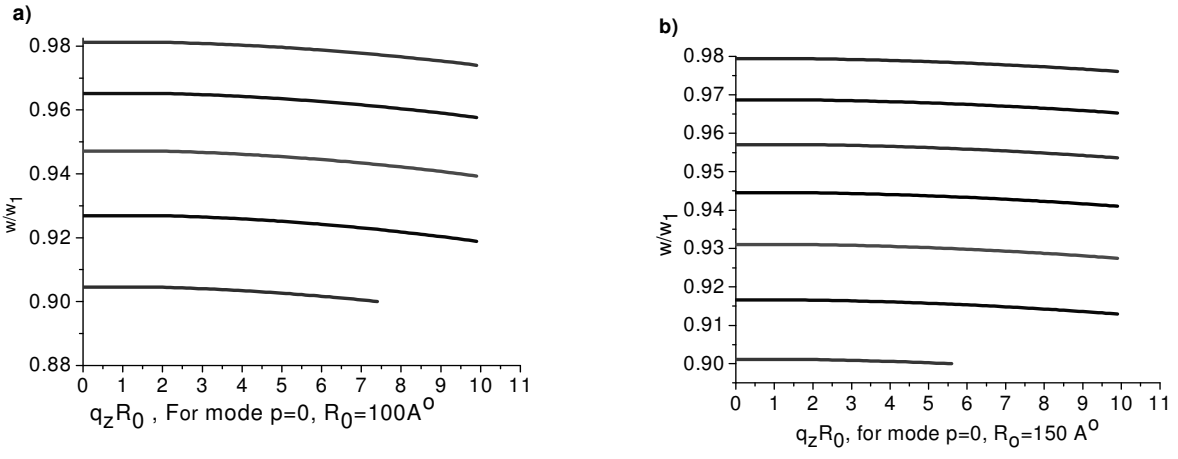

Fig 1. *The dispersion curves of the quantum wire with radius R_o 150 Å (a) and 100 Å (b).*

As can be seen from Figure 1, in the wire with radius R_o=100 Å, the phonon energy is quantized and separated into 5 energy levels farther apart. In the wire with radius R_o=150 Å, the energy is separated into 7 close levels.

2.3. Potential interaction

LO oscillation generated electric field which was calculated by the formula*:*

$$\mathbf{E} = -grad\phi \tag{17}$$

In the our situaion, electric field was written as below:

$$\mathbf{E} = -\rho_{oi}\mathbf{u}^{iL} \tag{18}$$

Where ρ_{oi} denote bulk charge density in material area *i*, $\mathbf{u}^{\mathbf{iL}}$ denote equations in (9), (10). In cylindrical coordinate, *grad*ϕ can be written as:

$$grad\phi = \boldsymbol{e}_r \frac{\partial \phi_i}{\partial r} + \boldsymbol{e}_\varphi \frac{1}{r}\frac{\partial \phi_i}{\partial \varphi} + \boldsymbol{e}_z \frac{\partial \phi_i}{\partial z} \tag{19}$$

From (17), (18) and take note of (19), we have:

$$\boldsymbol{e}_r \frac{\partial \phi_i}{\partial r} + \boldsymbol{e}_\varphi \frac{1}{r}\frac{\partial \phi_i}{\partial \varphi} + \boldsymbol{e}_z \frac{\partial \phi_i}{\partial z} = \rho_{0i}\mathbf{u}^{iL} \tag{20}$$
$$i = 1, 2$$

Put equation (9) into (20), we obtained equations for area 1

$$\begin{aligned}\frac{\partial\phi_1}{\partial r} &= \mathrm{A}^{(1)}\rho_{01}\frac{i\mathbf{q_1}}{\mathbf{q_z}}e^{ip\varphi}e^{i\mathbf{q}_z z}e^{-i\omega t}J_p'(\mathbf{q_1}r)\\ \frac{1}{r}\frac{\partial\phi_1}{\partial\varphi} &= -\mathrm{A}^{(1)}\rho_{01}\frac{p}{\mathbf{q_z}r}e^{ip\varphi}e^{i\mathbf{q}_z z}e^{-i\omega t}J_p(\mathbf{q_1}r)\\ \frac{\partial\phi_1}{\partial z} &= -\mathrm{A}^{(1)}\rho_{01}e^{ip\varphi}e^{i\mathbf{q}_z z}e^{-i\omega t}J_p(\mathbf{q_1}r)\end{aligned} \quad (21)$$

Taking integrals and transformations we have the potential interaction for the material area 1 as follows:

$$\phi_1 = A^{(1)}\rho_{01}\frac{i}{\mathbf{q_z}}J_p(\mathbf{q_1}r)e^{ip\varphi}e^{i\mathbf{q}_z z}e^{-i\omega t} \quad (22)$$

Completely similar, we can calculate the interaction potential for material area 2 as follows

$$\phi_2 = \tau\rho_{02}A^{(1)}\frac{i}{\mathbf{q_z}}H_p(\mathbf{q_2}r)e^{ip\varphi}e^{i\mathbf{q}_z z}e^{-i\omega t} \quad (23)$$

2.4. Hamilton interaction

We determine Hamilton's interaction between electrons and phonon in the form of Fröhlich:

$$H_{\text{int}} = -e\phi \quad (24)$$

Put equation (22) and (23) into equation (24), we have a Hamiltonian equation as follows:

$$\mathbf{H_{int}} = \begin{cases} -e\mathrm{A}\rho_{01}\dfrac{i}{\mathbf{q_z}}J_p(\mathbf{q_1}r)e^{iP\varphi}e^{i\mathbf{q}_z z}e^{-i\omega t}\left\{\hat{a}^+ + \hat{a}\right\} & khi\ \mathrm{r}<R_0 \\ -e\mathrm{A}\tau\rho_{02}\dfrac{i}{\mathbf{q_z}}H_p(\mathbf{q_2}r)e^{ip\varphi}e^{i\mathbf{q}_z z}e^{-i\omega t}\left\{\hat{a}^+ + \hat{a}\right\} & khi\ \mathrm{r}>R_0 \end{cases} \quad (25)$$

$$\mathbf{H_{int}} = -e\mathrm{A}\frac{i}{\mathbf{q_z}}\left[\begin{matrix}\rho_{01}J_p(\mathbf{q_1}r)\theta\left(R_0 - r\right)+ \\ +\tau\rho_{02}H_p(\mathbf{q_2}r)\theta\left(r - R_0\right)\end{matrix}\right]e^{iP\varphi}e^{i\mathbf{q}_z z}e^{-i\omega t}\left\{\hat{a}^+ + \hat{a}\right\} \quad (26)$$

$$\theta\left(R_0 - r\right) = \begin{cases} 0 \text{ when } \mathrm{r}>R_0 \\ 1 \text{ when } \mathrm{r}<R_0 \end{cases}; \qquad \theta\left(r - R_0\right) = \begin{cases} 0 \text{ when } \mathrm{r}<R_0 \\ 1 \text{ when } \mathrm{r}>R_0 \end{cases}$$

If we let

$$\mathbb{Z} = -e\mathrm{A}\frac{i}{\mathbf{q_z}}\left[\rho_{01}J_p(\mathbf{q_1}r)\theta\left(R_0 - r\right) + \tau\rho_{02}H_p(\mathbf{q_2}r)\theta\left(r - R_0\right)\right]e^{iP\varphi}e^{i\mathbf{q}_z z}e^{-i\omega t}$$

Hamiltonian interaction equation will be:

$$\mathbf{H}_{\mathbf{int}} = -\mathbb{Z}\left\{\hat{a}^{+} + \hat{a}\right\} \tag{27}$$

2.5. Interaction energy between electrons and LO

Energy expression

$$E = E_0^{(0)} + E_0^{(1)} + E_0^{(2)} + ...$$

We limit our consideration to the quadratic effect of energy as the fundamental energy. According to the perturbation theory, we have

$$E_0^{(1)} = \langle 0,0 | H_{\text{int}} | 0,0 \rangle \tag{28}$$

Where $|0,0\rangle$ is the fundamental status decribed electrons in lowest energy level and there is not any phonons with m =0, n=1, $\mathbf{k}_z$ =0:

$$|0,0\rangle \equiv |0\rangle = \frac{1}{J_1(\boldsymbol{\chi}_{01})\sqrt{R_0^{\,2}\pi L}} J_0\left(\frac{\boldsymbol{\chi}_{01}}{R_0} r\right) \tag{29}$$

Put (27) into (28), we obtained:

$$\begin{aligned} E_0^{(1)} = -\langle 0,0 | \mathbb{Z}(\hat{a}^{+} + \hat{a}) | 0,0 \rangle &= -\langle 0,0 | \mathbb{Z}\hat{a}^{+} | 0,0 \rangle - \langle 0,0 | \mathbb{Z}\hat{a} | 0,0 \rangle \\ &= -\langle 0,0 | \mathbb{Z} | 1,0 \rangle - \langle 0,0 | \mathbb{Z}\hat{a} | 0,0 \rangle = 0 \end{aligned}$$

Energy regulation in quadratic approximation

$$E_0^{(2)} = \sum \frac{\left| < 0,0 | \mathbf{H}_{\mathbf{int}} | \mathbf{k}, \mathbf{q} > \right|^2}{E_{|0,0\rangle}^{(0)} - E_{|\mathbf{k},1>}^{(0)}} \tag{30}$$

Xét $|\mathbf{k},\mathbf{1}>$ is the status where electrons in status with *m, n,* $\mathbf{k}_z$ and 1 phonon in the status p,s,q_z that contributed into $E_0^{(2)}$. So the equation (30) becomes to

$$E_0^{(2)} = \sum \frac{\left| < 0,0 | \mathbf{H}_{\mathbf{int}} | \mathbf{k},1 > \right|^2}{E_{|0,0\rangle}^{(0)} - E_{|\mathbf{k},1>}^{(0)}} \tag{31}$$

Where $|\mathbf{k},0\rangle \equiv |\mathbf{k}\rangle$. Put (27) into (31), one can get:

$$E_0^{(2)} = \sum \frac{\left| < 0,0 | \mathbb{Z}\left\{\hat{a}^{+} + \hat{a}\right\} | \mathbf{k},1 > \right|^2}{E_{|0,0\rangle}^{(0)} - E_{|\mathbf{k},1>}^{(0)}} = \sum \frac{\left| < 0,0 | \mathbb{Z}\hat{a}^{+} | \mathbf{k},1 > \right|^2}{E_{|0,0\rangle}^{(0)} - E_{|\mathbf{k},1>}^{(0)}} + \sum \frac{\left| < 0,0 | \mathbb{Z}\hat{a} | \mathbf{k},1 > \right|^2}{E_{|0,0\rangle}^{(0)} - E_{|\mathbf{k},1>}^{(0)}} \tag{32}$$

It is easy to see that the first term of (32) is zero. The second term becomes to

$$\sum \frac{\left|<0,0|\,\mathbb{Z}\hat{a}\,|\mathbf{k},1>\right|^2}{E^{(0)}_{|0,0\rangle}-E^{(0)}_{|\mathbf{k},1>}}=\sum \frac{\left|<0,0|\,\mathbb{Z}|\mathbf{k},0>\right|^2}{E^{(0)}_{|0,0\rangle}-E^{(0)}_{|\mathbf{k},1>}}$$

So (32) can be written as follows:

$$E_0^{(2)}=\sum \frac{\left|<0,0|\,\mathbb{Z}|\mathbf{k},0>\right|^2}{E^{(0)}_{|0,0\rangle}-E^{(0)}_{|\mathbf{k},1>}} \tag{33}$$

$$T=\left|<0,0|\,\mathbb{Z}|\mathbf{k},0>\right| \tag{34}$$

$$T=\left(\frac{2eA}{\mathbf{k_z}R_0{}^2J_1(\boldsymbol{\chi}_{01})J_{m+1}(\boldsymbol{\chi}_{mn})}\right)^2\left|\begin{array}{l}\rho_{01}\int_0^{R_0}J_0(\frac{\boldsymbol{\chi}_{01}}{R_0}r)J_m(\frac{\boldsymbol{\chi}^{(1)}_{-ms}}{R_0}r)J_m(\frac{\boldsymbol{\chi}_{mn}}{R_0}r)rdr+\\ +\tau\rho_{02}\int_{R_0}^{\infty}J_0(\frac{\boldsymbol{\chi}_{01}}{R_0}r)H_m(\frac{\boldsymbol{\chi}^{(2)}_{-ms}}{R_0}r)J_m(\frac{\boldsymbol{\chi}_{mn}}{R_0}r)rdr\end{array}\right|^2$$

Where

$$\left(\mathbf{q_1^2}\right)_{mn}=\left(\omega_1^2-\ \omega^2\right)\beta_1^{-2}-\mathbf{k}_z^2$$
$$\left(\mathbf{q_2^2}\right)_{mn}=\left(\omega_2^2-\ \omega^2\right)\beta_2^{-2}-\mathbf{k}_z^2$$

Electron energy in a quantum wire can be expressed as below:

$$E_T=\frac{\hbar^2\mathbf{k}_z^2}{2m^*}+\frac{\hbar^2\boldsymbol{\chi}_{mn}^2}{2m^*R_0{}^2} \tag{34}$$

Electron energy in the fundamental status is

$$E^{(0)}_{|0,0\rangle}=\frac{\hbar^2\boldsymbol{\chi}_{01}^2}{2m*R_0{}^2} \tag{35}$$

Electron-phonon energy at status $|\mathbf{k},1\rangle$

$$E^{(0)}_{|\mathbf{k},1\rangle}=\frac{\hbar^2\mathbf{k}_z^2}{2m*}+\frac{\hbar^2\boldsymbol{\chi}_{mn}^2}{R_0{}^2 2m*}+\frac{1}{2}\hbar\omega \tag{36}$$

With

$$\omega=\left\{\omega_1^2-\beta_1^2\left[\left(\mathbf{q_1^2}\right)_{mn}+\mathbf{k}_z^2\right]\right\}^{1/2} \tag{37}$$

If we let denominator of equation (33) be MS

$$MS = \frac{\hbar^2 \mathbf{k}_z^2}{2m^*} + \frac{\hbar^2}{2m^* R_0^{\,2}}\left(\boldsymbol{\chi}_{mn}^2 - \boldsymbol{\chi}_{01}^2\right) + \frac{\hbar}{2}\left\{\omega_1^2 - \beta_1^2\left[\left(\mathbf{q}_1^2\right)_{mn} + \mathbf{k}_z^2\right]\right\}^{1/2} \quad (38)$$

We can get the energy regulation as follws:

$$\left(\frac{2eA}{\mathbf{k}_z R_0^{\,2} J_1(\boldsymbol{\chi}_{01}) J_{m+1}(\boldsymbol{\chi}_{mn})}\right)^2 \left| \begin{array}{l} \rho_{01} \int_0^{R_0} J_0\left(\frac{\boldsymbol{\chi}_{01}}{R_0} r\right) J_m\left(\frac{\boldsymbol{\chi}_{-ms}^{(1)}}{R_0} r\right) J_m\left(\frac{\boldsymbol{\chi}_{mn}}{R_0} r\right) r dr + \\ + \tau\rho_{02} \int_{R_0}^{\infty} J_0\left(\frac{\boldsymbol{\chi}_{01}}{R_0} r\right) H_m\left(\frac{\boldsymbol{\chi}_{-ms}^{(2)}}{R_0} r\right) J_m\left(\frac{\boldsymbol{\chi}_{mn}}{R_0} r\right) r dr \end{array} \right|^2$$

$$E_0^{(2)} = \sum_{m,n,s,k_z} \frac{}{\frac{\hbar^2 \mathbf{k}_z^2}{2m^*} + \frac{\hbar^2}{2m^* R_0^{\,2}}\left(\boldsymbol{\chi}_{mn}^2 - \boldsymbol{\chi}_{01}^2\right) + \frac{\hbar}{2}\left\{\omega_1^2 - \beta_1^2\left[\left(\mathbf{q}_1^2\right)_{mn} + \mathbf{k}_z^2\right]\right\}^{1/2}}$$

Finally we have the interactive energy of the electron and phonon in the quantum wire

$$E = \frac{\hbar^2 \boldsymbol{\chi}_{01}^2}{2m^* R_0^{\,2}} + \sum_{m,n,s,k_z} \frac{T}{\frac{\hbar^2 \mathbf{k}_z^2}{2m^*} + \frac{\hbar^2}{2m^* R_0^{\,2}}\left(\boldsymbol{\chi}_{mn}^2 - \boldsymbol{\chi}_{01}^2\right) + \frac{\hbar}{2}\left\{\omega_1^2 - \beta_1^2\left[\left(\mathbf{q}_1^2\right)_{mn} + \mathbf{k}_z^2\right]\right\}^{1/2}}$$

Thus the energy of the electrons in the quantum wire is quantized and depends on the $\mathbf{k}_z$ vector of the electrons along the Oz axis and the radius of the wire.

3. CONCLUSIONS

We have sussesfully calculated the displacement of the lattice nodes in the quantum wire. Thereby building Hamilton's interaction between electrons and phonons in quantum wires and calculating dispersion expressions. Drew dispersion curves for modes p = 0 and wire with radius of 100 Å and 150 Å. Constructing an energy expression that interacts between the electron and the longitudinal optical phonon in polarized semiconductor quantum wires.

ACKNOWLEDGEMENTS

This research is a result from the HURE project 2019 without expense of the government budget.

REFERENCES

1. Babiker M., Ridley B. K. (1986), "Effective-mass eigenfunctions in superlattices and their role in well-capture", *Superlattices and Microstructures* 2, pp.287-291.
2. Constantinou N., K. Ridley B. (1990), *Interaction of electrons with the confined LO phonons of a free-standing GaAs quantum wire*.

3. Constantinou N. C. (1993), "Interface optical phonons near perfectly conducting boundaries and their coupling to electrons", *Physical Review B* 48, pp.11931-11935.

4. Ridley B. K. (1994), "Optical-phonon tunneling", *Physical Review B* 49, pp.17253-17258.

5. W. Kim K., Stroscio M., Bhatt A., Mickevicius R. V., Mitin V. (1991), *Electron□optical□ phonon scattering rates in a rectangular semiconductor quantum wire*.

6. Wiesner M., Trzaskowska A., Mroz B., Charpentier S., Wang S., Song Y., Lombardi F., Lucignano P., Benedek G., Campi D., Bernasconi M., Guinea F., Tagliacozzo A. (2017), "The electron-phonon interaction at deep Bi2Te3-semiconductor interfaces from Brillouin light scattering", *Scientific Reports* 7, p16449.

NĂNG LƯỢNG TƯƠNG TÁC GIỮA ELECTRONS VÀ PHONON QUANG DỌC TRONG DÂY LƯỢNG TỬ BÁN DẪN PHÂN CỰC

Tóm tắt*: Trong bài báo này chúng tôi tính độ dịch chuyển của nút mạng trong dây lượng tử, từ đó xây dựng Haminton tương tác giữa các điện tử và phô nôn trong các dây lượng tử và tính biểu thức tán sắc. Vẽ được đường cong tán sắc cho mode p = 0 và dây với bán kính 100 Å và 150 Å. Xây dựng biểu thức tính năng lượng tương tác của điện tử và LO trong dây lượng tử bán dẫn phân cực.*

Keywords: *Phonon quang dọc, biểu thức tán sắc, dây lượng tử, hàm Hamilton.*

POWER OF THE CONTROLLER IN CONTROLLED JOINT REMOTE STATE PREPARATION OF AN ARBITRARY QUBIT STATE

Nguyen Van Hop
Faculty of Physics, Hanoi National University of Education

Abstract: *The type of four-particle partially entangled state which is suitable for controlled joint remote state preparation of an arbitrary qubit state is designed. With the controller's assistance, the protocol is perfect as both its fidelity and total success probability are equal to one. In the opposite case, the analytical expression of the minimal averaged controller's power is calculated. Furthermore, the dependence of the minimal averaged controller's power on the parameter of the quantum channel is analyzed and the values of the parameter of the quantum channel to the controller is powerful are pointed out.*

Keywords: *Controlled joint remote state preparation, four-particle partially entangled channel, controller's power.*

Email: hopnv@hnue.edu.vn
Received 25 March 2019
Accepted for publication 25 May 2019

1. INTRODUCTION

Quantum entanglement [1] that has been recognized as a spooky feature of quantum machinery plays a vital role as a potential resource for quantum communication and quantum information processing. Quantum teleportation (QT) [2], which was firstly suggested by Bennett et al., is one of the most important applications of shared entanglement for securely and faithfully transmitting a quantum state from a sender to a spatially distant receiver without directly physical sending that state but only by means of local operation and classical communication. After the first appearance of QT, this method has not only attracted much attention in theory [3] but also obtained several significant results in experiment [4]. As an obvious extension of teleportation scheme, two modified versions to be established are remote state preparation (RSP) scheme [5 -10] which the sender knows the full identity of the to be prepared state and joint remote state preparation (JRSP) scheme [11-18] which each sender allowed to know only a partial information of the state to be prepared. In RSP, the sender completely knows the information of the state, while in QT, neither the sender nor the receiver has any knowledge of the state to be

transmitted. The catch of RSP is that the full identity of the prepared state is disclosed to the sender, who can reveal the information to outside. To overcome this drawback, joint remote state preparation, was proposed. In JRSP, the information of the initial state is secretly shared by two or more senders, located at distant sites, in such a way that none of the senders can know the full. In contrast to general RSP, in JRSP, the receiver can remotely reconstruct the original state only under the collective cooperation of all the senders. As a matter of fact, JRSP protocols are probabilistic with probabilities of less than one.

However, for practical purposes, it is often required to control the overall mission. This can be accomplished by the present of a controller in the protocol, who at the last moment decides ending of a mission after carefully judging all the related situations. Controlled joint remote state preparation [19] (CJRSP) have been studied. The controller, to be able to perform his role, has to share beforehand with the senders as well as the receiver a quantum channel which is general considered as a maximal entangled state.

In this paper, we use a partially entangled quantum channel but in case the controller agrees to cooperate, both protocols are perfect (the average fidelity and success probability are equal to unit). The problem of the role of the controller in the task is dedicated. What is the role of the controller in preventing unwanted situation from happening such as the receiver exposes information. This question is not considered in Ref. [19] but will be answered in our paper by virtue of quantitatively calculation of power of the controller in various situations. The results show that if the controller doesn't cooperate, i.e., he does nothing, the receiver cannot obtain with certainty a state with quality better than that obtained classically.

2. CONTENT

2.1. The working quantum channel

Suppose that Alice 1 and Alice 2 are in a task to help the Bob remotely prepare an arbitrary one-particle state under control of controller Charlie, the arbitrary state can be expressed as

$$|\psi\rangle = \cos\frac{\theta}{2}|0\rangle + \sin\frac{\theta}{2}e^{i\varphi}|1\rangle, \quad (1)$$

in which θ, φ are real.

To manipulate the task of CJRSP, we use the partially entangled state as the quantum channel

$$|Q(\beta)\rangle_{1234} = \frac{1}{\sqrt{2}}\left(\sin\beta|0111\rangle + \cos\beta|1111\rangle - |1000\rangle\right)_{1234}, \quad (2)$$

which can be generated from the GHZ state

$$|\mathrm{GHZ}\rangle_{1234} = 2^{-1/2}\sum_{j=0}^{1}(-1)^{j}|j, j\oplus 1, j\oplus 1, j\oplus 1\rangle_{1234}$$

as follows

$$|Q(\beta)\rangle_{1234} = R_1(\beta)\mathrm{CNOT}_{21}R_1(-\beta)|\mathrm{GHZ}\rangle_{1234}, \quad (3)$$

where CNOT_{21} is a controlled-NOT gate acting on two-qubit as

$$\mathrm{CNOT}_{21} = H_1 \otimes H_2\mathrm{CNOT}_{12}H_1 \otimes H_2$$

with $\mathrm{CNOT}_{12}|k,l\rangle_{12} = |k, k\oplus l\rangle_{12}$ and $H|x\rangle = \left(1/\sqrt{2}\right)\left(|0\rangle + (-1)^{x}|1\rangle\right)$. $R_1(\beta)$ is a rotation gate acting on a single-qubit state as

$$R_1(\beta)|k\rangle_1 = \cos(\beta/2)|k\rangle_1 - (-1)^{k}\sin(\beta/2)|k\oplus 1\rangle_1.$$

In this nonlocal resource, Alice 1 holds qubit 2 and the information about θ, Alice 2 holds qubit 3 and the information about φ, Bob holds qubit 4 and Charlie holds qubit 1. This state is characterized by angle β whose values to be known by only the controller. We are now in the position to employ the above-listed quantum channel for our purpose.

2.2. The controlled joint remote state preparation of an arbitrary qubit state

In order to realize the controlled joint remote state preparation of an arbitrary qubit state, our protocol is performed by four steps as follows.

In the first step, the Alice 1 acts on her qubit the unitary operator

$$U(\theta) = \begin{pmatrix} \cos\theta/2 & \sin\theta/2 \\ \sin\theta/2 & -\cos\theta/2 \end{pmatrix}, \quad (4)$$

then she measures her qubit on the basis $\left\{|k\rangle_2 ; k \in \{0,1\}\right\}$.

In the second step, depending on the result of the Alice 1, the Alice 2 exerts different operators on her qubit. If the Alice 1 obtains the result 0 and announces them to the Alice 2, respectively, the Alice 2 will apply to her qubit the unitary operator

$$V_2^{(0)}(\varphi) = \frac{1}{\sqrt{2}}\begin{pmatrix} 1 & e^{i\varphi} \\ 1 & -e^{i\varphi} \end{pmatrix}. \quad (5)$$

If the Alice 1 obtains the result 1 and announces them to the Alice 2, respectively, the Alice 2 will apply to her qubit the unitary operator

$$V_2^{(1)}(\varphi) = \frac{1}{\sqrt{2}}\begin{pmatrix} e^{i\varphi} & 1 \\ -e^{i\varphi} & 1 \end{pmatrix}. \quad (6)$$

Similar to the end of step 1, qubit of the Alice 2 is then measured in the basis $\{|l\rangle_3; l \in \{0,1\}\}$.

In the third step, because controller Charlie knows the value of β, he rotates qubit 1 by an angle $-\beta$ around the y-axis, then measures this qubit in the computational basis $\{|m\rangle_1; m \in \{0,1\}\}$.

In the fourth step, soon after the measurements of the sender Alice 1, Alice 2 and the controller Charlie, if both Alice and Charlie communicate with Bob via reliable classical channels about their measurement outcomes, then Bob can obtain the state by applying the recovery operator on his qubit 4. The correct recovery operator differently depend on the quantum channels used. For our protocol we have been able to work out explicit and compact formulae for the recovery operation. These operators have form as

$$R_{k/m} = X^k Z^{k \oplus l \oplus m}. \tag{7}$$

In the above recovery operators $\oplus$ stands for addition mod 2, while

$$X = \begin{pmatrix} 0 & 1 \\ 1 & 0 \end{pmatrix}, \tag{8}$$

and

$$Z = \begin{pmatrix} 1 & 0 \\ 0 & -1 \end{pmatrix}, \tag{9}$$

which are written in the qubit's computational basis $\{|0\rangle, |1\rangle\}$.

Because Bob always obtain the original state by using these recovery operators, so the total success probability and the fidelity of our scheme are one. It thus appears that the partially entangled state can implement the CJRSP as well as the maximally entangled state

2.3. Analysis of controller's power

We know that, Charlie is the controller and he has the decision role whether the task should be completed or not. So, he can permit to stop the task if the senders and the receiver are unreliable. Depending on the participation of Charlie, the fidelity of the task can be obtained unit. Now, let us compute the fidelity of this task without controller's collaboration. The controller's power is embodied in how much information Bob can achieve without the controller's help. If Charlie does not disclose his measurement results, Bob's state is a mixed one $\rho_4^{(kl)}(\beta, \theta, \varphi)$ even with Alice's result. The density matrix can be computed by

$$\rho_4^{(kl)}(\beta,\theta,\varphi) = \mathrm{Tr}_1\left(\left|\psi(\beta,\theta,\varphi)\right\rangle_{14}\left\langle\psi(\beta,\theta,\varphi)\right|\right), \quad (10)$$

where $\left|\psi(\beta,\theta,\varphi)\right\rangle_{14}$ is the state of Charlie and Bob's qubits after the measurements of Alice 1 and Alice 2.

The non-conditioned fidelity (NCF) of Bob's state without Charlie's help is

$$F_{kl} = \left\langle\psi\right|\rho_4^{(kl)}(\beta,\theta,\varphi)\left|\psi\right\rangle. \quad (11)$$

In order to calculate the NCF corresponding to random measurement results of Alice 1 and Alice 2. These fidelities are following

$$\begin{cases} F_{00} = \cos^4(\theta/2) + \sin^4(\theta/2) + 2\cos^2(\theta/2)\sin^2(\theta/2)\cos\beta, \\ F_{01} = 2\cos^2(\theta/2)\sin^2(\theta/2)[1+\cos(2\varphi)\cos\beta], \\ F_{10} = \cos^4(\theta/2) + \sin^4(\theta/2) - 2\cos^2(\theta/2)\sin^2(\theta/2)\cos\beta, \\ F_{11} = 2\cos^2(\theta/2)\sin^2(\theta/2)[1-\cos(2\varphi)\cos\beta]. \end{cases} \quad (12)$$

Then the average fidelity over all possible input states can be computed by

$$\overline{F}_{kl}(\beta) = \frac{1}{4\pi}\int_0^{2\pi} d\varphi \int_0^{\pi} F_{kl}(\beta,\theta,\varphi)\sin\theta d\theta. \quad (13)$$

Substituting F_{kl} from Eqs. (12) into Eq. (13) and carrying out the integrations we obtain the following results

$$\overline{F}_{00}(\beta) = \frac{2+\cos\beta}{3}, \quad \overline{F}_{10}(\beta) = \frac{2-\cos\beta}{3} \quad (14)$$

and

$$\overline{F}_{01} = \overline{F}_{11} = \frac{1}{3}. \quad (15)$$

The measurements on particles 2 and 3 performed by Alice 1 and Alice 2 will project the joint state of particles 1 and 4 onto one of the four possible states with equal probability of 1/4. To assess quality of the whole protocol we calculate the average fidelity

$$\overline{F} = \frac{1}{4}\left(\overline{F}_{00} + \overline{F}_{01} + \overline{F}_{10} + \overline{F}_{11}\right) = \frac{1}{2}. \quad (16)$$

The average fidelity calculated according to the Eq. (16) equal to the minimal average fidelity of prediction [21]. From the Eqs. (14) and (15), we can infer that the maximal average fidelity is

$$\overline{F}_{max} = \max\left\{\overline{F}_{00}, \overline{F}_{10}\right\}, \quad (17)$$

and the minimal average fidelity is

$$\overline{F}_{min} = \frac{1}{3}. \tag{18}$$

The average controller's power $\overline{C}$ [21] is defined as

$$\overline{C} = 1 - \overline{F}. \tag{19}$$

To limit the power of the controller, after hearing the results of measurements of Alice 1 and Alice 2, Bob can use appropriate operators on qubit that he holds so the average controller's power is as small as possible. As receiver Bob doesn't not know the value of β so that the control power of the controller is minimum when the average fidelity is maximal

$$\overline{C}_{min} = \min\{\overline{C}_{00}, \overline{C}_{10}\}, \tag{20}$$

with

$$\overline{C}_{00} = 1 - \overline{F}_{00},\ \overline{C}_{10} = 1 - \overline{F}_{10}. \tag{21}$$

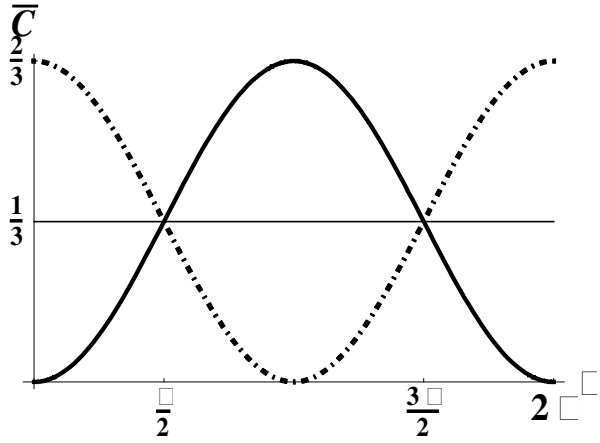

Figure 1. *The dependence of the minimal average controller's power* $\overline{C}_{00}$, *and* $\overline{C}_{10}$, *Eq (21), on the angle* θ. *The horizontal line at 1/3 represents the classical limit of the averaged controller's power*

At that point, we notice that the best value of the fidelity that can be obtained only by classical means is equal to $f_{av}^{cl} = 2/3$ [20, 21]. This means that the minimal average controller's power should be $C_{cl} = 1/3$.

Figure displays the dependences of $\overline{C}_{min}$ on β. Figure shows that: If $\beta \neq \pi/2$ and $\beta \neq 3\pi/2$, then between the two values of $\overline{C}_{00}$ and $\overline{C}_{01}$, one is bigger than 1/3 and the other is smaller than 1/3. However, the receiver can't recognize which value is smaller because he has no idea about the value of β (only the controller knows β). In summary,

in controlled joint remote state preparation protocol, if we choose the value of β which satisfies the conditions $\beta \neq \pi/2$ and $\beta \neq 3\pi/2$, the receiver will never recover for sure the desired state having the average fidelity higher than the classical value.

3. CONCLUSION

In conclusion, one protocol for controlled joint remote state preparation is proposed. This protocol considered is perfect as both its fidelity and total success probability are equal to one, despite the partial entanglement. The controller's power in the controlled joint remote state preparation is evaluated. Furthermore, we analyzed the dependence of the averaged controller's power on the parameter of the quantum channel and point out the values of the parameter of the quantum channel to the controller is powerful. The study joint remote state preparation of a two-qubit state under control of a controller via a set of partially entangled quantum channels would be proceeded.

Acknowledgments: This work is supported by the Vietnam Ministry of Education and Training under grant number B2018-SPH-48.

REFERENCES

1. Schrodinger, E (1935), Naturwissenschaften **23** pp. 807.
2. C. H. Bennett, G. Brassard, C. Crepeau, R. Jozsa, A. Peres, W. K. Wootters (1993), *Teleporting an unknown quantum state via dual classical and Einstein-Podolsky-Rosen channels*. Phys. Rev. Lett. 70 pp. 1895.
3. M. Ikram, S. Y. Zhu and M. S. Zubairy (2000), *Quantum teleportation of an entangled state*. Phys. Rev. A 62 pp. 022307.
4. D. Bouwmeester, J. W. Pan, K. Martle, M. Eibl, H. Weinfurter and A. Zeilinger (1997), *Experimental quantum teleportation*. Nature **390** pp. 575.
5. H. K. Lo (2000), *Classical-communication cost in distributed quantum-information processing: a generalization of quantum communication complexity*. Phys. Rev. A **62**, pp. 012313.

A. K. Pati (2000), *Minimum classical bit for remote preparation and measurement of a qubit*. Phys. Rev. A **63** pp. 014302.

B. H. Bennett, D. P. DiVincenzo, P. W. Shor, J. A. Smolin, B. M. Terhal, W. K. Wootters (2001), *Remote state preparation*. Phys. Rev. Lett **87** pp. 077902.

6. J. M. Liu, Y. Z. Wang (2003), *Remote preparation of a two-particle entangled state*. Phys. Lett. A **316** pp. 159.
7. W. T. Liu, W. Wu, B. Q. Ou, P. X. Chen, C. Z. Li, J. M. Yuan (2007), *Experimental remote preparation of arbitrary photon polarization states*. Phys. Rev. A **76** pp. 022308.

8. J. T. Barreiro, T. C. Wei, P. G. Kwiat (2010), *Remote preparation of single-photon hybrid entangled and vector-polarization states*. Phys. Rev. Lett **105** pp. 030407.
9. N. B. An, and K. Jaewan (2008), *Joint remote state preparation*, J. Phys. B: At. Mol. Opt.
10. Phys. **41** pp. 095501.
11. Y. Xia, J. Song, H. S. Song (2007), *Multiparty remote state preparation*. J. Phys. B At. Mol. Opt. Phys. **40** pp. 3719.
12. N. B. An (2009), *Joint remote preparation of a general two-qubit state*. J. Phys. B At. Mol. Opt. Phys. **42** pp. 125501.
13. K. Hou, J. Wang, Y. L. Lu, S. H. Shi (2009), *Joint remote preparation of a multipartite GHZ-class state*. Int. J. Theor. Phys. **48** pp. 2005.
14. N. B. An, C. T. Bich, N. V. Don (2011), *Joint remote preparation of four-qubit cluster-type states revisited*. J. Phys. B At. Mol. Opt. Phys. **44** pp. 135506.
15. X. Q. Xiao, J. M. Liu, G. H. Zeng (2011), *Joint remote state preparation of arbitrary two- and three-qubit states*. J. Phys. B At. Mol. Opt. Phys. **44** pp. 075501.
16. N. B. An, C. T. Bich, N. V. Don (2011), *Deterministic joint remote state preparation*. Phys. Lett. A **375** pp. 3570.
17. Q. Q. Chen, Y. Xia, J. Song (2012), *Deterministic joint remote preparation of an arbitrary three-qubit state via EPR pairs*. J. Phys. A Math. Theor. **45** pp. 055303.
18. N. B. An, and C. T. Bich (2014), *Perfect controlled joint remote state preparation independent of entanglement degree of the quantum channel*. Phys. Lett. A **378**, pp. 35823585.
19. X. H. Li, S. Ghose (2014), *Control power in perfect controlled teleportation via partially entangled channels*. Phys. Rev. A **90** pp. 052305.
20. X. H. Li, S. Ghose (2015), *Analysis of N-qubit perfect controlled teleportation schemes from the controller's point of view*. Phys. Rev. A **91** pp. 012320.

QUYỀN LỰC CỦA NGƯỜI ĐIỀU KHIỂN TRONG ĐỒNG VIỄN TẠO TRẠNG THÁI LƯỢNG TỬ MỘT QUBIT BẤT KÌ CÓ ĐIỀU KHIỂN

Tóm tắt: *Trong bài báo này chúng tôi nghiên cứu đồng viễn tạo trạng thái lượng tử của một qubit bất kì có điều khiển qua kênh lượng tử rối riêng phần không cực đại. Bằng chiến lược hợp lí, khi người điều khiển hợp tác, giao thức đồng viễn tạo trạng thái lượng tử là hoàn hảo vì xác suất thành công và độ tin cậy bằng một. Khi người điều khiển không hợp tác, chúng tôi xây dựng biểu thức giải tích quyền lực trung bình nhỏ nhất của người điều khiển. Từ biểu thức quyền lực trung bình nhỏ nhất này, sự phụ thuộc của quyền lực trung bình nhỏ nhất theo tham số của kênh lượng tử đã được phân tích để chỉ ra miền giá trị của tham số của kênh lượng tử bảo đảm quyền lực cho người điều khiển.*

APPLICATION OF ORIGIN SOFTWARE TO RESEARCH FLUORESCE EMISSION SPECTRUM DATA

Ho Xuan Huy
An Giang University

Abstract: *In studying materials science, the instruments used for measuring fabrication are: Micro-Raman oscillator, infrared absorption spectrum, absorption spectrum, fluorescence emission spectrum. The received data from measurement systems is data files. Researchers must process these empirical datas; and, show them through graphs to determine the structure and characteristic properties of the material. Origin software is used to graph, process data, match functions, find errors, calculate quantities.*

In this paper, Origin is applyed to analyze samples and give some results about the fluorescence spectrum of SiO_2-Al_2O_3 glass material, which is produced by Sol-Gel method. The emission spectra of two widebands with a peak around 1533nm and 1550nm, corresponding to the $^4I_{13/2} \rightarrow {}^4I_{15/2}$ transition.The principal emission intensity of Er^{3+} ion in a multi-component Al^{3+} ionic glass at 1530nm is increased several times, the width of spectrum is extended appreciably.

Keywords: *Origin, luminescent emission, ion Er^{3+}, ion Al^{3+}*

Email: hoxuanhuy69@gmail.com
Received 22 April 2019
Accepted for publication 25 May 2019

1. INTRODUCTION

Materials science is an interdisciplinary field involving the properties of matter. It is interested in electrical materials, electronic materials, nanomaterials, optical fiber materials. The devices used for measuring fabrication are: Micro-Raman oscillator, infrared absorption spectrum, absorption spectrum, fluorescence emission spectrum...The results allow for studying the lattice structure, basal energy levels and the energy levels in the ground state and the corresponding excited states of rare-earth ions.

During the implementation of scientific projects, researchers must process these empirical datas; and, show them through diagrams to determine the structure and characteristic properties of the material. There are many softwares available in researching and teaching such as Origin, Matlab, Excel ... These software can process the statistical datas, show the empirical results by diagram, extract the report of analysis results.

Origin software has spreadsheets like Excel so you can import data from Excel or Word tables by copy, paste; Or you can import the digital data files of the measurement system with the Import command. This software has the advantage that after importing data and selecting the quantities to be calculated, the software will automatically output the specified statistics, whereas if using Matlab or Excel we must write or program the calculational functions.

Application of Origin software to process the datas of aluminosilicate glass samples ($Si0_2.Al_2O_3$) measured by the Triax 320 spectrophotometer.

2. RESEARCH METHODS

2.1. The Triax 320 spectrophotometer

The spectral system Triax 320 uses optical fiber to receive IR emission signals directly, emitted from the sample. The light source emitted from the diode laser with λ_{kt} = 980nm is the source of excitation for fluorescence emission.

This method saves the time of optical adjustment and allows to reduce the loss in the signal received from the sample.. Then the lead emission signal in the fiber is inserted into the measuring device, they will first be adjusted by a mirror system so that all optical signals fall into the slot of the machine, from this slot, they will be analyzed by a grating suitable for the emission zone and separated by each signal component corresponding to the wavelength.

This signal component will be delivered to an InGaAs photodiode detector operating in the IR area, then the signal from this detector will be directly moved to the microprocessor, amplified and then connected to the computer.

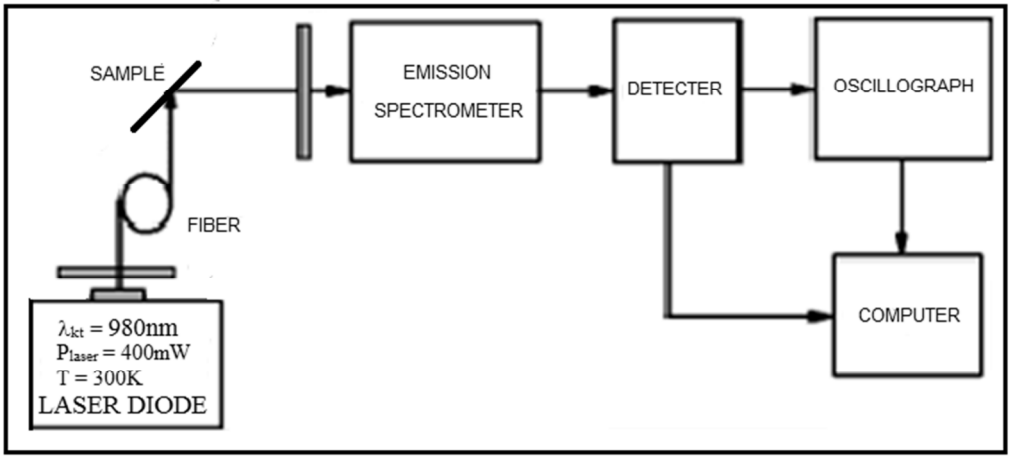

Fig 1. *Basic construction of Triax 320 spectrophotometer system*

The software that comes with the measuring device will handle the signals received from the grating and detector, then draw into a spectrum, noting that it is stored in the form of data files.

Triax 320 measuring system of JOBIN-YVON (France), located at Lab.Materials and Engineering of Opyical fiber - Institute of Materials Science - Vietnam Academy of Science and Technology.

2.2. Processed data from the TRIAX 320 Spectrophotometer with Origin

Origin is a powerful and full featured data analysis software. Powerful visualization tools with accompanying descriptive statistics to assist with hypothesis testing, model development and modeling, and data analysis [6].

The main interface of Origin is the Menus bar, toolbars, active windows such as tables, graphs. The Origin menu provides commands to perform operations during data processing. In each submenu, the tags also change to correspond to each specific window: Analysis for the Worksheet window or Analysis for the Graph window.

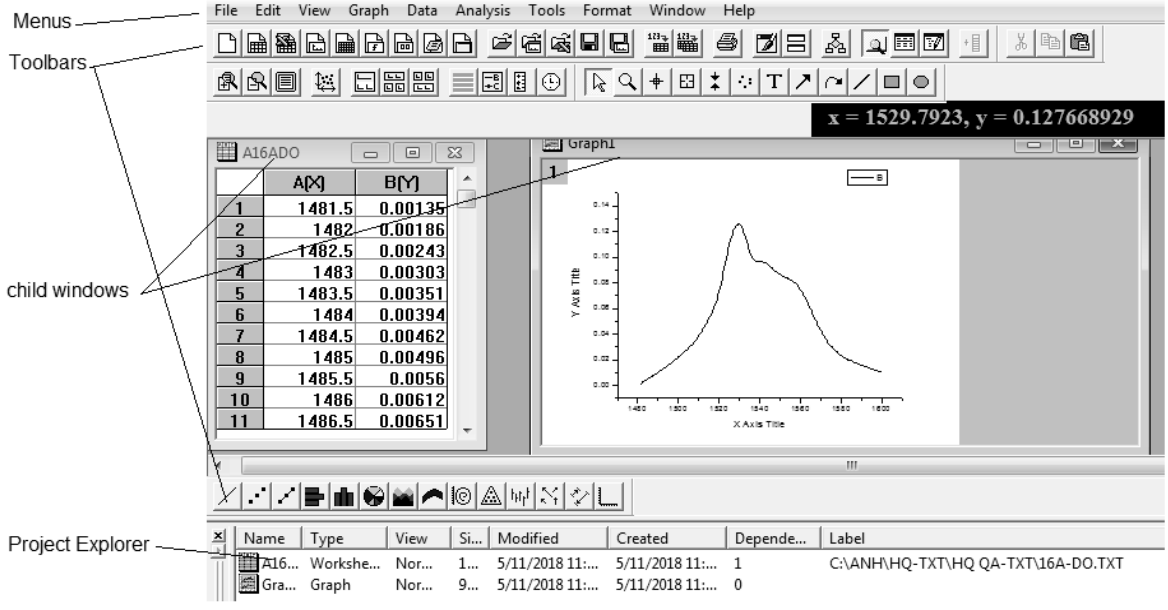

Fig 2. *The main interface of Origin*

The worksheet viewer uses data organizers and provides tools for using, analyzing, analyzing, and graphing data from worksheet data. The columns in the worksheet are relative to each other by the axis specified as the X axis, the Y axis, and their location.

The Graph window is where the graphs are displayed and edited. Each graph window contains a single edit page. You can annotate different objects such as axes, annotations,

and drawing data. Origin handles data from the measurement system through the following steps:

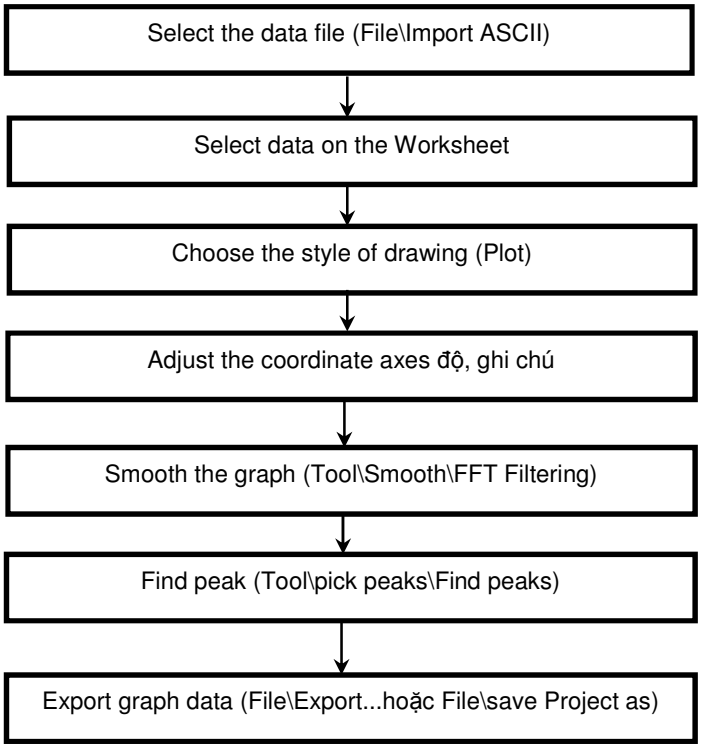

Fig 3. *Origin procedures for processing experimental data*

3. RESULTS AND DISCUSSION

3.1. Processing manipulation on the TRAX 320 spectrophotometer

The light source emitted from the diode laser is considered as a source of fluorescence emission stimulation for research samples to record emission signals from samples corresponding to the electronic shifts of rare earth ions in glass samples.

During the experimental process, in order to obtain a high-resolution spectrum, it is necessary to adjust the machine's entrance and exit slots, the distance from the receiver to the sample, the signal receiving angle, the change of excitation power etc…

Fluorescence emission spectra give information about the energy levels corresponding to the shift, spectral line expansion and movement between multiple levels of Er^{3+} ion in a home network. Samples are measured under the same conditions to compare their relative emission intensity With:

- Stimulus wavelength λ_{kt} = 980nm of diode laser, will be used to stimulate Er^{3+} ions from basic level $4I_{15/2}$ to level $4I_{11/2}$

- Laser output power is P_{laser} = 400mW và T = 300K

- Spectral region observed from 1480nm – 1600nm

3.2. Analysis of fluorescence emission spectra

The samples used in this work were prepared by sol gel method as reported. Silica glass series with an erbium oxide concentration of 1, 3, 4 and 5wt%. The main focus of this work is to optimize the material composition and hence to improve the fluorescence property, broader and smooth of gain profile of erbium ion in the sol gel aluminosilicate glass system with the composition as $SiO_2.E^{3+}$, $SiO_2.Al_2O_3.E_2O_3$.

In Figure 4, the emission spectrum of SiO_2 samples. 1% Er^{3+} (line 1), SiO_2. 5% Er^{3+} (line 2), SiO_2. 3% Er^{3+} (line 3), SiO_2. 4% Er^{3+} (line 4) the heated at 1000°C were measured for 1 hour. We can see that the emission spectra of non-sample samples have high concentrations of Er^{3+} ionic ions, the emission spectrum has a high emission intensity.

The strongest fluorescence intensity is the sample of $SiO_2.Er^{3+}$ (4%wt). With the sample of $SiO_2.Er^{3+}$ (5%wt), the intensity of fluorescence emission is much weaker.

People can explain this case the sample of $SiO_2.Er^{3+}$ (5%wt) has a fluorescence quenching effect due to the concentration of Er^{3+} ions in clumping at high temperature, this phenomenon affects the fluorescence emission of Er^{3+} ions.

When crowding occurs, transmission of emission energy between ions and non-radiative recovery between sub-levels will occur, which reduces the fluorescence efficiency in the emission spectrum at nearly 1530 nm.

In Figure 5, the fluorescence emission spectra of the samples $SiO_2.Er^{3+}$ samples (3%wt) (line 2) with heated at 1000°C for 1 hour and $98SiO_2.1{,}5Al_2O_3.0{,}5Er_2O_3$ (line 1) with heated at 850°C for 1 hour.

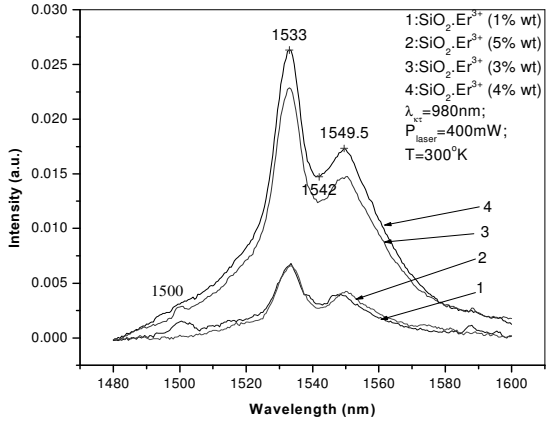

Fig 4. *Luminescence spectrum of samples SiO_2: Er^{3+} with different concentrations*

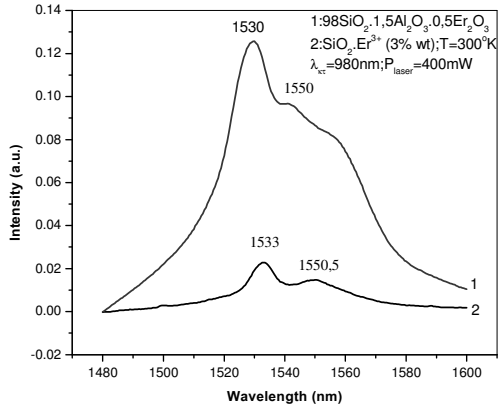

Fig 5*. Luminescence spectrum of samples $SiO_2.Er^{3+}$ (3% wt) và $98SiO_2.1{,}5Al_2O_3.0{,}5Er_2O_3$.*

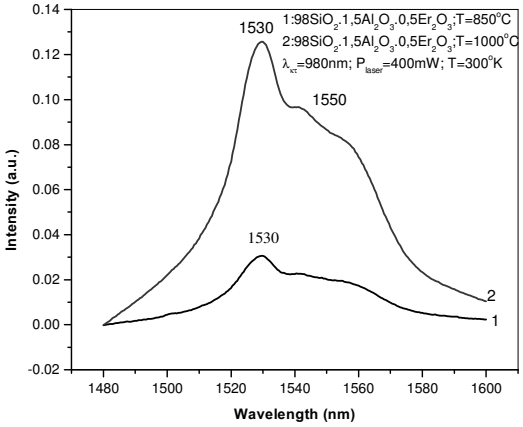

Fig 6. *Luminescence spectrum of samples $98SiO_2.1.5Al_2O_3.0.5Er_2O_3$*

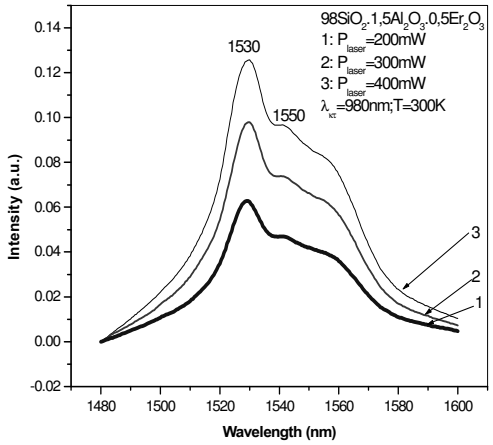

Fig 7. *Luminescence spectrum of samples $98SiO_2.1.5Al_2O_3.0.5Er_2O_3$*

Al^{3+} ions have formed an outer layer of oxygen ions and stretched Er-O bonds, increase the number of non-bridging oxygen groups in the structure and facilitate better dispersion of Er^{3+} ions and add more Er^{3+} ions into the network , it reduces the concentration of Er^{3+} ions to increase the emission intensity. [5]

Thus, Al^{3+} ion makes the emission range of Er^{3+} more expanded, It can be explained that Er^{3+} ions are better distributed and less clustered when Al^{3+} ion doped.

Figure 6 shows the fluorescence emission spectra of $98SiO_2.1,5Al_2O_3.0,5Er_2O_3$ samples (line 1), with heated at 1000°C for 1 hour and $98SiO_2.1,5Al_2O_3.0,5Er_2O_3$ (line 2), with heated at 850°C in 0.5 hours.

We see that the fluorescence signal from Er^{3+} ions increased many times when the calcination temperature increased to 1000°C compared to 850°C . This may be explained by the reduction of the remaining OH groups in the samples.

The OH groups reduce the fluorescence emission of rare earth ions due to the high level of phonon energy making the probability of non-radiative recovery increase. [1,2,5]

When firing samples at high temperatures, the amount of OH- groups decreases significantly. With a temperature of 1000°C, the emission spectrum increased significantly and the linewidth was also expanded but not much.

In Figure 7, the fluorescence emission spectra of the $98SiO_2.1,5Al_2O_3.0,5Er_2O_3$ sample, with heated 1000°C in 1 hour.

Spectra are recorded with different output power of diode lasers. The same type of spectrum is recorded, the received emission intensity increases with the size of the lasing

laser and at 400mW, the strongest intensity was obtained. But with a large capacity, the intensity does not increase and will damage the sample.

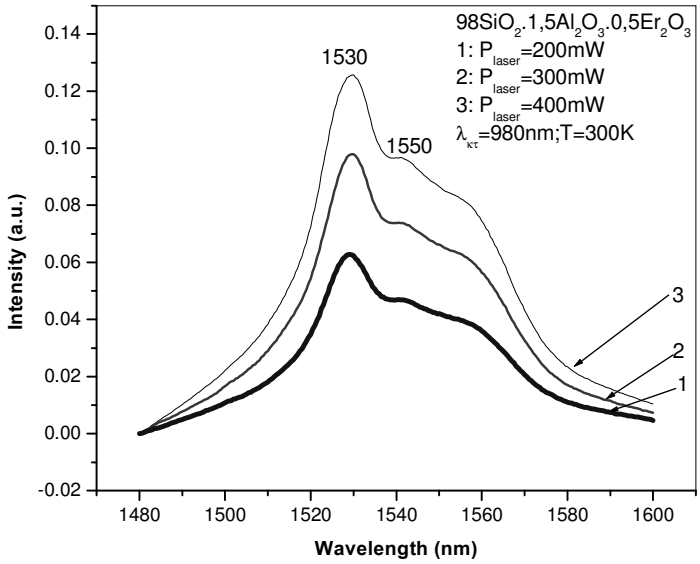

Fig 7. *Luminescence spectrum of sample $98SiO_2.1.5Al_2O_3.0.5Er_2O_3$*

We see the output power at 400mW, the width is also expanded compared to the output power at 200mW, 300mW. So, with the output power of the diode laser is suitable at 400mW.

4. CONCLUSION

Effective application of Origin software is able to display graphs of fluorescence emission spectra. Study and analyze the spectra of the multi-component glass samples $SiO_2.Al_2O_3$ doped Er^{3+} were surveyed and obtained as follows:

The emission spectra of these samples recorded two wide bands with peaks around 1533nm and 1550 nm corresponding to the shift between levels $^4I_{13/2} \rightarrow {}^4I_{15/2}$

Radiation displacement at nearly 1530 nm is very interested. The width of the emission spectral band is enlarged, we see an increase in the spectrum and the width when the Er^{3+} doped ion content increases.These samples show the spectral properties necessary for fiber optic amplification applications used in optical information.

From the fluorescence emission spectra of the samples, we see the concentration of Er^{3+} ion doped on the most effective SiO_2 glass at 4% wt for the spectrum with the largest fluorescence intensity.

The main emission intensity at 1530 nm of Er^{3+} ions in a multi-component glass substrate with Al^{3+} ions is increased, the linewidth is expanded. Ion Al^{3+} plays a role in evenly distributing Er^{3+} ions in SiO_2 glass substrate.

REFERENCES

1. Arai K (1986), "Aluminium or phospharus co-doping sffects on fluorescence and structural properties of neodymium-doped silica glass", *J.Appl, phys,* 59(1986), pp.3430-3436.
2. Benatson M and Bouazaoui (1997), "Fluorescenceproperties of sol-gel derived Er^{3+}:SiO_2.GeO_2 planar waveguids",- *Optics communi-cation,* 137(1997), pp.143-150.
3. Dejneka M and Samson B (1999), "Rare-Earth-Doped Fibers for telecommications Application", *Material Research Society Bulletin*, 24(1999), pp.39-45.
4. C.Hernandez, A.C. Pierre (2000), "E volution of the texture abd structure of SiO_2.Al_2O_3 xerogeels and Aerogels as a Function of Si to Al Molar Reatio", - *Journal of Sol-gel and technology*, 20(2000), pp.227-243.
5. Zhou, Y.L.Lam, S.S.Wang, H.L.Liu, C.H.Kam,Y.C.Chan (1997), "Fluorescence enhancement of Er^{3+} doped sol-gel glass by aluminum codoping",- *Appl Phys Lett,* 71(1997), pp.587-589.
6. Https://www.originlab.com

ỨNG DỤNG PHẦN MỀM ORIGIN TRONG NGHIÊN CỨU SỐ LIỆU PHỔ PHÁT XẠ HUỲNH QUANG

Tóm tắt: *Quá trình nghiên cứu khoa học vật liệu, các thiết bị được sử dụng để nghiên cứu đo các mẫu chế tạo là các hệ đo như: phổ dao động Micro-Raman, phổ hấp thụ hồng ngoại, phổ hấp thụ, phổ phát xạ huỳnh quang. Dữ liệu nhận từ các hệ đo là các tập tin số liệu. Nhà nghiên cứu khoa học thường phải xử lý số liệu thực nghiệm và biểu diễn qua đồ thị để xác định các cấu trúc, tính chất của vật liệu. Origin là một phần mềm được dùng để vẽ đồ thị, xử lý số liệu, khớp hàm, tìm sai số, va tính toán các đại lượng.*

Trong báo cáo đã ứng dụng Origin để phân tích các mẫu và thu được một số kết quả về phổ phát xạ huỳnh quang của vật liệu thủy tinh SiO_2-Al_2O_3 được chế tạo bằng phương pháp Sol – Gel. Phổ phát xạ các mẫu ghi được hai dải rộng có đỉnh xung quanh 1533nm và 1550nm tương ứng với dịch chuyển giữa các mức $^4I_{13/2} \rightarrow {}^4I_{15/2}$. Cường độ phát xạ chính tại 1530nm của ion Er^{3+} trong nền thuỷ tinh nhiều thành phần có ion Al^{3+} thì tăng lên nhiều lần, độ rộng vạch phổ được mở rộng đáng kể.

Từ khóa*: Origin, phát xạ huỳnh quang, ion Er^{3+} , ion Al^{3+}*

THE HEAT CAPACITY C_V OF THE SYSTEM OF THE q- DEFORMED HARMONIC OSCILLARORS

Luu Thi Kim Thanh, Man Van Ngu
Hanoi Pedagogical University no.2

Abstract: *We investigate some physical content of the q- deformed harmonic oscillator, with q is real and q is a phase factor. The expressions for the partition function and the average energy of one q- deformed harmonic oscillator are derived, we have caculated the heat capacity C_V of one mol of the q- deformed harmonic oscillators.*

Keywords: *q-deformed harmonic oscillators; average energy; heat capacity.*

Email: luuthikim.thanh888@gmail.com
Received 5 April 2019
Accepted for publication 20 May 2019

1. INTRODUCTION

Quantum algebras [1,2] are defomed versons of the usual Lie algebras, to which they reduce when the deformation parameter q is set equal to unity. Quantum algebras have attracted considerable attention in recent years particulaly, because quantum algebra have subsequently found applications in several branches of physics, as, for example, in the description of spin chains, anyons, quantum optics, quantum statistics and in conformal field theories…

The interest for possible applications of quantum algebras in physics has been triggered in 1989 by the introduction of the q-deformed harmonic oscillators [3,4,5] as a tool for providing a boson realization of the quantum algebras $SU_q(2)$. It is clear that quantum algebras provide us with a class of symmetries which is richer than the class of Lie symmetries, which are contained in the former as a special case. It is therefore conservable that quantum algebras can turn out to be appropriate for descibing symmetries of physical systems which are outside the realm of Lie algebras.

In this paper, we investigate some physical content of the q- deformed harmonic oscillator, with q is real and q is a phase factor. The expressions for the partition function and the average energy of one q- deformed harmonic oscillator are derived, we have caculated the heat capacity C_V one mol of the q- deformed harmonic oscillators.

2. QUANTUM Q - OSCILLATOR

The single mode boson oscillators obey the commutation rules:

$$[\hat{a}, \hat{a}^+] = 1, \widehat{N} = \hat{a}^+\hat{a}, \left[\widehat{N}, \hat{a}\right] = -\hat{a}, \left[\widehat{N}, \hat{a}^+\right] = \hat{a}^+ \tag{1}$$

The basis of the Fock space is defined by repeated action of the creation operator $\hat{a}^+$ on the vacuum state, which is annihilated by $\hat{a}$:

$$\hat{a}|0\rangle = 0, |n\rangle = \frac{(\hat{a}^+)^n}{\sqrt{n!}}\,|0\rangle \tag{2}$$

The action of the operators on the basis is given by

$$\begin{aligned} &\widehat{N}|n\rangle = n|n\rangle \\ &\hat{a}^+|n\,\rangle = \sqrt{n+1}|n+1\rangle \\ &\hat{a}|n\rangle = \sqrt{n}|n-1\rangle \end{aligned} \tag{3}$$

The matrix representation of the operators $\hat{a}^+, \hat{a}$ in the basis (2) have the known expressions

$$\hat{a}^+ = \begin{pmatrix} 0 & 0 & 0 & \cdots \\ \sqrt{1} & 0 & 0 & \cdots \\ 0 & \sqrt{2} & 0 & \cdots \\ \cdots & \cdots & \cdots & \cdots \end{pmatrix}, \tag{4}$$

$$\hat{a} = \begin{pmatrix} 0 & \sqrt{1} & 0 & \cdots \\ 0 & 0 & \sqrt{2} & \cdots \\ 0 & 0 & 0 & \cdots \\ \cdots & \cdots & \cdots & \cdots \end{pmatrix}, \tag{5}$$

while the number operator $\widehat{N}$ is described by the matrix

$$\widehat{N} = \begin{pmatrix} 0 & 0 & 0 & \cdots \\ 0 & 1 & 0 & \cdots \\ 0 & 0 & 2 & \cdots \\ \cdots & \cdots & \cdots & \cdots \end{pmatrix}. \tag{6}$$

The q-oscillators may be introduced by generalizing the matrices (4), (5) and (6) with the help of the q-number $[n]_q$,

$$[n]_q = \frac{q^n - q^{-n}}{q - q^{-1}} \tag{7}$$

where q is a parameter. The same definition holds if n is an operator. We remark that q-numbers remain invariant under the substitution $q \to q^{-1}$.

If q is real, q-numbers can be written as

$$[n]_q = \frac{\sinh(\tau n)}{\sinh(\tau)} \tag{8}$$

where $q = e^{\tau}$ and τ is real.

If q is a phase factor, can easily be put in the form

$$[n]_q = \frac{\sin(\tau n)}{\sin(\tau)} \tag{9}$$

where $q = e^{i\tau}$ and τ is real.

Then, replacing the intergers in (4) and (5) by the q-number $[n]_q$ we obtain matrices which define the creation and annihilation operators of the quantum q-oscillator,

$$\hat{a}^+{}_q = \begin{pmatrix} 0 & 0 & 0 & \cdots \\ \sqrt{[1]_q} & 0 & 0 & \cdots \\ 0 & \sqrt{[2]_q} & 0 & \cdots \\ \cdots & \cdots & \cdots & \cdots \end{pmatrix}, \tag{10}$$

$$\hat{a}_q = \begin{pmatrix} 0 & \sqrt{[1]_q} & 0 & \cdots \\ 0 & 0 & \sqrt{[2]_q} & \cdots \\ 0 & 0 & 0 & \cdots \\ \cdots & \cdots & \cdots & \cdots \end{pmatrix}. \tag{11}$$

The above matrices obey the commutation relations

$$\left[\hat{N}, \hat{a}^+{}_q\right] = \hat{a}^+{}_q, \left[\hat{N}, \hat{a}_q\right] = -\hat{a}_q. \tag{12}$$

$$\hat{a}_q \hat{a}^+{}_q - q^{\mp 1} \hat{a}^+{}_q \hat{a}_q = q^{\pm \hat{N}} \tag{13}$$

An immediate coseqnence of (13) is that

$$\hat{a}^+{}_q \hat{a}_q = \left[\hat{N}\right]_q;\ \hat{a}_q \hat{a}^+{}_q = \left[\hat{N}+1\right]_q \tag{14}$$

in addition, the following commutation relation holds

$$\left[\hat{a}_q, \hat{a}^+{}_q\right] = \left[\hat{N}+1\right]_q - \left[\hat{N}\right]_q$$

The Fock space spanned by the orthonormalised eigenstates of the operator $\hat{N}$,

$$|n\rangle = \frac{(\hat{a}^+)^n}{\sqrt{[n]_q!}} |0\rangle . \tag{15}$$

It is useful to notice that the q-deformed boson operators $\hat{a}^+{}_q$ and $\hat{a}_q$ can be expressed in terms of usual boson operators $\hat{a}^+$ and $\hat{a}$ through the relations

$$\hat{a}^+{}_q = \hat{a}^+ \sqrt{\frac{[\hat{N}+1]_q}{\hat{N}+1}} = \sqrt{\frac{[\hat{N}]_q}{\hat{N}}}\, \hat{a}^+, \tag{16}$$

$$\hat{a}_q = \sqrt{\frac{[\hat{N}+1]_q}{\hat{N}+1}}\, \hat{a} = \hat{a} \sqrt{\frac{[\hat{N}]_q}{\hat{N}}}. \tag{17}$$

3. THE HEAT CAPACITY C_V

Let us consider some physical content of the q- deformed harmonic oscillator.

The Hamiltonian of the q- deformed harmonic oscillator is

$$H = \frac{\omega\hbar}{2}\left(\hat{a}_q\hat{a}^+{}_q + \hat{a}^+{}_q\hat{a}_q\right) \tag{18}$$

and its eigenvalues in the basis given above are

$$E(n) = \frac{\omega\hbar}{2}\left([n]_q + [n+1]_q\right) \tag{19}$$

In particular, for q real ($q = e^{\tau}$) the eigenvalues can be written as

$$E(n) = \frac{\omega\hbar}{2}\frac{\sinh\left(\tau\left(n+\frac{1}{2}\right)\right)}{sinh\left(\frac{\tau}{2}\right)} \tag{20}$$

while for q being a phase factor ($q = e^{i\tau}$) one has

$$E(n) = \frac{\omega\hbar}{2}\frac{\sin\left(\tau\left(n+\frac{1}{2}\right)\right)}{sin\left(\frac{\tau}{2}\right)} \tag{21}$$

One can easily see that for q real the energy eigenvalues increase more rapidly than the ordinary case, in which the spectrum is equidistant, i.e. the spectrum gets "expanded". In contrast, for q being a phase factor the eigenvalues of the energy increase less rapidly than the ordinary (equidistant) case, i.e. the spectrum is "compressed".

For small values of τ one can take Taylor expansions of the functions appearing there and thus find an expansion of the q-number $[n]_q$ of equations (8) and (9) in terms of powers of τ^2. The final result is

$$[n]_q = n \mp \frac{\tau^2}{6}(n - n^3) + \frac{\tau^4}{360}(7n - 10n^3 + 3n^5) \mp \frac{\tau^6}{15120}(31n - 49n^3 + 21n^5 - 3n^7) + \cdots \tag{22}$$

where the upper (lower) sing corresponds to q being a real (phase factor). The energy of the q-deformed harmonic oscillator can be rewritten as

$$E(n) = \omega\hbar\left\{\left(n+\frac{1}{2}\right)\left(1 \mp \frac{\tau^2}{24}\right) \pm \frac{\tau^2}{6}\left(n+\frac{1}{2}\right)^3 + \cdots\right\} \tag{23}$$

The partition function for one q- deformed harmonic oscillator is given by

$$Z = \sum_{n=0}^{\infty} e^{-\frac{E(n)}{kT}} \tag{24}$$

for the case of the energy of the quantum q-oscillator (23) has been the expansion in the first order of n, the following relation holds

$$Z = \frac{e^{-\frac{\hbar\omega}{2kT}}}{1 - e^{-\frac{\hbar\omega\left(1\pm\frac{\tau^2}{12}\right)}{kT}}} \tag{25}$$

The average energy of the q-deformed harmonic oscillator is

$$\bar{E} = \frac{\hbar\omega}{2} + \frac{\hbar\omega\left(1\pm\frac{\tau^2}{12}\right)}{e^{\frac{\hbar\omega\left(1\pm\frac{\tau^2}{12}\right)}{kT}-1}} \tag{26}$$

The internal energy of an Einstein solid is

$$U = 3N\frac{\hbar\omega}{2} + \frac{3N\hbar\omega\left(1\pm\frac{\tau^2}{12}\right)}{e^{\frac{\hbar\omega\left(1\pm\frac{\tau^2}{12}\right)}{kT}-1}} \tag{27}$$

The calculations give the folowing result of the heat capacity of the one mol of the an Einstein solid :

$$C_V = \left(\frac{\partial U}{\partial T}\right)_V = \frac{3N_A\hbar^2\omega^2}{kT^2}\frac{e^{\frac{\hbar\omega}{kT}\left(1\pm\frac{\tau^2}{12}\right)}}{\left(e^{\frac{\hbar\omega}{kT}\left(1\pm\frac{\tau^2}{12}\right)}-1\right)} \tag{28}$$

where N_A is Avogadro constant.

4. ACKNOWLEDGMENTS

We would like to thank Prof. Dao Vong Duc for useful discussions and the valuable comments.

The present work was supported by Hanoi Pedagogical University No.2 for Science and Technology under grant number C.2018.27

REFERENCES

1. R. W. Gray and C. A. Nelson, J. Phys. A: Math. Gen. **23** (1990) L945.
2. V. G. Drinfeld, Proceedings of the Intern. Congress of Mathematicians. Berkeley, CA, USA (1986) 793.
3. M. K. Kumari, P. Shanta and S. Chaturvedi, Mod. Phys. Lett. **A7** (1992) 2513.
4. R. N. Mohapatra, Phys. Lett. **B242** (1990) 407.
5. Dao Vong Duc, Proceedings of the Intern. Conference on Frontiers in Quantum Physics, Kuala Lumpur, Springer – Verlag, p. 272.
6. F.Ammar, A.Makhlouf, S.Silvertrov, J. Physics. A, Math.Theor., **43** (2010), p.265204
7. Lu Ding, Xiao-Yu Jia, Ke Wu, Zhao-Wen Yan, Wei-Zhong Zhao, Nuclear Physics B.**904** (2016) 18-38

NHIỆT DUNG C_V CỦA HỆ CÁC DAO ĐỘNG TỬ ĐIỀU HÒA BIẾN DẠNG Q

Tóm tắt: *Chúng tôi quan tâm đến một số nội dung vật lý của dao động tử điều hòa biến dạng q. Chúng tôi đã thu được các biểu thức về tổng trạng thái và năng lượng trung bình của một dao động tử điều hòa biến dạng q từ đó chúng tôi tính được nhiệt dung mol C_V của dao động tử điều hòa biến dạng q.*

Từ khóa: *dao động điều hòa biến dạng q; năng lượng trung bình, nhiệt dung.*

QUANTUM THEORY OF ABSORPTION OF ELECTROMAGNETIC WAVE IN TWO - DIMENSIONAL GRAPHENE

Nguyen Vu Nhan[1], Tran Anh Tuan[2], Do Tuan Long[2], Nguyen Quang Bau[2]
[1]*Hanoi Metropolitan University*
[2]*Hanoi University of Science*

Abstract: *Quantum theory of absorption of electromagnetic wave (EMW) by confined electrons in two - dimensional (2D) graphene has been studied by using the quantum kinetic equation in assumption of electron - optical phonon scattering. The analytic expression of absorption coefficient is obtained in 2D graphene. The results in this case are compared with the case of the bulk semiconductors show the difference and the novelty of the results. The results numerically calculated and graphed show the dependence of absorption coefficient on the frequency of the electronmagnetic wave, the temperature of the system and characteristic parameters of 2D graphene.*

Keywords: *Absorption coefficient, Quantum kinetic equation, 2D Graphene, confined electron, Electron - phonon scattering, Electromagnetic wave.*

Email: anhtuanphysics@gmail.com
Received 27 March 2019
Accepted for publication 25 May 2019

1. INTRODUCTION

In recent years, 2D Graphene has been used extensively in electronic devices. This has led to a revolution in science and technology. Therefore, researching on graphene materials becomes scientists's interest. One of the recent studies of graphene materials is Magnetophonon Resonance in Graphene monolayers. Specifically, the author Borysenko K. M. [1] investigated the process of electron-phonon interaction in graphene. The author Deacon R. S. and colleagues [2] studied cyclotron resonance to determine the velocity of electrons and holes in single-layer graphene. Or the author group Mori N. and Ando T. [3] have studied magnetic-phonon resonance in Graphene monolayers by using Kubo formula. However, the problem of absorption of the electromagnetic wave in the case of the presence of an external magnetic field in 2D Graphene has not been studied, so, in this work, we used the quantum kinetic equation method to calculate the nonlinear absorption

coefficient in 2D Graphene under the influence of electromagnetic wave. We saw some differences between the results obtained in this case and in the case of the bulk semiconductors. Numerical calculations are carried out with a specific 2D Graphene. And the final section show remarks and conclusions.

2. NONLINEAR ABSORPTION COEFFICIENT IN THE CASE OF THE PRESENCE OF AN EXTERNAL MAGNETIC FIELD

In this report, we use quantum kinetic equation method to obtain nonlinear absorption coefficient in 2D Graphene in the presence of electromagnetic wave. We consider a 2D Graphene subjected to a static magnetic field $B = (0; 0; B)$ is perpendicular to the system. The wave function and the corresponding energy [4] are given by the formula below:

$$\vec{F}_{nX}(\vec{r}) = \frac{C_n}{\sqrt{L}} \exp\left(-i\frac{Xy}{l^2}\right) \begin{bmatrix} \operatorname{sgn}(n)\, h_{|n|-1}(x-X) \\ h_{|n|-1}(x-X) \end{bmatrix}, \tag{1}$$

with:

$$C_n = \begin{cases} 1 & n = 0 \\ \frac{1}{\sqrt{2}} & n \neq 0 \end{cases}, \quad \operatorname{sgn}(n) = \begin{cases} 1 & n > 0 \\ 0 & n = 0 \\ -1 & n < 0 \end{cases}$$
$$h_{|n|}(x) = \frac{i^{|n|}}{\sqrt{2^{|n|}\,|n|!\sqrt{\pi}l}} \exp\left[-\frac{1}{2}\left(\frac{x}{l}\right)^2\right] H_{|n|}\left(\frac{x}{l}\right), \tag{2}$$

where L is the linear dimension of the system, X is a center coordinate, $Hn(t)$ is Hermite polynomial, $\ell = \sqrt{\frac{c\hbar}{eB}}$ and $n = 0; \pm 1; \ldots$.

$$\varepsilon_n = \operatorname{sgn}(n)\hbar\omega_B\sqrt{|n|}, \tag{3}$$

with effective magnetic energy given by:

$$\hbar\omega_B = \frac{\sqrt{2}}{\ell}\gamma. \tag{4}$$

The Hamiltonian of the electron - optical phonon systein 2D Graphene in the second quantization presentation can be written as:

$$H = \sum_{n,\vec{k}_\perp} \varepsilon_n \left[\overrightarrow{k_\perp} - \frac{e}{\hbar c}\overrightarrow{A}(t)\right] a^+_{n,\vec{k}_\perp} a_{n,\vec{k}_\perp} + \sum_{\vec{q}} \hbar\omega_{\vec{q}} \left(b^+_{\vec{q}} b_{\vec{q}} + \frac{1}{2}\right)$$
$$+ \sum_{\vec{q},n,n',\vec{k}_\perp} M_{n,n'}(\vec{q})\, a^+_{n',\vec{k}_\perp+\vec{q}} a_{n,\vec{k}_\perp} \left(b^+_{-\vec{q}} + b_{\vec{q}}\right), \tag{5}$$

where: ε_n is energy of electron (3), $\vec{A}(t)$ is the vector potential of an external electromagnetic wave, *n* denotes the quantization of the energy spectrum in the z direction (n = 1, 2, 3, ...); $\vec{k},\vec{q}$ respectively are wave vectors of electron, phonon, $(n,\vec{k}_\perp),(n',\vec{k}_\perp+\vec{q}_\perp)$ are electron states before and after scattering, respectively, $\vec{k}_\perp$ is in plane (x,y) wave vector of the electron. $a^+_{n,\vec{k}_\perp}$, $a_{n,\vec{k}_\perp}$, $b^+_{\vec{q}}$, $b_{\vec{q}}$ are the creation and annihilation operators of electron,phonon, respectively, $\vec{q}=(\vec{q}_\perp,q_z)$; $M_{n,n'}(\vec{q})$ is the matrix factor of electron, given by:

$$|M_{n,n'}(\vec{q})|^2 = |C(\vec{q})|^2 |J_{n,n'}(u)|^2, \tag{6}$$

with: $\left|C(\vec{q}_\perp)\right|^2 = \dfrac{\hbar D_{op}^2}{2\rho L^2 \omega_{\vec{q}}}$ is the electron { optical phonon interaction constant, ρ = 7*:*7 × 10^{-8} g/cm2 is mass density of 2D Graphene, *Dop* =1*:*4 × 10^{-9} eV/cm is deformed potential of optical phonon.

$$|\mathrm{J}_{n,n'}(u)|^2 = C_n^2 C_{n'}^2 \frac{m!}{(m+j)!} e^{-u} u^j \left[L_m^j(u) + S_n S_{n'} \sqrt{\frac{m+j}{m}} L_{m-1}^j(u) \right]^2, \tag{7}$$

with $L_j^m(u)$ is the associated Laguerre polynomial, $u = \dfrac{\ell^2 q^2}{2}, q^2 = q_x^2 + q_y^2$,

$$m = \min(|n|,|n'|),\ j = \big||n|-|n'|\big|,\ S_n \equiv sng(n). \tag{8}$$

2.1. Quantum kinetic equation for electron in 2D Graphene

When a high-frequency electromagnetic wave is applied to the system in the z direction with electric field vector $\vec{E}=\vec{E}_0 \sin\Omega t$ (where $\vec{E}_0$ and Ω are the amplitude and the frequency of the electromagnetic wave), the quantum kinetic equation of average number of electron $n_{n,\vec{k}_\perp} = \left\langle a^+_{n,\vec{k}_\perp} a_{n,\vec{k}_\perp} \right\rangle$ is:

$$i\hbar \frac{\partial \left\langle a^+_{n,\vec{k}_\perp} a_{n,\vec{k}_\perp} \right\rangle_t}{\partial t} = \left\langle \left[a^+_{n,\vec{k}_\perp} a_{n,\vec{k}_\perp}, H \right] \right\rangle_t . \tag{9}$$

Starting from the Hamiltonian (5) and using the commutative relations of the creation and the annihilation operators, we obtain the quantum kinetic equation for electrons in 2D Graphene:

$$\frac{\partial n_{n,\vec{k}_\perp}(t)}{\partial t} = -\frac{1}{\hbar^2}\sum_{\vec{q},n,n'}|M_{n,n'}(q)|^2\sum_{l,s=-\infty}^{+\infty}J_l\left(\frac{e\vec{q}_\perp\vec{E_0}}{m\Omega^2}\right)J_s\left(\frac{e\vec{q}_\perp\vec{E_0}}{m\Omega^2}\right)\times\exp\left[-i(s-l)\Omega\right]$$
$$\times\int_{-\infty}^{t}dt_1\left\{\left[n_{n,\vec{k}_\perp}(t_1)N_{\vec{q}}-n_{n',\vec{k}_\perp+\vec{q}_\perp}(t_1)(N_{\vec{q}}+1)\right]\right.$$
$$\times\exp\left[\frac{i}{\hbar}\left(\varepsilon_{n',\vec{k}_\perp+\vec{q}_\perp}-\varepsilon_{n,\vec{k}_\perp}-\hbar\omega_{\vec{q}}-l\hbar\Omega+i\hbar\delta\right)(t-t_1)\right]$$
$$+\left[n_{n,\vec{k}_\perp}(t_1)(N_{\vec{q}}+1)-n_{n',\vec{k}_\perp+\vec{q}_\perp}(t_1)N_{\vec{q}}\right]$$
$$\times\exp\left[\frac{i}{\hbar}\left(\varepsilon_{n',\vec{k}_\perp+\vec{q}_\perp}-\varepsilon_{n,\vec{k}_\perp}+\hbar\omega_{\vec{q}}-l\hbar\Omega+i\hbar\delta\right)(t-t_1)\right]$$
$$-\left[n_{n',\vec{k}_\perp-\vec{q}_\perp}(t_1)N_{\vec{q}}-n_{n,\vec{k}_\perp}(t_1)(N_{\vec{q}}+1)\right]$$
$$\times\exp\left[\frac{i}{\hbar}\left(\varepsilon_{n,\vec{k}_\perp}-\varepsilon_{n',\vec{k}_\perp-\vec{q}_\perp}-\hbar\omega_{\vec{q}}-\hbar l\Omega+i\hbar\delta\right)(t-t_1)\right]$$
$$-\left[n_{n',\vec{k}_\perp-\vec{q}_\perp}(t_1)(N_{\vec{q}}+1)-n_{n,\vec{k}_\perp}(t_1)N_{\vec{q}}\right]$$
$$\left.\times\exp\left[\frac{i}{\hbar}\left(\varepsilon_{n,\vec{k}_\perp}-\varepsilon_{n',\vec{k}_\perp-\vec{q}_\perp}+\hbar\omega_{\vec{q}}-\hbar l\Omega+i\hbar\delta\right)(t-t_1)\right]\right\}, \quad (10)$$

It is well known that to obtain the explicit solutions from (10) is very difficult. In this paper, we use the first-order tautology approximation method to solve this equation. In detail, in (10), we use the approximation:

$$n_{n,\vec{k}_\perp}(t_1)\approx\overline{n_{n,\vec{k}_\perp}}\quad n_{n,\vec{k}_\perp+\vec{q}_\perp}(t_1)\approx\overline{n_{n,\vec{k}_\perp+\vec{q}_\perp}},\ n_{n,\vec{k}_\perp-\vec{q}_\perp}(t_1)\approx\overline{n_{n,\vec{k}_\perp-\vec{q}_\perp}}$$

where $\overline{n_{n,\vec{k}_\perp}}$ is the time - independent component of the electron distribution function. The approximation is also applied for a similar exercise in bulk semiconductor [5, 6]. We perform the integral with respect to t. Next, we perform the integral with respect to t of (10). The expression of electron distribution function can be written as:

$$n_{n,\vec{k}_\perp}(t) = -\frac{1}{\hbar(s-l)\Omega}\sum_{\vec{q},n,n'}|M_{n,n'}(q)|^2\times\sum_{l,s=-\infty}^{+\infty}J_l\left(\frac{e\vec{q}_\perp\vec{E_0}}{m\Omega^2}\right)J_s\left(\frac{e\vec{q}_\perp\vec{E_0}}{m\Omega^2}\right)\exp\left[-i(s-l)\Omega\right]$$
$$\times\left[-\frac{\overline{n_{n,\vec{k}_\perp}}N_{\vec{q}}-\overline{n_{n',\vec{k}_\perp+\vec{q}_\perp}}(N_{\vec{q}}+1)}{\varepsilon_{n',\vec{k}_\perp+\vec{q}_\perp}-\varepsilon_{n,\vec{k}_\perp}-\hbar\omega_{\vec{q}}-l\hbar\Omega+i\hbar\delta}-\frac{\overline{n_{n,\vec{k}_\perp}}(N_{\vec{q}}+1)-\overline{n_{n',\vec{k}_\perp+\vec{q}_\perp}}N_{\vec{q}}}{\varepsilon_{n',\vec{k}_\perp+\vec{q}_\perp}-\varepsilon_{n,\vec{k}_\perp}+\hbar\omega_{\vec{q}}-l\hbar\Omega+i\hbar\delta}\right.$$
$$\left.+\frac{\overline{n_{n',\vec{k}_\perp-\vec{q}_\perp}}N_{\vec{q}}-\overline{n_{n,\vec{k}_\perp}}(N_{\vec{q}}+1)}{\varepsilon_{n,\vec{k}_\perp}-\varepsilon_{n',\vec{k}_\perp-\vec{q}_\perp}-\hbar\omega_{\vec{q}}-\hbar l\Omega+i\hbar\delta}+\frac{\overline{n_{n',\vec{k}_\perp-\vec{q}_\perp}}(N_{\vec{q}}+1)-\overline{n_{n,\vec{k}_\perp}}N_{\vec{q}}}{\varepsilon_{n,\vec{k}_\perp}-\varepsilon_{n',\vec{k}_\perp-\vec{q}_\perp}+\hbar\omega_{\vec{q}}-\hbar l\Omega+i\hbar\delta}\right], \quad (11)$$

where $\overrightarrow{N}_q$ is the time-independent component of the phonon distribution function, $J_k(x)$ is the Bessel function and the quantity δ is infinitesimal and appears due to the assumption of an adiabatic interaction of the electromagnetic wave.

2.2. Calculation of nonlinear absorption coefficient in 2D Graphene

The carrier current density formula in 2D Graphene takes the form:

$$\vec{J}_\perp(t) = \frac{e\hbar}{m}\sum_{n,\vec{k}_\perp}\left[\vec{k}_\perp - \frac{e}{\hbar c}\vec{A}(t)\right] n_{n,\vec{k}}(t)$$

.

Because the motion of electrons is confined along the z direction in a 2D Graphene, we only consider the in plane (x, y) current density vector of electrons $\vec{J}_\perp(t)$. Using (11), we find the expression for current density vector:

$$\overrightarrow{J_\perp}(t) = -\frac{e^2}{mc}\sum_{n,\vec{k}_\perp}\vec{A}(t)\, n_{n,\vec{k}_\perp}(t) + \sum_{l=1}^{\infty}\overrightarrow{J_l}\sin(l\Omega t) \quad , \tag{12}$$

here:

$$\overrightarrow{J_\ell} = \frac{2\pi e\hbar^2}{ml\Omega}\sum_{n,n',\vec{k}_\perp,\vec{q}}|M(\vec{q})|^2\sum_{k=-\infty}^{\infty}\vec{q}_\perp J_k\left(\frac{e\vec{q}_\perp\overrightarrow{E_0}}{m\Omega^2}\right)\left[J_{k+l}\left(\frac{e\vec{q}_\perp\overrightarrow{E_0}}{m\Omega^2}\right) + J_{k-l}\left(\frac{e\vec{q}_\perp\overrightarrow{E_0}}{m\Omega^2}\right)\right]$$
$$\times N_{\vec{q}}\left(\overline{n_{n,\vec{k}_\perp}} - \overline{n_{n',\vec{k}_\perp+\vec{q}_\perp}}\right)\delta\left(\varepsilon_{n',\vec{k}_\perp+\vec{q}_\perp} - \varepsilon_{n,\vec{k}_\perp} + \hbar\omega_0 - k\hbar\Omega\right) \quad , \tag{13}$$

By using the matrix factor, the electron - optical phonon interaction factor in (6) and the Bessel function [7, 8], from the expression for the current density vector (12) we establish the nonlinear absorption coefficient of the electromagnetic wave:

$$\alpha = \frac{8\pi}{c\sqrt{\chi_\infty}E_0^2}\left\langle\vec{J}_\perp(t)\overrightarrow{E_0}\sin\Omega t\right\rangle_t$$
$$= \frac{32\pi^2\Omega}{c\sqrt{\chi_\infty}E_0^2}\sum_{\vec{k}_\perp,\vec{q},n,n'}|M_{n,n'}(\vec{q})|^2\,\overline{N_{\vec{q}}}\,\overline{n_{n,\vec{k}_\perp}}\sum_\ell \ell J_\ell^2\left(\frac{e\vec{q}_\perp\overrightarrow{E_0}}{m\Omega^2}\right)\delta\left(\varepsilon_{n',\vec{k}_\perp+\vec{q}_\perp} - \varepsilon_{n,\vec{k}_\perp} + \hbar\omega_{\vec{q}} - \ell\hbar\Omega\right) \quad , \tag{14}$$

where $\langle X\rangle_t$ means the usual thermodynamic average of X at moment t, and $\chi 1$ is the high-frequency dielectric constants, $\delta(x)$ is the Dirac delta function. For simplicity, we limit the problem to case of $\ell = 0, \ell = 1$:

$$\sum_{\ell=0,1}\ell J_\ell^2\left(\frac{e\vec{q}_\perp\overrightarrow{E_0}}{m\Omega^2}\right) = J_1^2\left(\frac{e\vec{q}_\perp\overrightarrow{E_0}}{m\Omega^2}\right) \approx \left(\frac{e\vec{q}_\perp\overrightarrow{E_0}}{2m\Omega^2}\right)^2 . \tag{15}$$

Let consider the electron - optical phonon interaction when the temperature of the system is high (T > 50K), the electron - optical phonon interaction is higher than other interactions. In this case, electron gas is assumed that non-generated gas and abided by the Boltzmann distribution. Simultaneously, let assume that phonon is not dispersive, means, $\omega_0 = const.$ const is the optical phonon frequency non-dispersion:

$$\hbar\omega_{\vec{q}} \approx \hbar\omega_0, \langle N_{\vec{q}}\rangle_{eq} = N_0 \approx \left[\exp\left(\frac{\hbar\omega_0}{k_BT}\right) - 1\right]^{-1} \quad , \tag{16}$$

$\left\langle N_{\vec{q}} \right\rangle_{eq}$ is the equilibrium distribution function of phonons. By replacing (16), (15) on (14), change $\vec{k}_\perp + \vec{q}_\perp \to n, \vec{k}_\perp \to n'$ in Dirac delta function, denote $\overrightarrow{n_{\vec{k}}} = f_{n,\vec{k}_\perp}$ we get the absorption coefficient :

$$\alpha = \frac{4\pi^2 \hbar e^2 D_{op}^2}{c\sqrt{\chi_\infty}\rho L^2 \omega_0 m^2 \Omega^3}\left[\exp\left(\frac{\hbar\omega_0}{k_B T}\right) - 1\right]^{-1} \sum_{n,n'} f_{n,\vec{k}_\perp} \sum_{\vec{k}_\perp,\vec{q}_\perp} |J_{n,n'}(u)|^2 q_\perp^2 \delta\left(\varepsilon_n - \varepsilon_{n'} + \hbar\omega_{\vec{q}} - \hbar\Omega\right) \quad ,(17)$$

Transforming the summations over $\vec{q}_\perp$ and $\vec{k}_\perp$ to integrals as follows:

$$\sum_{\vec{q}_\perp} \to \frac{S_0}{(2\pi)^2} \int_0^\infty q_\perp dq_\perp \int_0^{2\pi} d\varphi = \frac{S_0}{2\pi} \int_0^\infty q_\perp dq_\perp, \sum_{\vec{k}_\perp} \to \frac{L_y}{2\pi} \int_{-L_x/2l^2}^{L_x/2l^2} dk_\perp \int_0^\pi d\theta = \frac{L_x L_y}{2l^2}\pi \quad . \quad (18)$$

The expression (17) becomes:

$$\alpha = \frac{\pi^2 \hbar^2 e^2 D_{op}^2 S_0 L_x L_y}{c\sqrt{\chi_\infty}\rho L^2 \omega_0 m^2 \Omega^3 l^2}\left[\exp\left(\frac{\hbar\omega_0}{k_B T}\right) - 1\right]^{-1} \sum_{n,n'} f_n \delta\left(\varepsilon_n - \varepsilon_{n'} + \omega_{\vec{q}} - \Omega\right) \int_0^\infty q^3 |J_{n,n'}(u)|^2 dq \quad . \quad (19)$$

We use the calculation results in [9]:

$$\int_0^\infty q_\perp^3 |J_{n,n'}(u)|^2 dq_\perp = \frac{2C_n^2 C_{n'}^2}{l^4}\left[(2m+j+1) - 2S_n S_{n'}\sqrt{m(m+j)} + S_n^2 S_{n'}^2 (2m+j-1)\right] \quad . \quad (20)$$

Finally, inserting (20) into (19) we obtain the explicit expression for the absorption coefficient as:

$$\alpha = \frac{2\pi^2 \hbar e^2 D_{op}^2 S_0 L_x L_y}{c\sqrt{\chi_\infty}\rho L^2 \omega_0 m^2 \Omega^3 l^6}\left[\exp\left(\frac{\hbar\omega_0}{k_B T}\right) - 1\right]^{-1} \sum_{n,n'} f_n C_n^2 C_{n'}^2 \left[(2m+j+1)\right.$$
$$\left. -2S_n S_{n'}\sqrt{m(m+j)} + S_n^2 S_{n'}^2 (2m+j-1)\right] \delta\left(\varepsilon_n - \varepsilon_{n'} + \hbar\omega_{\vec{q}} - \hbar\Omega\right) \quad . \quad (21)$$

The delta functions in (21) are divergent as their arguments equals to zero. To avoid this, we replace them phenomenology by Lorentzians as [10]:

$\delta(\varepsilon) = \frac{\Gamma_K}{\pi(\varepsilon^2 + \Gamma_K^2)}$, where $\Gamma_K = \hbar\omega_B\sqrt{W_K}$ is the level width, $W_K = \frac{\hbar D_{op}^2}{8\pi\rho\gamma^2\omega_K}$ is the dimensionless parameter characterizing the scattering strength.

3. NUMERICAL RESULTS AND DISCUSSION

In order to clarify the mechanism for the nonlinear absorption of a electromagnetic wave in 2D graphene, in this section, we will evaluate, plot and discuss the expression of the nonlinear absorption coefficient for the case of a special 2D Graphene. We use some results for linear absorption in [11] to make the comparison between the linear and the nonlinear absorption phenomena. For this section, the parameters used in computational calculations are as follows [3, 10] in Table I:

TABLE I. The parameters

Symbols	Units	Values
ρ	g/cm^2	$7,7.10^{-8}$
D_{op}	eV/cm	$1,4.10^{-9}$
k_B	J/K	$1,3807.10^{-23}$
$\hbar\omega_0 = \hbar\omega_K$	meV	162
$L_x = L_y = L$	m	2.10^{-9}
$S_0 = L_x L_y$	m^2	4.10^{-18}
c	m/s	3.10^8
$\hbar$	J.s	$1,05459.10^{-34}$
$\chi\infty$		10,9
γ	eV. Å	6,46

3.1. The dependence of absorption coefficient on temperature

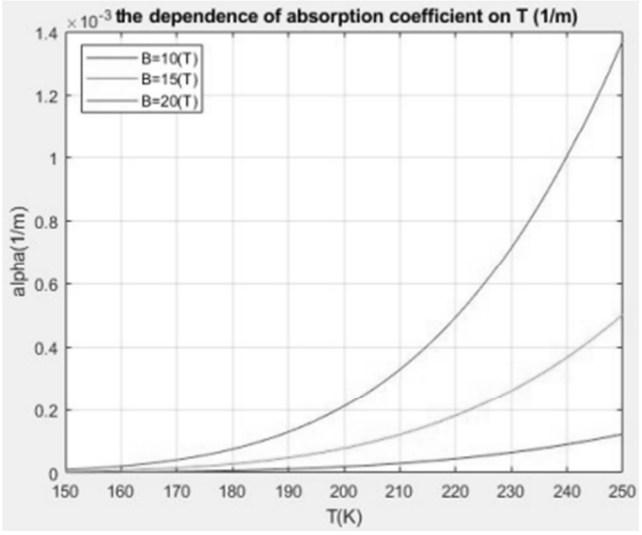

Fig 1. *The dependence of α on T*

Figure 1 shows the dependence of the nonlinear absorption coefficient α on the temperature T of the system at different values of the magnetic field. It can be seen from this figure that the nonlinear absorption coefficient α depends strongly and non-linearly on T. We can see that non-linear absorption coefficient reaches at the saturated value when temperature is very low and increases quickly when temperature is high.

Therefore, the presence of electromagnetic wave influence on the absorption coefficient is quite remarkable, the absorption coefficient value is the same in domain of low temperature and have different values in the region with higher temperatures. This result is consistent with those previously reported by using Boltzmann kinetic equation in other two-dimensional systems [12]. This coefficient absorption is the same as the results which gained in bulk semiconductor. The smaller magnetic the smaller absorption coefficient. When B is high, the absorption increases.

3.2. The dependence of absorption coefficient on magnetic field

In figure 2 the dependence of absorption coefficient in case electron - optical phonon scattering on magnetic is non-linear. As can be seen, form the graph, in each case of the magnetic field, the absorption coefficient reaches a peak with the specific value of electromagnetic wave frequency Ω. When magnetic field value increases, absorption coefficient at the peak position tends to upwards.

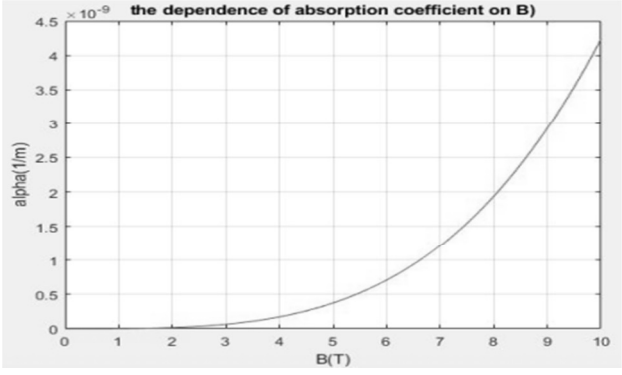

Fig 2. *The dependence of α on B*

3.3. The dependence of absorption coefficient on the frequency of electromagnetic wave

In figure 3 the dependence of absorption coefficient on frequency electromagnetic wave at presence on magnetic field, at three different magnetic field points. In this case, absorption peak is so sharp and absorption coefficient has significant value when near absorption peak. From the graph, we see that the oscillations have appeared and oscillation is controlled by the ratio of the Fermi energy and the cyclotron energy. The mechanism of the oscillations can be easily explained as follows. At low temperature and strong magnetic field, the free electrons in 2D Graphene will move as simple harmonic oscillator. When the magnetic field changes, the cycle of the oscillations also change. The energy levels of electrons are separated into Landau level, with each Landau level, cyclotron energy, and the electron state linearly increase with the magnetic field. When the energy level of the Landau levels excesses the value of Fermi level, the electron can move up freely and move

in the line, which makes the absorption coefficient oscillate circulating with the magnetic field. That means the external magnetic has a significant effect on absorption coefficient, the transfer energy level of electron after absorption electromagnetic wave must satisfy condition $\Omega - \omega_0 = 0$. This result is one of the new findings that we have studied.

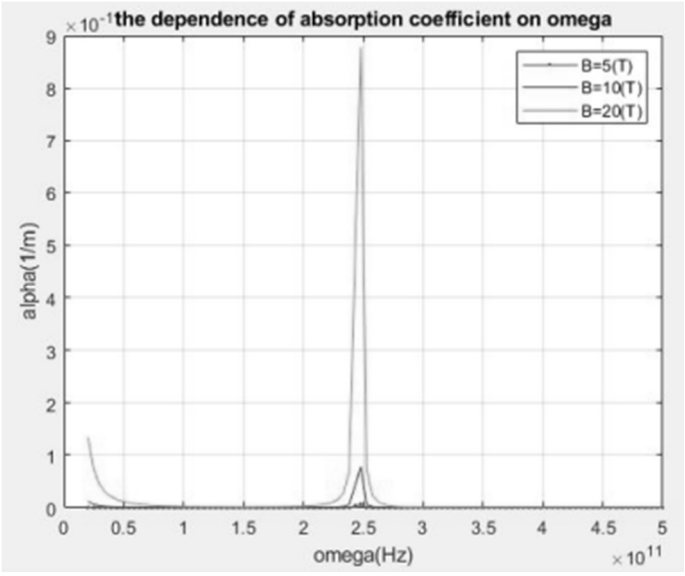

Fig 3. *The dependence of α on* Ω

4. CONCLUSION

In this paper, by using quantum kinetic equation, we anlytically calculated the absorption coefficient in 2D Graphene under the influence of weak electromagnetic wave. After obtained the analytical expression of absorption coefficient by electrons confined in 2D Graphene for the presence of an external magnetic field, we graphed them numerically to clarify the dependence of absorption coefficient on the frequency Ω of the electromagnetic wave, the temperature T of the system, the magnetic field B. The coefficient absorption in graphene is the same as the results which gained in bulk semiconductor. It is found in this paper that the absorption coefficient oscillates when the electromagnetic wave frequency changes. At each specific point of magnetic field, absorption coefficient reaches peaks and oscillates with different amplitudes. The stronger magnetic field is, the higher peaks are. Moreover, in this paper, we used the quadratic approximation of the Bessel function to eliminate the influence of electromagnetic wave intensity on the nonlinear absorption coefficient to simplify the problem. However, calculations in the 2D Graphene are still much more complicated than calculating weak electromagnetic wave non-linear absorption coefficients in other two-dimensional systems like quantum wells, doped superlattices by Kubo - Mori method [13, 14].

REFERENCES

1. K. M. Borysenko, J. T. Mullen, E. A. Barry, S. Paul, Semenov, and K. W. Kim (2010), "First-principles analysis of electron-phonon interactions in graphene", - *Phy. Rev B.*, **Vol. 81**, **No. 12**, pp. 3-6.
2. R. S. Deacon, K. Chuang, R. J. Nicholas, K. S. Novoselov, and A. K. Geim (2007), "Cyclotron resonance study of the electron and hole velocity in graphene monolayers", - *Phy. Rev. B*, pp. 2-5.
3. N. Mori and T. Ando (2011), "Magnetophonon resonance in monolayer graphene", - *J. Phys. Soc. Jpn*, **Vol. 80**, **No. 4**.
4. T. Ando (2007), "Magnetic oscillation of optical phonon ingraphene", - *J. Phys. Soc. Jpn*, **Vol. 76**, **No. 2**.
5. E. M. Epstein (1975), Sov. Communicacattion of HEE of USSR, Ser, p.785.
6. V. L. Malevich and E. M. Epstein (1974), Sov. Quantum Electronic 1, p.1468.
7. G. B. Arfken, H. J. Weber, and F. E. Harris (2013), *Mathematical Methods for Physicists*.
8. H. B. Dwight (2006), *Tables of Integrals and Other Mathematical Data.*, **Vol.50**. JSTOR.
9. L. T. Phuong, T. M. Duyen, V. T. Lam, and B. D. Hoi (2017), "Investigation of Magneto-phonon Resonance in Graphene Monolayers", - *VNU Journal of Science: Mathematics-Physics*, **Vol.33**, **No.4**, pp.45-56.
10. H. V. Phuc, N. N. Hieu, L. Dinh, and T. C. Phong (2015), "Nonlinear optical absorption in parabolic quantum wellvia two-photon absorption process", - *Optics Communications*, **Vol.335**, pp.37-41.
11. N. Q. Bau, N. V. Nhan, and T. C. Phong (2002), "Calculations of the absorption coefficient of a weak electromagnetic wave by free carriers in doped superlattices by using the Kubo-Mori method", - *J. Kor. Phys. Soc.*, p.149.
12. Shik (1999), *Quantum wells in Physics and Electronics oftwo-dimensional systems*.
13. N. Q. Bau and T. C. Phong (1998), "Calculations of the absorption coefficient of a weak emw by free carriers in quantum wells by the kubo-mori method", - *J. Phys. Soc. Jpn*.

LÝ THUYẾT LƯỢNG TỬ HẤP THỤ SÓNG ĐIỆN TỪ TRONG GRAPHENE HAI CHIỀU

Tóm tắt: *Nghiên cứu lý thuyết lượng tử hấp thụ sóng điện từ (EMW) trong Graphene hai chiều (2D) bằng phương trình động lượng tử với giả thiết cơ chế tán xạ electron-phonon quang. Thu được biểu thức giải tích cho hệ số hấp thụ trong Graphene 2D. Các kết quả là mới và được so sánh với trường hợp trong bán dẫn khối để thấy sự khác biệt. Kết quả thu nhận được tính số và vẽ đồ thị biểu thị sự phụ thuộc của hệ số hấp thụ vào tần số EMW, nhiệt độ của hệ và các tham số đặc trưng cho Graphene 2D.*

Từ khóa: *Hệ số hấp thụ, phương trình động lượng tử, 2D Graphene, electron giam cầm, tán xạ electron-phonon, sóng điện từ.*

THE FIRST STEP TO ISOLATE AND DETERMINE THE STRUCTURE OF SOME ORGANIC COMPOUNDS OF THE TICH DUONG MUSHROOMS (RHOPALOCNEMIS PHALLOIDES JUNGHUN) COLLECTED IN SON LA

Pham Van Cong, Nguyen Thi Hai, Seng Cay Hom Ma Ni,
Son Am Phon Keo Pa Sot
Tay Bac University

Abstract: *2- (3,4-hydroxyphenyl) chroman-3,5,7-triol has been isolated from the Rhopalocnemis phalloides junghun. Chemical structure of these compounds have been confirmed by NMR (1D and 2D) and compared with reference .*

Keywords: *Balanophoraceae, Rhopalocnemis phalloides junghun, phenolic*

Email: pvhoan@hnmu.edu.vn
Received 24 April 2019
Accepted for publication 25 May 2019

1. PREAMBLE

Tich duong mushrooms has the scientific name of Rhopalocnemis phalloides junghun, belonging to parasitic, non-chlorophyll fungus; tubers are 2-10cm large, smooth or melancholy; the stem is 2-10 cm long, along with 6-20 cm long oval flowers, at the young age, there is a flowering leaf. Single flowers between feathers; male flowers with 5 teeth, including the heroic part; female flowers with perches have 2 long stents. Positive fungi are usually reddish-brown or yellowish, ivory, often found on parasitic roots of tree roots.

Tich duong mushrooms is a precious medicinal herb, which has long been widely used in traditional medicine; It has a sweet taste, mild temperament, has a kidney-replenishing effect, has a strong back and lumbar field, used in cases where men are impotent, women are infertile, blood is dry, constipation, back weak pillows

Regarding chemical composition: in Tich duong mushrooms, fat, derivatives of cinnamic acid, tannin, lignan, glycosides,... [5-7] were discovered.

According to recent studies, Tich duong mushrooms fungi contain a number of compounds that are able to resist oxidation, inhibit HIV, hypoglycemia, and the ability of

some cytotoxic cytotoxic cells [8-10]. This paper will inform the isolation and structure of some compounds from n-hexane, ethyl acetate extract of the Tich duong mushrooms in Son La.

2. EXPERIMENTAL AND RESEARCH METHODS

2.1. Plant samples

Tich duong mushrooms (4 kg of fresh plants) were harvested in October 2018 in Bac Yen mountain area - Son La. Scientific name is Rhopalocnemis phalloides junghun was identified by Pham Quynh Anh, Department of Biochemistry – Tay Bac University

2.2. Chemicals and equipment

- Thin layer chromatography (TLC): Performed on a thin, pre-coated sheet of DC-Alufolien 60 F254 (Merck-Germany). Detect the substance with ultraviolet light in two wavelengths 254 and 368 nm, sulfuric acid reagent (H2SO4 + methanol + vanillin) dried at a temperature of> 100 oC until the color appears.

- Column chromatography (CC) is carried out with normal phase adsorbents (Silica gel 60-160 and 240-430 mesh, Merck).

- IR spectrum (KBr) is recorded on the machine SIMP4.

- Flow point is measured on Electrothermal IA- 9200 (UK).

- High resolution mass spectra HR-ESI-MS measured on the mass spectrometer of the FT-ICR / MS.

- Nuclear magnetic resonance spectrum (NMR) was measured on the Bruker AM500 FT-NMRSpectrometer.

2.3. Extraction and isolation of substances

Tich duong mushrooms has a mass of 0.7 kg (dry, powder) soaked in solvent H2O: MeOH = 20:80 (5 liters). Samples are soaked for 1 week, ultrasonic extraction many times. Filter the yellow and residue solution. The residue is further soaked in solvent H2O: MeOH. Repeat several times until the filtered water remains light yellow. The solution was carried out to store the spinning machine, resulting in a high total of dark yellow, liquid, viscous (LT).

Then, the total height was treated according to the fractional extraction direction: Dissolve high alcohol in 1 liter of water, stir well then ultrasound to completely dissolve and then extract with the solvents: n-hexane, ethyl acetate followed ratio 1: 1 (extract each segment 3 times), extract the fractional extracts, store and recover the solvent under pressure to reduce those segments to the corresponding residue: n-hexane residue (denoted

as LTH, 1, 42g), ethyl acetate residue (LTE, 11.69 g). The n-hexane, ethyl acetate residues are separated on the silica gel column with the elution solvent system as follows: the LTH residue with the n-hexane-ethyl acetate system has increased polarization, the residue of LTE using the elution solvent system (EtOAc: MeOH) = (80:20), (80:20), (70:30), (60:40), (50:50) to collect segments. After purification by re-running the silica gel phase often repeat or recrystallize from the fractions obtained with clean compounds, denoted by: LTH1 (115 mg); LTE1 (189 mg).

3. RESULTS

3.1. Compound 1 (LTH1)

+ 1H NMR spectrum of compound 1 has 5 protons, including:

- A proton of R-CH3 group has a chemical shift at 0.8 ppm.

- A proton with a chemical shift at 1.3 ppm is expected to be a proton of the R-CH2-R group

- A proton with a chemical shift at 2.3 ppm is expected to be a proton of the R-CO-CH group

- Two equivalent protons, with a chemical displacement of 4.2 ppm are expected to be the proton of the group –CH2-O-

From the analysis of spectral data of LTH1 and comparison with reference materials, it is possible to confirm that LTH1 belongs to trigixerite group:

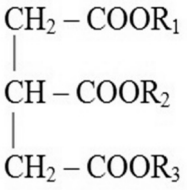

3.2. Compound 2 (LTE1)

Data on the 1H-NMR spectrum and the ^{1}H-NMR spectrum of the E1 substance showed 14 protons in the molecule. ^{13}C-NMR spectral data show the signal of 15 carbon. Spectral line characteristics and atomic number correlations C and H in E1 molecule allow prediction of E1 as a substance of frame flavan

+ ^{1}H-NMR spectrum (MeOH, 500MHz)

-NMR spectrum of this substance shows cluster signal of 4 aromatic proton signals of group -CH with 2 pairs of equivalent protons, having a chemical shift at 6,729 ppm (2H, d, J = 8.36 Hz) and 7.239 ppm (2H, d, J = 8.36 Hz) suggests that the aromatic ring is replaced twice in the para position. A -CH2 group with two multiplet signals of two protons in ở =

2.50 and 2.71 ppm respectively. In addition, the signal δ = 5,734 and 5,904 ppm are 2 protons of the aromatic ring indicating that positions 7 and 5 have been replaced.

+ **^{13}C-NMR spectrum** (^{13}C-NMR spectrum of E1 shows 14 carbon signals, of which 1 group signal –CH2 characteristic at δ = 28.2ppm at high field, 4 signals of group –CH aromatic (C cycle), with the chemical displacement là = 114ppm (C5 ', C3') and δ = 128 ppm (C6 ', C2') corresponding to the four protons above. The signals in the 98.4 to 130 ppm transition range show the signals of group-CH of the round.

The group position of –CH2 in position C4 was confirmed by interactions via a link between C4 and 2 H4 (1-2) protons on the HSQC spectrum.

Similarly, the positions of the –CH protons of rings A and B in positions 3, 2, 8 and 6 are expressed through direct C-H interactions on the spectrum of spectra.

The position of the three –OH groups was confirmed by the interactions on the HMBC spectrum of H4 (1) with C9, C10 and C3; interaction of H2 with C9, C1 ', C6' and C2 '; interaction of H6 with C10, C8 and C7; Interaction of H8 with C10, C7 and C6.

From analyzing the spectrum data of E1 and comparing with the reference, it is confirmed that E1 is 2- (3,4-hydroxyphenyl) chroman-3,5,7-triol.

Structural formula of LTE1E1:

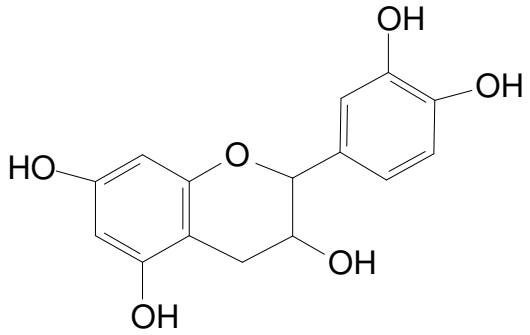

4. CONCLUSION

By repeating chromatographic method, 2 compounds from n-hexane and ethyl acetate segments of the positive fungi (Rhopalocnemis phalloides junghun) were isolated. Combining methods of infrared spectroscopy, mass spectra, one-way, two-dimensional nuclear magnetic resonance spectroscopy, and comparing their spectral data with published literature, the chemical structure of triglixerite (1), 2- (3,4-dihydroxyphenyl) chromane-3,5,7-triol (2).

This is the first time these compounds have been isolated from the Tich duong mushrooms collected in Son La.

REFERENCES

1. Pham Hoang Ho (2004), "Vietnam Grass", Episode 2, Young Publisher, pp. 140-141
2. Do Huy Bich and colleagues, *Medicinal plants and medicinal animals in Vietnam*, Publisher. Science and Technology, T1, Tr. 555 (2006).
3. Do Tat Loi (2000), *Vietnamese medicinal herbs and herbs*, Publisher. Medicine, Tr. 914.
4. Cam Thi Dinh, Nguyen Thi Hong Van, Tran Thi Quynh Trang, Phan Anh Tuan, Nguyen Thanh Huong, Pham Quoc Long (2014), *Study on chemical composition of ethyl acetate extract of poplar tree* (Balanophora laxiflora Hemsl.) In Vietnam, Journal of Science and Technology, 52 (5A), 96-100.
5. Gai-Mei She, Ying-Jun Zhang, Chong-Ren Yang (2009), *Phenolic Constituents from Balanophora laxiflora with DPPH Radical-Scavenging Activity*, Chemistry Biodiversity, 6 (6), 875-880.
6. Xiaohong Wang, Zizhen Liu, Wenlin Qiao, Ruiyang Cheng, Bin Liu and Gaimei She (2012), *Phytochemicals and biological studies of plants from the genus Balanophora*, Chemistry Central Journal, 10, 1186-1752.
7. Jiang ZH., Wen XY., Tanaka T., Wu SY., Liu Z., Iwata H., Hirose Y., Wu S., Kouno I. (2008), *Cytotoxic Hydrolyzable Tannins from Balanophora japonica*, J. Nat. Prod., 71(4), 719-723.
8. Wen-Fei Chiou, Chien-Chang Shen and Lie-Chwen Lin (2011), *Anti-Inflammatory Principles from Balanophora laxiflora*, Journal of Food and Drug Analysis, 19(4), 502-508.
9. Shang-Tse Ho, Yu-Tang Tung, Chi-Chang Huang, Chao-Lin Kuo, Chi-Chen Lin, Suh-Ching Yang, and Jyh-Horng Wu (2012), *The Hypouricemic Effect of Balanophora laxiflora Extracts and Derived Phytochemicals in Hyperuricemic Mice*, Evidence - Based Complementary and Alternative Medicine **2012**, 1-7.
10. Babady-Byla, Werner Herz (1996), *Triterpenes and 1-(ω hydroxyceratyl)glycerols from Pentaclethra eetveldeana root bark*, Phytochemistry, 42(2), 501- 504.

BƯỚC ĐẦU PHÂN LẬP VÀ XÁC ĐỊNH CẤU TRÚC MỘT SỐ HỢP CHẤT HỮU CƠ CỦA CÂY NẤM TÍCH DƯƠNG (*RHOPALOCNEMIS PHALLOIDES JUNGHUN*) THU TẠI SƠN LA

Tóm tắt: *2-(3,4- hydroxyphenyl) chroman-3,5,7-triol đã được phân lập từ cây nấm tích dương Rhopalocnemis phalloides junghun. Cấu trúc hóa học của các hợp chất này được xác định bằng các phương pháp phổ cộng hưởng từ hạt nhân 1 chiều và 2 chiều cũng như kết hợp so sánh với tài liệu tham khảo.*

Từ khóa: *Balanophoraceae, Rhopalocnemis phalloides junghun, phenolic.*

RESEARCH ON MANUFACTURING MATERIALS FROM LATERITE TO TREAT WASTEWATER IN NOODLE PRODUCTION VILLAGES, NOODLES IN SUBURBAN AREAS OF HANOI

Pham Van Hoan, Ngo Thanh Son, Nguyen Xuan Trinh, Ngo Thi Van Anh
Hanoi Metropolitan University

Abstract: *The noodle production village play an important role in the development of the local economy, as well as preserving the long-standing value of cultural traditions. However, the recent expansion of production has increased the risk of environmental pollution, greatly affecting the health of local people as well as landscape and ecology. Based on the analysis of Phu Do noodle production village wastewater, the study determined the ability of laterite to treat wastewater, contributing to environmental protection as well as the sustainable development of region as well as the country in the near future*

Keywords: *Laterite, Noodle production, Phu Do, Wastewater, Treatment…*

Email: pvhoan@hnmu.edu.vn
Received 27 April 2019
Accepted for publication 25 May 2019

1. INTRODUCTION

Among handicraft villages in Hanoi, noodle making village, noodle cake, in the field of food and food processing, is one of the traditional trade villages that have long been known. In Hanoi, especially in the suburbs, there are many establishments, households involved in the production of noodles, noodle cake, providing dozens to hundreds of tons of vermicelli and noodles every day. Dynamic eating, processing of not only the people of the capital, but also for neighboring provinces and regions to export to other countries.

However, currently in the city, there are only a few villages producing vermicelli, noodles with the focus of Phu Do trade village, or Minh Khai craft village (Hoai Duc district), and other areas of employment, vermicelli, noodle cake is only a small scale of a few households, such as the village of Mang Trach (Co Loa, Dong Anh), or in Quoc Oai and Thach That districts.

Due to manual and dispersed production, the treatment of trade village wastewater in general and noodle production villages in particular is very difficult. This has

consequences for air pollution, pollution of surface water and groundwater, greatly affecting the health of residents living in the village area [3].

There have been a number of studies evaluating the environment of craft villages, vermicelli production villages and noodle cakes. However, the treatment of this wastewater with materials made on laterite has not been studied [1; 2; 5].

To overcome this problem, the study of treatment at the source of noodle production, noodle cake is necessary and suitable to the local economic conditions.

This article introduces the initial studies using laterite to make materials to treat wastewater in noodle production villages, pho noodles in Phu Do, Tu Liem, Hanoi.

2. EXPERIMENT

2.1. Survey and assess the status of pollution in craft villages

- Reference documents
- Actual survey

2.2. Research on manufacturing treatment materials from natural sources (laterite)

Within the scope of research on resources and funding of the topic, the research team selected the determination of the waste water composition of the village identified by the surface water system in the production area.

To assess the current status of surface water environment in the village Phu Do, the research team took samples at 5 locations in 2 phases: October 2018 and February 2019.

Table 1. *Sampling location*

No	Sample of waste water	Places	Coordinates	
1	NM1	Nhue River	21°00'48.5"N	105°45'51.8"E
2	NM2	Phu Do pond	21°00'35.5"N	105°46'01.5"E
3	NM3	Nhue River	21°00'37.1N	105°45'44.0"E
4	NM4	Phu Do Lake	21°00'37.7"N	105°45'47.8"E
5	NM5	Phu Do channel	21°00'39.2"N	105°45'49.3"E

The sample collected by the research team was then analyzed at the Center for Environmental Monitoring and Modeling, University of Science, Hanoi National University.

Table 2. *Environmental monitoring data of surface water in Phu Do village in phase 1 (October 2018)*

Sample of waste water	Targets						
	pH	**TSS (mg/l)**	**BOD_5 (mg/l)**	**COD (mg/l)**	**Total Coliform (MPN/100ml)**	**NH_4^+ (mgN/l)**	**PO_4^{3-} (mgP/l)**
MN1	6,11	227	4213	5013	170000	68.88	16,03
MN2	5,47	394	5656	8666	22000	85,12	16,19
MN3	6,26	474	5506	6406	900000	154,02	29,93
MN4	6,59	55	3473	5010	8000	39,76	8,48
MN5	6,1	96	108,3	278	300000	93,52	0,08
QCVN 08: 2008/BTNMT	5,5 – 9	50	15	30	7500	0,5	0,3

The analytical results show that, in addition to the target of pH of organic substances at the monitoring positions, it is many times higher than the regulations of QCVN 08: 2008 / BTNMT national technical regulations on quality. surface water. COD content is 9.3 - 288.87 times higher; BOD is 7.22 - 377.1 times higher; The concentration of TSS is 1.1 - 9.48 times higher, the total Coliform is 1.1 - 120 times higher; NH4 + content is 79.53 - 308.04 times higher, PO43- content is 28. 27 - 99.77 times higher than Column B1 (regulating water quality for irrigation or other purposes) Other uses) of QCVN 08: 2008 / BTNMT.

The presence of high concentrations of NH4 + and PO43- has caused the water environment in the ponds to be enriched, the algae thrive, causing the phenomenon of water blooming, stinking water.

Table 3. *Environmental monitoring data of surface water in Phu Do trade village, phase 2 (February 2019)*

Sample of waste water	Targets						
	pH	**TSS (mg/l)**	**BOD_5 (mg/l)**	**COD (mg/l)**	**Total Coliform (MPN/100ml)**	**NH_4^+ (mgN/l)**	**PO_4^{3-} (mgP/l)**
MN1	6,0	211	3275	3202	150230	57.88	16,03
MN2	5,1	312	4423	6533	20234	68.11	12.34
MN3	5,8	212	5237	5328	670564	134,02	13,7
MN4	6,1	62	2138	4231	7008	42.23	8,48
MN5	5,9	78	114,2	250	26900	84.56	0,05
QCVN 08: 2008/BTNMT	5,5 – 9	50	15	30	7500	0,5	0,3

Analysis results show that, in addition to the target of pH of organic matters in the lake is many times higher than the regulations of QCVN 08: 2008 / BTNMT national technical regulations on surface water quality. COD content is 8.33 - 217.77 times higher; BOD is 7.61 - 349.1 times higher; TSS content is 1.24 - 4.22 times higher.

Total Coliform: Particularly, the parameter content at the monitoring point NM4 = 7008 is within the permitted limit of QCVN08: 2008 / BTNMT. Total Coliform content at positions NM1 - 2- 3 - 5 is higher than the permitted limit of QCVN08: 2008 / BTNMT from 2.7 to 89.41 times. ; NH4 + content is 79.53 - 308.04 times higher.

The concentration of PO43- is 28.3 - 53.43 times higher than that of QCVN 08: 2008 / BTNMT (except for the position NM5 of PO43- within the permitted limit of the method). The value of surface water environmental monitoring parameters through the two assessments is shown on the charts below.

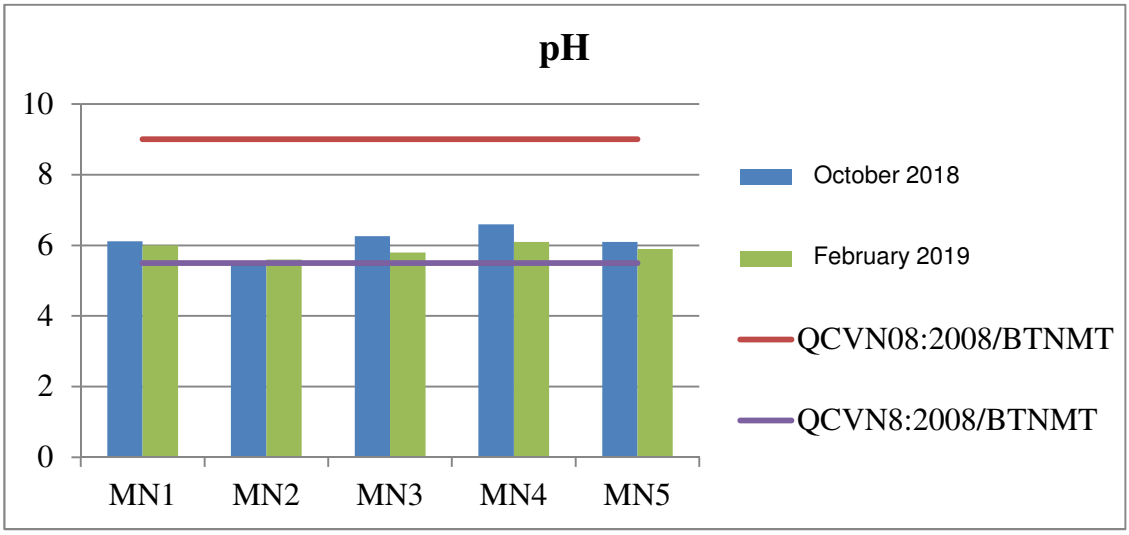

Figure 1. *pH at two monitoring sites*

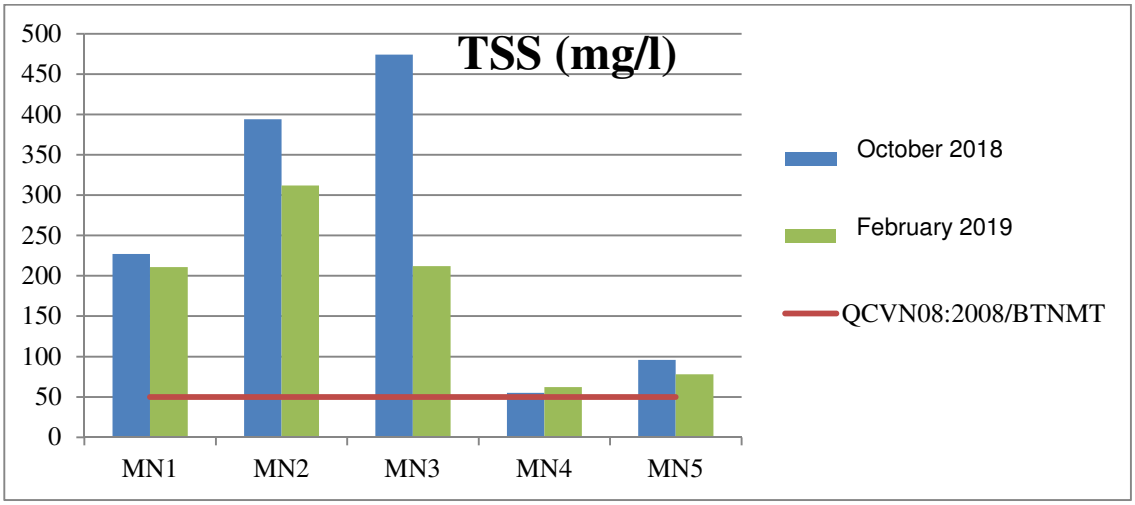

Figure 2. *TSS at 2 monitoring points*

pH value of surface water environment ranged from 5.5 - 7.0 within the permitted limit of QCVN 08: 2008 / BTNMT national technical standards for surface water quality. The value of the second phase pH decreased compared to the first phase.

TSS content in water tends to decrease through 2 monitoring periods. However, the TSS content in both monitoring periods in all sampling locations exceeded the permitted limit of QCVN 08: 2008 / BTNMT.

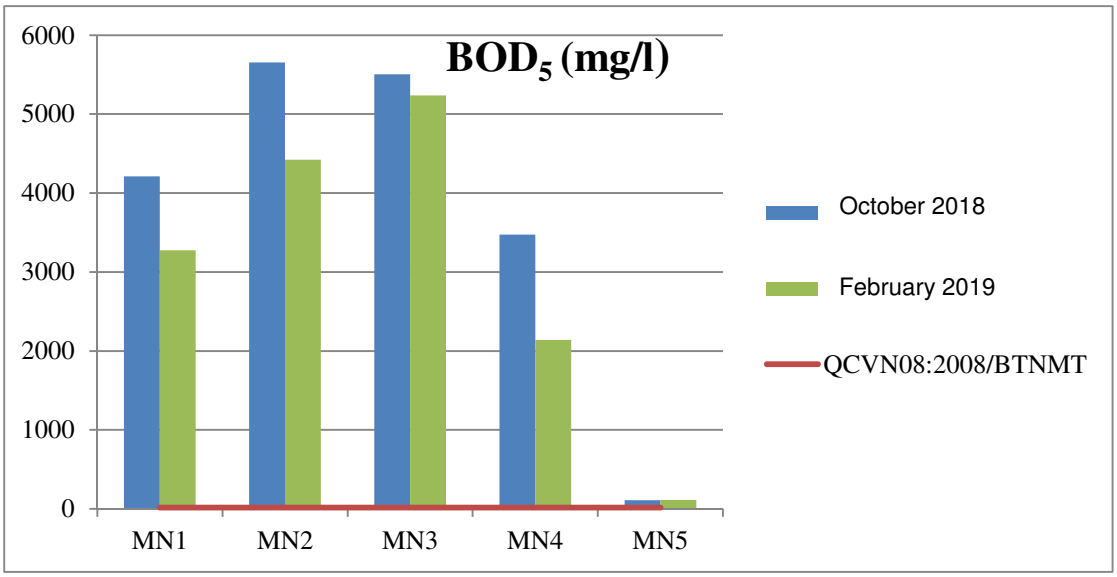

Figure 3. *BOD5 at 2 monitoring points*

BOD5 content in the regional water environment exceeds the permitted limits of QCVN 08: 2009 / BTNMT many times and tends to decrease.

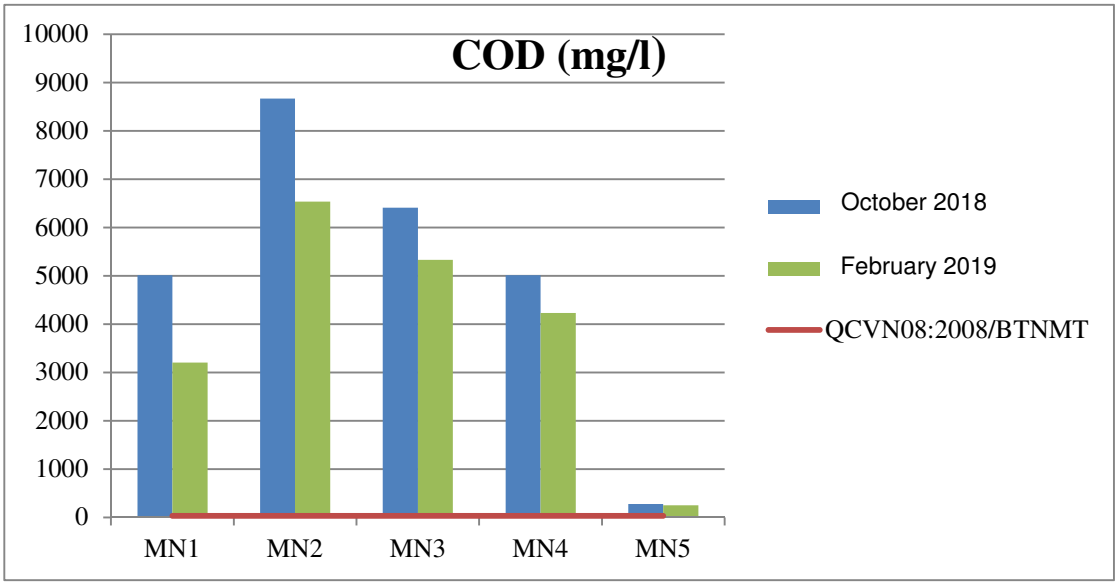

Figure 4. *COD at 2 monitoring points.*

Like BOD5, the COD content in the water in the local Phu Do village area is very high, exceeding the permitted standard of QCNV08: 2008 / BTNMT on surface water quality and tends to decrease.

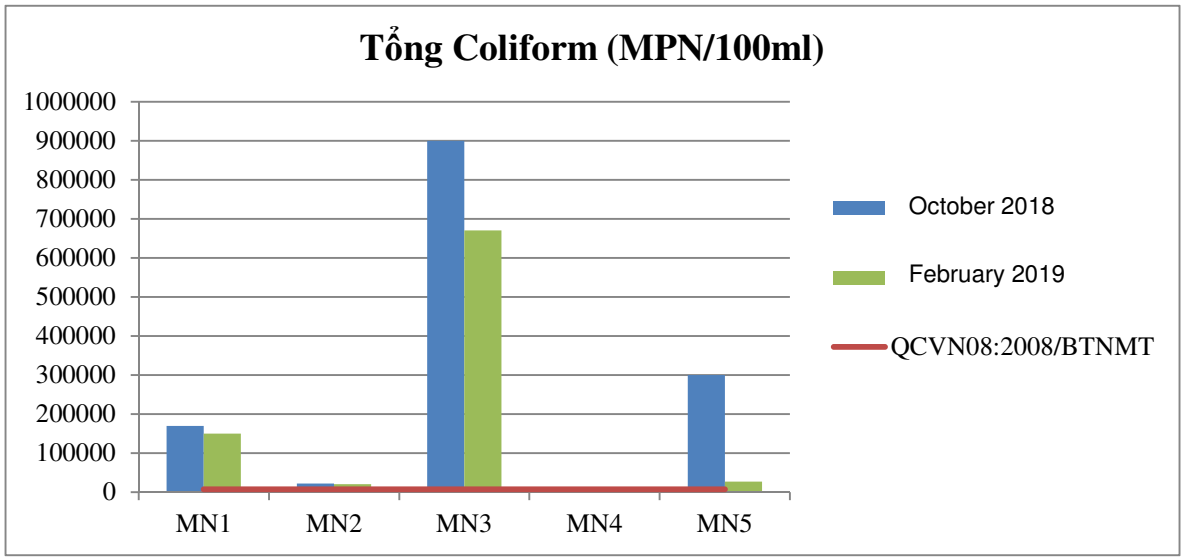

Figure 5. *Total value of Coliform at 2 monitoring points*

The total value of Coliform in the environment in the area tends to decrease but not significantly. The content in the positions MN1, MN3, MN5 is very high in excess of the permitted limit of QCVN 08: 2008 / BTNMT many times. Particularly, position MN4 in phase 2 has a total Coliform content below the permitted limit of surface water quality standards.

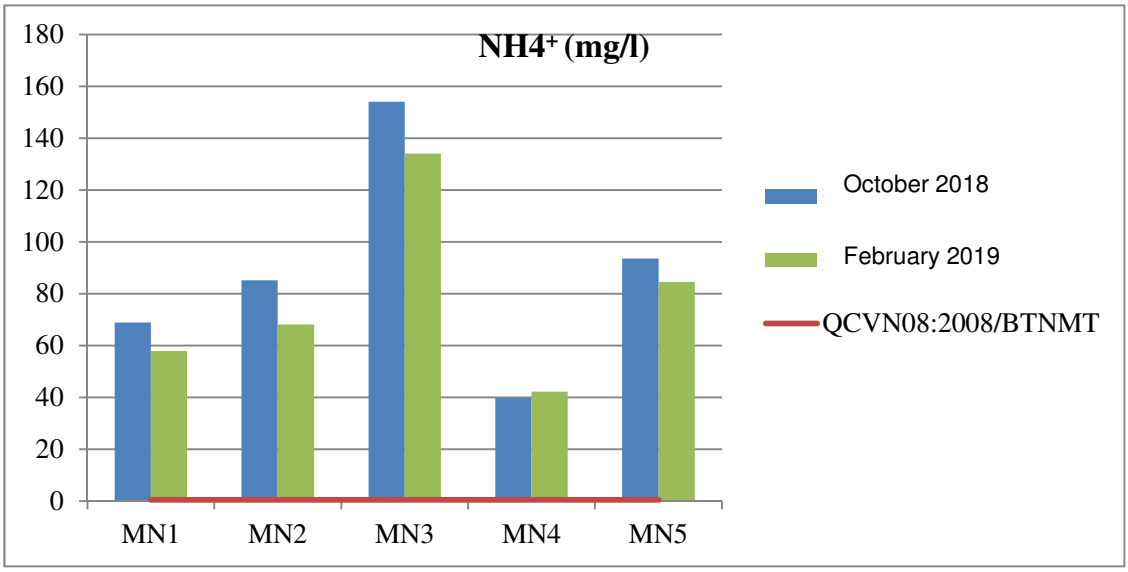

Figure 6. *NH_4^+ at 2 monitoring points*

Based on the chart, it is easy to see that the content of ammonium in the country tends to decrease, except for the MN4 point, but it is not significant. The content of ammonium in water at two monitoring periods is very high, exceeding the permitted limit of QCVN 08: 2008 / BTNMT.

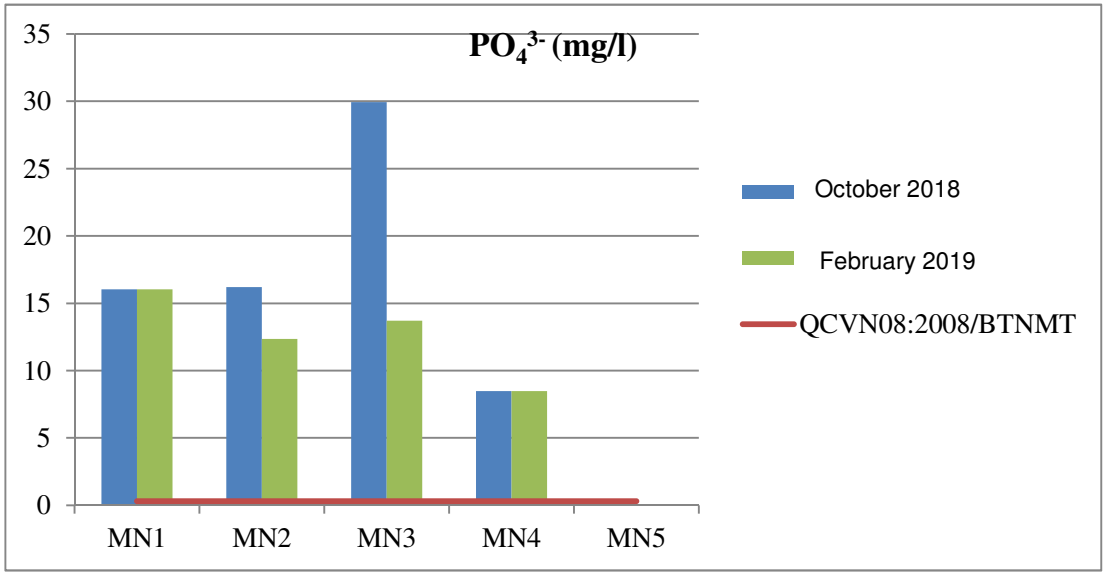

Figure 7. *PO_4^{3-} in surface water at 2 monitoring points*

The concentration of PO43- in surface water in Phu Do vermicelli production village tended to decrease slightly through 2 monitoring periods. However, the content of PO43- in both batches is very high, exceeding the permitted limit of QCVN 08: 2008 / BTNMT on surface water quality.

3.3. Fabrication of laterite materials is taken from Thach That district, Hanoi and processed according to the following process

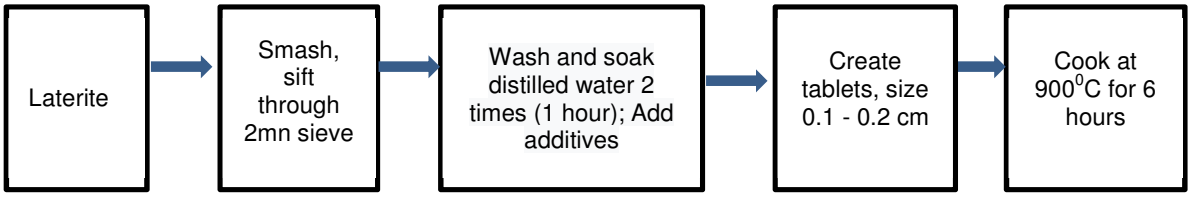

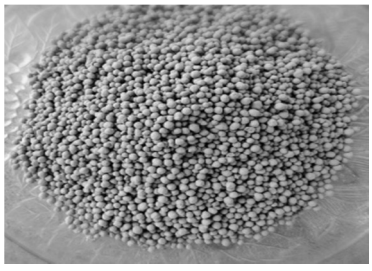

Figure 8. *Material made of laterite (M1)*

3.4. Examine the ability of materials in wastewater treatment of vermicelli production villages, pho noodles

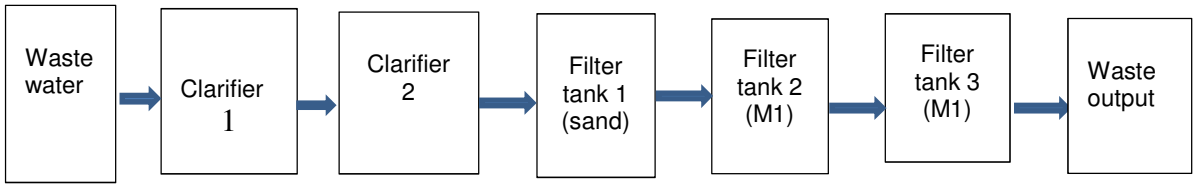

Figure 9. *Layout diagram of wastewater treatment experiment*

To determine the role of materials (M1), water samples through settling tanks 1, 2 and filter tank 1 were taken out to assess color and odor.

By observation, waste water through settling tanks and filter tanks 1 still has an unpleasant odor and is slightly turbid. Because sand only retains insoluble suspended matter, the removal of dissolved substances is entirely due to the material made from laterite (M1).

Results of quality evaluations of waste water after treatment are as follows.

3.4.1. Feelings

Odor: the original sour smell has been exhausted, indicating that evaporation solvents have been removed;

Color: clear, demonstrating that colored or suspended solids components have been removed.

3.4.2. Other soluble ingredients

Adsorption efficiency (%) is calculated by the following formula:

$$\text{Adsorption (\%)} = (Ci - Co) / Ci \times 100$$

In which Ci: the input concentration of the target

Co: output concentration

The indicators after analysis are shown as follows:

a. Target of TSS (Total suspended solid content)

Table 4. *TSS index and processing efficiency*

Sample of waste water	TSS (mg/l)		processing efficiency
	Input	Output	
MN1	277	45	84%
MN2	394	47	88%
MN3	475	62	87%

Thus, the wastewater treatment system for vermicelli, noodles with laterite material is proposed, capable of handling suspended solids with an average efficiency of 86%. The content of TSS in the outlet water is also approximately the permitted limit according to QCVN

b. BOD5 index (Biochemical oxygen demand)

Table 5. *BOD5 index and processing performance*

Sample of waste water	BOD_5 (mg/l)		processing efficiency
	Input	Output	
MN1	4213	1023	75%
MN2	5656	1540	72%
MN3	5506	1450	73%

Treatment system with laterite material as proposed, has the ability to handle BOD5 with an average efficiency of 73%. However, the amount of BOD5 in the output water is still very high, far exceeding QCVN many times.

c. COD criteria (Chemical oxygen demand)

Table 6. *COD index and processing efficiency*

Sample of waste water	COD (mg/l)		processing efficiency
	Input	Output	
MN1	5013	1290	74%
MN2	8666	2020	76%
MN3	6406	1415	78%

The system has the ability to handle COD, the average efficiency is 76%, but the COD content is still very large, far exceeding QCVN many times.

d. Total coliform

Table 7. *Coliform index and treatment performance*

Sample of waste water	Tổng coliform (MPN/100ml)		processing efficiency
	Input	Output	
MN1	150230	29540	80%
MN3	670564	102430	84%
MN5	26900	5400	80%

The ability to treat coliform of the proposed system is relatively high, the average yield is 81%. However, at times when the total coliform is abnormally high, the output index is still very large, exceeding the QCVN.

e. NH_4^+

Table 8. *NH4 + index and processing efficiency*

Sample of waste water	NH_4^+		processing efficiency
	Input	Output	
MN2	85,12	12,04	85%
MN3	154,02	19,46	87%
MN5	93,52	14.01	85%

The proposed system is capable of handling NH4 + Ion in a sample of vermicelli wastewater, average performance reaches 85%. However, the amount of ammonium ion in the output water is still higher than the permitted level according to QCVN.

g. PO_4^{3-}

Table 9. *PO43- index and processing performance*

Sample of waste water	PO_4^{3-}		processing performance
	Input	Output	
MN1	16,03	2,4	85%
MN2	16,19	1,96	88%
MN3	29,93	3,06	89%

Thus, the wastewater treatment system has the ability to process ion PO43-, the processing efficiency is relatively high, averaging 87%.

4. CONCLUSION

The water treatment system proposed with mechanical methods combined with laterite materials to treat wastewater of the vermicelli production village, Phu Do is the deodorant and color. Using materials to treat waste water from laterite - an available and cheap materials is a promising research direction that needs further study.

However, the treatment is not really thorough, the processing efficiency has not really met the expectations, need to be studied further.

REFERENCES

1. Ministry of Natural Resources and Environment (2013), *National Environmental Status Report.*
2. Circular 46/2011/ TT-BTNMT, December 26, 2011 of the Ministry of Natural Resources and Environment promulgating Regulations on environmental protection of craft villages.
3. Sub-Department of Environmental Protection (2013), *Specialized report on the current situation of natural environment, topography and socio-economic conditions*, Production and technology of Phu Do noodle village, Hanoi.
4. Dang Kim Chi, Nguyen Ngoc Lan, Tran Le Minh (2005), *Vietnam Craft Village and Environment*, Science and Technology Publishing House.
5. Le Ngoc Anh (2013), *Graduation project: Applying DPSIR model in assessing the current state of water environment in Bai Do trade village, Tri Thuy commune, Phu Xuyen district, Hanoi*.
6. QCVN 08: 2008 / BTNMT National technical regulation on surface water quality.

NGHIÊN CỨU CHẾ TẠO VẬT LIỆU XỬ LÍ NƯỚC THẢI LÀNG NGHỀ SẢN XUẤT BÚN, BÁNH PHỞ TẠI KHU VỰC NGOẠI THÀNH HÀ NỘI 55TỪ ĐÁ ONG

Tóm tắt: *Làng sản xuất bún, bánh phở đóng một vai trò quan trọng trong sự phát triển của nền kinh tế địa phương, cũng như bảo tồn giá trị lâu đời của truyền thống văn hóa. Tuy nhiên, việc mở rộng sản xuất gần đây đã làm tăng nguy cơ ô nhiễm môi trường, ảnh hưởng lớn đến sức khỏe của người dân địa phương cũng như cảnh quan và sinh thái. Dựa trên phân tích nước thải làng sản xuất mì Phú Đô, nghiên cứu đã xác định khả năng xử lý nước thải của đá ong, góp phần bảo vệ môi trường, đóng góp sự phát triển bền vững của khu vực cũng như đất nước trong tương lai.*

Từ khóa: *Laterit (Đá ong), sản xuất bún, Phú Đô, nước thải, xử lý…*

THỂ LỆ GỬI BÀI

1. *Tạp chí Khoa học* là ấn phẩm của Trường ĐH Thủ đô Hà Nội, công bố các công trình nghiên cứu và bài viết tổng quan trong nhiều lĩnh vực khoa học. Tạp chí được xuất bản định kì, mỗi số về một lĩnh vực cụ thể: Khoa học Xã hội và Giáo dục; Khoa học Tự nhiên và Công nghệ.
2. Tác giả có thể gửi toàn văn bản thảo bài báo cho Tổng biên tập, Phó Tổng biên tập hoặc biên tập viên theo địa chỉ email ghi ở dưới. Tất cả bản thảo bài báo gửi công bố đều được thẩm định về nội dung khoa học bởi các nhà khoa học chuyên ngành có uy tín. Tạp chí không nhận đăng các bài đã công bố trên các ấn phẩm khác và không trả lại bài nếu không được duyệt đăng. Tác giả bài báo chịu hoàn toàn trách nhiệm về pháp lí đối với nội dung kết quả nghiên cứu được đăng tải.
3. Bố cục bài báo cần được viết theo trình tự sau: *tóm tắt* (nêu ý tưởng và nội dung tóm tắt của bài báo); *mở đầu* (tổng quan tình hình nghiên cứu, tính thời sự của vấn đề, đặt vấn đề); *nội dung* (phương pháp, phương tiện, nội dung nghiên cứu đã thực hiện); *kết luận* (kết quả nghiên cứu, hướng nghiên cứu tiếp theo) và *tài liệu tham khảo*.

   Bài báo toàn văn không dài quá 10 trang đánh máy trên khổ giấy A4, phông chữ Times New Roman (Unicode), cỡ chữ (Size) 12 thống nhất cho toàn bài, lề trái 3 cm, lề phải 2 cm, cách trên, cách dưới 2.5 cm, giãn dòng (Multiple) 1.25. Các thuật ngữ khoa học và đơn vị đo lường viết theo quy định hiện hành của Nhà nước; các công thức, hình vẽ cần được viết theo các ký hiệu thông dụng; tên hình vẽ đặt dưới hình, tên bảng, biểu đồ đặt trên bảng. Khuyến khích các bài sử dụng chương trình LaTex với khoa học tự nhiên, công thức hóa học có thể dùng ACD/Chem Sketch hoặc Science Helper for Word. Bài báo phải có tóm tắt bằng tiếng Việt và tiếng Anh. *Tóm tắt* viết không quá 10 dòng. *Tóm tắt tiếng Việt* đặt sau tiêu đề bài báo và tên tác giả, *tóm tắt tiếng Anh* gồm cả tiêu đề bài báo đặt sau *tài liệu tham khảo*. Các tên nước ngoài được ghi bằng kí tự Latinh. Cuối bài có ghi rõ cơ quan công tác, số điện thoại, địa chỉ email của tác giả.
4. Phần *Tài liệu tham khảo* xếp theo thứ tự xuất hiện trong bài báo và sắp xếp theo mẫu dưới đây:

   1. John Steinbeck (1994), *Chùm nho phẫn nộ* (Phạm Thủy Ba dịch, tập 2), - Nxb Hội nhà văn, H., tr.181.
   2. Bloom, Harold (2005), *Bloom's guides: John Steinbeck's The Grapes of Wrath*, New York: Chelsea House, pp.80-81.
   3. W.A Farag, V.H Quintana,. G Lambert-Torres (1998), "A Genetic-Based Neuro-Fuzzy Approach to odelling and Control of Dynamical Systems", *IEEE Transactions on neural Networks Volume*: 9 Issue: 5, pp.756-767.

Phòng Tạp chí - Trường Đại học Thủ đô Hà Nội
Số 98, Dương Quảng Hàm, Cầu Giấy, Hà Nội
Tel: 04.3.767.1409; Fax: 04.3. 833.5426
Email: tapchikhoahoc@hnmu.edu.vn